Design of an Unmanned Aerial Vehicle for Kinetic Attack Applications

---

A Final Year Project Report

Presented to

SCHOOL OF MECHANICAL & MANUFACTURING ENGINEERING

Department of Mechanical Engineering

NUST

ISLAMABAD, PAKISTAN

In Partial Fulfillment
of the Requirements for the Degree of
Bachelor of Mechanical Engineering

---

by

Muhammad Taimoor Asif
Muhammad Saqib Irshad
Muhammad Hanzla
Ali Yasir

June 2023

EXAMINATION COMMITTEE

We hereby recommend that the final year project report prepared under our supervision by:

MUHAMMAD SAQIB IRSHAD	293083
MUHAMMAD HANZLA	288124
ALI YASIR	285010
MUHAMMAD TAIMOOR ASIF	291006

Titled: "DESIGN OF AN UNMANNED AERIAL VEHICLE FOR KINETIC ATTACK APPLICAITONS" be accepted in partial fulfilment of the requirements for the award of BACHELOR OF MECHANICAL ENGINEERING degree with grade ___

Supervisor: Dr. Emad Ud Din, HOD Mechanical Engineering, SMME - NUST	Dated:
Committee Member: Name, Title (faculty rank) Affiliation	Dated:
Committee Member: Name, Title (faculty rank) Affiliation	Dated:

_____ _____

(Head of Department) (Date)

COUNTERSIGNED

Dated: _____ _____

(Dean / Principal)

Abstract

Recently, the world has seen a considerable growth in the number of utilized drones, with a global and ongoing increase in demand for their multi-purpose applications. Their use is not limited to reconnaissance, surveillance applications but UAVs can also be used as a suicide drone or kamikaze drone. The use of kinetic attack drones allows for quicker reaction times while dealing with concealed or hidden targets.

This project aims to design an autonomous aerial vehicle for kinetic attack applications by conducting a thorough analysis of the literature to focus on the design implications for such drone systems. The objective is to design UAV based on mission requirements and to select a configuration which best suits to the case using a decision matrix. Predictive analysis is used to select performance and design parameters based on the visual inspection of data from more than 80 previously designed UAVs for attack applications. The design requirements include the capability of a UAV to be launched without much infrastructure requirement, easy to transport, ability to track and lock on to the target, detonate on target with impact, and cost-effectiveness. The selected design parameters include top speed, span, maximum take-off weight, range, payload weight, endurance, and other relevant parameters. This project's outcome will be a scaled drone for kinetic attack applications designed, fabricated, and evaluated using appropriate design specifications.

Acknowledgement

We would like to extend our sincere gratitude to all those who provided us the possibility to complete this report. We would also like to thank our Advisors “Dr. Emad Ud Din” and “Dr. Basharat Ali” for their unwavering support and guidance throughout the project.

Furthermore, we would also like to acknowledge the invaluable contributions of our final year project coordinator “Dr. Rehan Zahid” and Lab Engineer “Ali Hassan” whose insightful suggestions and constant encouragement helped us to coordinate our project effectively. We must also recognize the guidance provided by our other supervisors, as well as the feedback given by the panel during our last project presentation. Their constructive input enabled us to make significant improvements and present our work with a clear and practical approach. Once again, we appreciate the efforts of all those who helped us in completing this project.

Originality Report

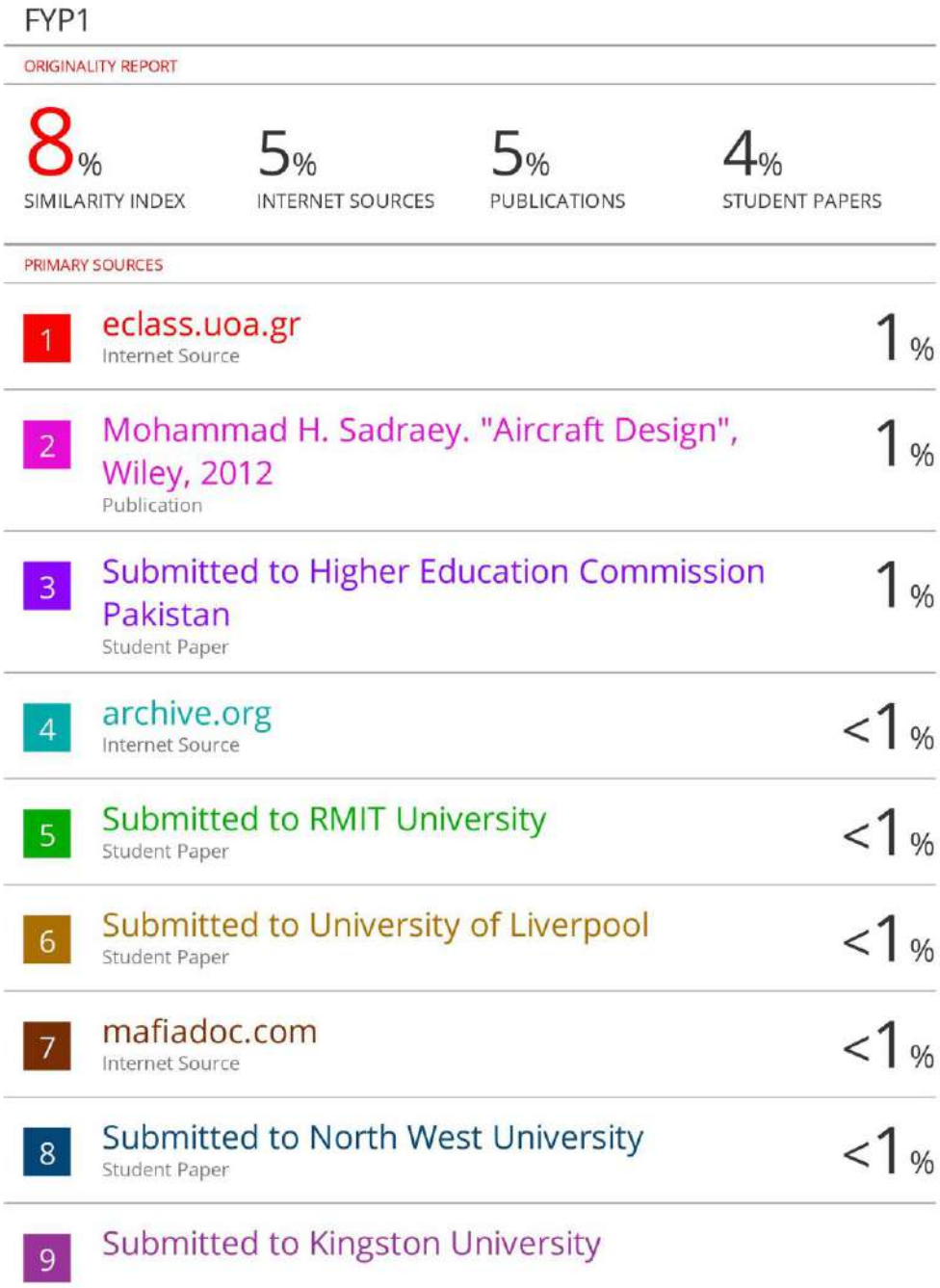

FYP1

ORIGINALITY REPORT

8%	5%	5%	4%
SIMILARITY INDEX	INTERNET SOURCES	PUBLICATIONS	STUDENT PAPERS

PRIMARY SOURCES

1	eclass.uoa.gr Internet Source	1%
2	Mohammad H. Sadraey. "Aircraft Design", Wiley, 2012 Publication	1%
3	Submitted to Higher Education Commission Pakistan Student Paper	1%
4	archive.org Internet Source	<1%
5	Submitted to RMIT University Student Paper	<1%
6	Submitted to University of Liverpool Student Paper	<1%
7	mafiadoc.com Internet Source	<1%
8	Submitted to North West University Student Paper	<1%
9	Submitted to Kingston University	

	Student Paper	<1%
10	Submitted to Middle East Technical University Student Paper	<1%
11	www.aero.us.es Internet Source	<1%
12	Jay Gundlach. "Designing Unmanned Aircraft Systems", American Institute of Aeronautics and Astronautics (AIAA), 2012 Publication	<1%
13	Jose Luis Rivera Gil, Juliana Serna, Javier A. Arrieta - Escobar, Paulo César Narváez Rincón, Vincent Boly, Veronique Falk. "Triggers for Chemical Product Design: A Systematic Literature Review", AIChE Journal, 2022 Publication	<1%
14	Submitted to Universiti Putra Malaysia Student Paper	<1%
15	Mohammad H. Sadraey. "Design of Unmanned Aerial Systems", Wiley, 2020 Publication	<1%
16	www2.mdpi.com Internet Source	<1%
17	Submitted to Coventry University Student Paper	<1%

18	Submitted to Multimedia University Student Paper	<1 %
19	spectrum.library.concordia.ca Internet Source	<1 %
20	ultraexotics.shop Internet Source	<1 %
21	Submitted to The Scientific & Technological Research Council of Turkey (TUBITAK) Student Paper	<1 %
22	Submitted to Universidad Europea de Madrid Student Paper	<1 %
23	Submitted to University of Hertfordshire Student Paper	<1 %
24	Submitted to University of Witwatersrand Student Paper	<1 %
25	Submitted to Defence Institute of Advanced Technology, Pune Student Paper	<1 %
26	ardupilot.org Internet Source	<1 %
27	rahauav.com Internet Source	<1 %
28	www.researchgate.net Internet Source	<1 %

29	Submitted to De Montfort University Student Paper	<1 %
30	Submitted to Emirates Aviation College, Aerospace & Academic Studies Student Paper	<1 %
31	R.P.G. Collinson. "Introduction to Avionics Systems", Springer Science and Business Media LLC, 2023 Publication	<1 %
32	people.utm.my Internet Source	<1 %
33	Submitted to Southern New Hampshire University - Continuing Education Student Paper	<1 %
34	Submitted to University of Bath Student Paper	<1 %
35	plane.ardupilot.com Internet Source	<1 %
36	Submitted to Florida Institute of Technology Student Paper	<1 %
37	Submitted to University of Glamorgan Student Paper	<1 %
38	Submitted to Federal University of Technology Student Paper	<1 %
	hdl.handle.net	

39	Internet Source	<1%
40	Cavagna, L.. "NeoCASS: An integrated tool for structural sizing, aeroelastic analysis and MDO at conceptual design level", Progress in Aerospace Sciences, 201111 Publication	<1%
41	www.slideshare.net Internet Source	<1%
42	Submitted to Universiti Teknologi Malaysia Student Paper	<1%
43	digitalcommons.njit.edu Internet Source	<1%
44	prism.ucalgary.ca Internet Source	<1%
45	systemarchitect.mit.edu Internet Source	<1%
46	Submitted to Universiti Tunku Abdul Rahman Student Paper	<1%
47	faculty.dwc.edu Internet Source	<1%
48	www.wiley.com Internet Source	<1%
49	Submitted to North Penn School District Student Paper	<1%

50	repository.tudelft.nl Internet Source	<1 %
51	www.srielectronics.com Internet Source	<1 %
52	Mohammad H. Sadraey. "Chapter 5 Longitudinal Control", Springer Science and Business Media LLC, 2022 Publication	<1 %
53	Submitted to South Bank University Student Paper	<1 %
54	Submitted to Swinburne University of Technology Student Paper	<1 %
55	Submitted to University of Derby Student Paper	<1 %
56	publikace.k.utb.cz Internet Source	<1 %
57	www.unicef.org Internet Source	<1 %
58	"An UAV with Twin Propellers Driven by Single Motor", International Journal of Innovative Technology and Exploring Engineering, 2019 Publication	<1 %
59	Submitted to University of Leeds Student Paper	<1 %

60	slideplayer.com Internet Source	<1 %
61	wpage.unina.it Internet Source	<1 %
62	Anmin Zhao, Jun Zhang, Ke Li, Dongsheng Wen. "Design and implementation of an innovative airborne electric propulsion measure system of fixed-wing UAV", Aerospace Science and Technology, 2020 Publication	<1 %
63	Hidehiro Segawa, Ashok Gopalarathnam. "Optimum Flap Angles for Roll Control on Wings with Multiple Trailing-Edge Flaps", 46th AIAA Aerospace Sciences Meeting and Exhibit, 2008 Publication	<1 %
64	123docz.net Internet Source	<1 %
65	Submitted to Cranfield University Student Paper	<1 %
66	Nicolosi, Fabrizio, Pierluigi Della Vecchia, and Salvatore Corcione. "Design and aerodynamic analysis of a twin-engine commuter aircraft", Aerospace Science and Technology, 2015. Publication	<1 %
67	Submitted to University of Wales Swansea Student Paper	

		<1 %
68	Yousef Alghamdi, Arslan Munir, Hung Manh La. "Architecture, Classification, and Applications of Contemporary Unmanned Aerial Vehicles", IEEE Consumer Electronics Magazine, 2021 Publication	<1 %
69	byjusexamprep.com Internet Source	<1 %
70	cgi.temp.ekohudochhalsa.se.php54.levonline.com Internet Source	<1 %
71	en.wikipedia.org Internet Source	<1 %
72	keep.lib.asu.edu Internet Source	<1 %
73	lib.buet.ac.bd:8080 Internet Source	<1 %
74	scholarworks.rit.edu Internet Source	<1 %
75	ujcontent.uj.ac.za Internet Source	<1 %
76	www.aerostudents.com Internet Source	<1 %

77	"Morphing Aerospace Vehicles and Structures", Wiley, 2012 Publication	<1 %
78	"Springer Handbook of Mechanical Engineering", Springer Science and Business Media LLC, 2009 Publication	<1 %
79	Adekunle Taofeek Oyelami, Oladipupo Maothon Bamgbose, Olusola Akinbolaji Akintunlaji. "Mission-Planner Mapped Autonomous Robotic Lawn Mower", Journal Européen des Systèmes Automatisés, 2023 Publication	<1 %
80	Michael Kryger, Brock Wester, Eric A. Pohlmeyer, Matthew Rich et al. "Flight simulation using a Brain-Computer Interface: A pilot, pilot study", Experimental Neurology, 2017 Publication	<1 %
81	Na Xu, Mao Sun. "Lateral dynamic flight stability of a model hoverfly in normal and inclined stroke-plane hovering", Bioinspiration & Biomimetics, 2014 Publication	<1 %
82	Nhan T. Nguyen, Eric Ting, Daniel Y. Nguyen, Khanh V. Trinh. "Flight Dynamic Modeling and Stability Analysis of Flexible Wing Generic	<1 %

	Transport Aircraft", 55th AIAA/ASME/ASCE/AHS/ASC Structures, Structural Dynamics, and Materials Conference, 2014 Publication	
83	Nianhong Han, Haiyang Hu, Hui Hu. "An Experimental Investigation on the Dynamic Ice Accretion Process over the Blade Surface of a Rotating UAV Propeller", AIAA SCITECH 2022 Forum, 2022 Publication	<1 %
84	api.intechopen.com Internet Source	<1 %
85	cpanel.thescipub.com Internet Source	<1 %
86	fenix.tecnico.ulisboa.pt Internet Source	<1 %
87	mediatum.ub.tum.de Internet Source	<1 %
88	open.uct.ac.za Internet Source	<1 %
89	scholarsmine.mst.edu Internet Source	<1 %
90	tigerprints.clemson.edu Internet Source	<1 %

91	Aircraft Engineering and Aerospace Technology, Volume 89, Issue 1 (2017) Publication	<1 %
92	eteze.bg.ac.rs Internet Source	<1 %
93	"Unmanned Aerial Vehicle Cellular Communications", Springer Science and Business Media LLC, 2023 Publication	<1 %
94	Yong Zeng, Qingqing Wu, Rui Zhang. "Accessing From the Sky: A Tutorial on UAV Communications for 5G and Beyond", Proceedings of the IEEE, 2019 Publication	<1 %
95	kc.umn.ac.id Internet Source	<1 %

Exclude quotes	On	Exclude matches	Off
Exclude bibliography	On		

TABLE OF CONTENTS

List of Tables

List of Figures

Symbol and Abbreviation

$N_b = \textit{Number of Batteries}$

$K = \textit{Induced Drag Coefficient}$

$N_{sm_1} = \textit{Number of Servos of Type } 1$

$C_D = \text{" } \textit{Drag Polar} \text{ "}$

$N_{sm} = \textit{Number of Servos}$

$V_c = \textit{Cruise Speed}$

$N_m = \textit{N umber of Motors}$

$V_s = \text{" } \textit{Stalling Speed} \text{ "}$

$V_{max} = \textit{Maximum Speed}$

$W_b = \textit{Weight of Battery}$

$ROC = \textit{Rate of Climb}$

$W_m = \textit{Weight of Motor}$

$ROC_{ceil} = \textit{Rate of Climb at Ceiling Altitude}$

$e = \textit{Ostwald's Efficiency}$

$W_{ESC} = \textit{Weight of Electronic Speed Controller}$

$W_p = \textit{Weight of Propellers}$

$\left(\frac{W}{S}\right)_{stall} = \textit{Wing Loading as a function of Stall Speed}$

$W_{FC} = \textit{Weight of Flight Controller}$

$\left(\frac{W}{S}\right)_{Max} = \textit{Wing Loading as a function of Max Speed}$

$W_{misc} = \textit{Weight of Miscellaneous Components } (GPS)$

$Cl_{max_{w,2D}} = \textit{Maximum lift coefficient of wing Airfoil}$

$W_{sm} = \textit{Weight of Servos}$

$\left(\frac{W}{S}\right)_{ROC} = \textit{Wing Loading as a function of Rate of Climb}$

$W_{CB} = Weight\ of\ Cables\ or\ Wires$

$\left(\frac{W}{S}\right)_{Ceiling} = Wing\ Loading\ as\ a\ function\ of\ Rate\ of\ Climb$

$W_{AF} = Weight\ of\ Airframe\ of\ Structure$

$\left(\frac{W}{P}\right)_{stall} = Power\ Loading\ as\ a\ function\ of\ Stall\ Speed$

$W_{PL} = Weight\ of\ Payload$

$W_{\text{MTow}} = Maximum\ Take - off\ Weight$

$\rho_{\text{sea}} = Density\ of\ Air\ at\ Sea - Level$

$\left(\frac{W}{P}\right)_{Max} = Power\ Loading\ as\ a\ function\ of\ Max\ Speed$

$\rho_{\text{ceiling}} = Density\ of\ Air\ at\ Ceiling\ Altitude$

$\rho_{\text{alt}} = Density\ of\ Air\ at\ Cruising\ Altitude$

$CD_o = Zero - Lift\ Drag\ Coefficient$

$\left(\frac{W}{P}\right)_{ROC}$ = Power Loading as a function of Rate of Climb

$\left(\frac{W}{P}\right)_{\text{Ceiling}}$ = Power Loading as a function of Rate of Climb

h_{Ceiling} = Absolute Ceiling

h_{alt} = Cruising Altitude

P_{alt} = Power at cruising altitude

P_{SL} = Power at sea level

$K = Induced$ Drag Factor

σ_c = Relative Air Density at Required Ceiling

$(\eta_p)_{\text{Stall}}$ = Efficiency of Propeller during Stall

$(\eta_p)_{Max}$ = Efficiency of Propeller during Maximum Speed

$(\eta_p)_{ROC}$ = Efficiency of Propeller during Climb

$(\eta_p)_{\text{Ceiling}}$ = Efficiency of Propeller at Ceiling

$(\eta_p)_{\text{Stall}}$ = **Efficiency of Propeller during Stall**

σ_c = **Relative Air Density at Ceiling**

σ_{alt} = **Relative Air Density at Cruising Altitude**

$\left(\frac{W}{P}\right)_{DP}$ = **Power Loading Design Point**

$\left(\frac{W}{S}\right)_{DP}$ = **Wing Loading Design Point**

S_w = **Wing Area**

b_w = **Wing Span**

AR_w = **Wing Aspect Ratio**

$C_{\text{root},w}$ = **Wing Root Chord**

P_{DP} = **Power of Motor From Design Point**

$\left(\frac{L}{D}\right)_{w,2-D_{\max}}$ = **Maximum Wing Airfoil Lift to Drag Ratio**

$\left(\frac{L}{D}\right)_{W,3-D_{\max}}$ = **Maximum Wing Lift to Drag Ratio**

g = **Gravitational Acceleration**

λ_w = **Taper Ratio of Wing**

$\alpha_{i,w}$ = **W ing Incidence Angle or Setting Angle**

$C_{\alpha_{w,2D}}$ = **Lift coefficient Slope of Wing Airfoil**

$Cl_{\alpha_{w,3D}}$ = **Lift coefficient Slope of Wing**

$\alpha_{o_{w,2D}}$ = **Zero Lift Angle of Attack of Airfoil**

C_w = **Mean Aerodynamic Chord of Wing**

Λ_w = **Wing Sweep Angle**

$Cl_{LT_{w,3D}}$ = **Lift Coefficient of Wing from Lift Line Theory**

$Cl_{c_{req,2D}}$ = = **Required Lift Coefficient of Airfoil at Cruising**

$Cl_{c_{req,3D}}$ = = **Required Lift Coefficient of Wing at Cruising**

S_w = **Mean Wing Area**

$\left(\frac{t}{c}\right)_{max,w}$ **=Wing Airfoil Maximum Thickness to Chord Ratio**

R_{plane} = **Range of Aircraft**

t_{cruise} = **Time of Total Cruise**

E_{cruise} = **Energy Consumption in Cruise**

$FOS_{Battery}$ = **Safe Discharge of Battery**

$E_{Descend}$ = **Energy Consumption in Descend**

E_{Total} = **Total Energy Consumption**

$(W_b)_{req}$ = $Required\ Weight\ of\ Battery$

$\bar{V}_H$ = $Horizontal\ Tail\ Volume\ Coefficient$

D_F = $Diameter\ of\ Fuselage$

K_c = $Fudge\ Factor$

$l_{h_{opt}}$ = $Optimum\ Moment\ -\ Arm\ of\ Horizontal\ Tail$

S_h = $Horizontal\ Tail\ Area$

$C_{m_{w,2D}}$ = $Wing\ Airfoil\ Maximum\ Pitching\ Moment$

$C_{m_{w,3D}}$ = $Wing\ Maximum\ Pitching\ Moment$

h
= $Distance\ of\ Center\ of\ gravity\ from\ wing\ leading\ edge\ in\ terms\ of\ chord\ length$

h_o
= $Distance\ of\ Aerodynamic\ center\ from\ wing\ leading\ edge\ in\ terms\ of\ chord\ length$

$Cl_{h_{req}}$ = $Required\ Lift\ Coefficient\ of\ Horizontal\ Tail$

AR_h = **Horizontal Tail Aspect Ratio**

λ_h = **Taper Ratio of Horizontal Tail**

$\left(\frac{t}{c}\right)_{max,h}$ = **Horizontal Tail Airfoil Maximum Thickness to Chord Ratio**

Cl $l_{\alpha_{h,2D}}$ = **Lift coefficient Slope of Horizontal Tail Airfoil**

Cl $l_{\alpha_{h,3D}}$ = **Lift coefficient Slope of Horizontal Tail**

$\alpha_h =$ **Horizontal Tail Angle of Attack**

$b_h =$ **Horizontal Tail Span**

$\alpha_{t,h} =$ **Horizontal Tail Twist Angle**

$\alpha_{t,h} =$ **Horizontal Tail Incidence Angle**

$C_h =$ $Mean\ Aerodynamic\ Chord\ of\ Horizontal\ Tail$

$\mathrm{S_h} =$ $Mean\ Horizontal\ Tail\ Area$

$\eta_h =$ $Horizontal\ Tail\ Efficiency$

$C_{m\alpha} =$ $Longitudinal\ Stability\ Contribution\ by\ Horizontal\ Tail$

$V_v =$ $Vertical\ Tail\ Volume\ Coefficient$

$l_{v_{opt}} =$ $Optimum\ Moment\ -\ Arm\ of\ Vertical\ Tail$

$S_v =$ $Vertical\ Tail\ Area$

$\left(\frac{t}{c}\right)_{\mathrm{max},V} =$ $Vertial\ Tail\ Airfoil\ Maximum\ Thickness\ to\ Chord\ Ratio$

$\lambda_v =$ $Taper\ Ratio\ of\ Vertical\ Tail$

$AR =$ $Vertical\ Tail\ Aspect\ Ratio$

$\alpha_{t,v} =$ $Vertical\ Tail\ Twist\ Angle$

$\Gamma_v =$ $Dihedral\ Angle\ of\ Vertical\ Tail$

$b_v =$ $Vertical\ Tail\ Span$

$C_{tip,v} =$ $Vertical\ Tail\ Tip\ Chord$

$C_{root,v} =$ $Vertical\ Tail\ Root\ Chord$

$\mathrm{C}_v =$ $Mean\ Aerodynamic\ Chord\ of\ Vertical\ Tail$

$\mathrm{S}_v =$ $Mean\ Vertical\ Tail\ Area$

$FOS_p =$ $Propulsion\ Factor\ of\ Safety$

$V_{p,2D} =$ $Propeller\ Airofil\ Lift\ Coefficient$

$\eta_p =$ $Propeller\ Efficiency$

$AR =$ $Maximum\ Propeller\ Tip\ Speed$

$D_p =$ $Propeller\ Aspect\ Ratio$

$\omega_p =$ **Propeller** RPM

$S.F_t = Tail\ Safety\ Factor$

$\mathbf{C_{tip,E/h}}$ **= Elevator to Horizontal Tail Tip Chord Ratio**

$\mathbf{C_{tip,R/h}}$ **= Rudder to Vertical Tail Tip Chord Ratio**

$L_f =$ **Length of Fuselage**

$W_{MTOW_{est}} = Estimated\ Total\ Aircraft\ Weight$

$\frac{b_{a_i}}{b} = inboard\ position\ of\ aileron\ w.r.t\ wingspan$

$\frac{b_{a_o}}{b} = outboard\ position\ of\ aileron\ w.r.t\ wingspan$

$b_A = aileron\ span$

$C_A = aileron\ chord$

$S_A = aileron\ area$

$\frac{S_A}{S} = ratio\ of\ aileron\ area\ to\ wing\ area$

$\frac{b_A}{b} = ratio\ of\ aileron\ span\ to\ wingspan\ of\ aileron\ chord\ to\ wing\ chord$

$\tau_a = aileron\ effectiveness$

$C_{l_{\delta A}} = rolling\ moment\ coefficient\ derivative$

$\delta_A = max\ aileron\ deflection$

$C_l = rolling\ moment\ coefficient$

$L_A = aircraft\ rolling\ moment$

$P_{ss} = steady\ state\ roll\ rate$

$\phi_l = bank\ angle\ for\ steady\ state\ roll\ rate$

$\dot{P} = aircraft\ rate\ of\ roll\ rate$

$t_2 = roll\ time$

$b_E = elevator\ span$

$C_E = elevator\ chord$

$S_E = elevator\ area$

$\frac{b_E}{b_h} = ratio\ of\ elevator\ span\ to\ horizontal\ tail\ span$

$\frac{C_E}{C_h} = ratio\ of\ elevator\ chord\ to\ horizontal\ tail\ chord$

$\frac{S_E}{S_h} = ratio\ of\ elevator\ area\ to\ horizontail\ tail\ area$

$\tau_E = elevator\ effectiveness$

$\delta_E = max\ elevator\ deflection$

$\frac{\partial C_m}{\partial \delta_E}$
$= rate\ of\ change\ of\ pitching\ moment\ coefficient\ w.r.t\ elevator\ deflection$

$C_{L_{\delta E}} = elevator\ contribution\ to\ aircraft\ lift$

$\frac{\partial C_L}{\partial \delta_E} = rate\ of\ change\ of\ lift\ coefficient\ w.r.t\ elevator\ deflection$

$C_{L_{h\delta E}} = elevator\ contribution\ to\ horizontal\ tail\ lift$

$C_{L_l} = steady\ state\ lift\ coefficient\ at\ cruising\ speed$

C_{L_o} = lift coefficient at zero angle of attack

C_{m_o} = pitching moment coefficient at zero angle of attack

$\bar{q}$ = Dynamic Pressure

δ_R = Max Rudder deflection

V_{mc} = Minimum controllable speed

η_v = Vertical tail efficiency

$\frac{b_R}{b_V}$ = ratio of rudder span to vertical tail span

$C_{n_{\delta R}}$ = directional control derivative

C_R = Rudder angle of attack effectiveness of rudder chord to vertical tail chord

$\frac{S_R}{S_V}$ = ratio of rudder area to vertical tail area

C_{α_V} = vertical tail lift curve slope

S_{V_e} = effective vertical tail area

α_{spin} = **angle of attack during spin**

$\bar{V}_{V_e}$ = **effective vertical tail volume coefficient**

I_{xx_w} = **rolling inertia in wind axis**

I_{zz_w} = **product inertia in wind axis**

I_{xz_w} = **inertia in wind axis**

I_{xx_B} = **rolling inertia in body axis**

N_{SR} = **counteracting yawming moment**

I_{z_B} = **product inertia in body axis**

I_{xz_B} = **inertia in body axis**

$\dot{R}_{SR}$ = **rate of spin recovery**

$\gamma = attack\ angle$

Chapter 1: Introduction to UAVs

1.1 Introduction

Kinetic Attack Drones, often referred to as loitering munitions or suicide drones, are a kind of unmanned aerial vehicles (UAVs) that have drawn attention for their distinctive capabilities. Kamikaze drones are designed to be flown directly into a target and explode upon contact, unlike conventional drones that are employed for surveillance or reconnaissance. This makes them an effective weapon for both offensive and defensive missions. [1]

These drones exist in a variety of sizes, from small hand-launched devices to larger fixed-wing platforms and can be either remotely controlled or autonomous. Some models are made to loiter in the air for long periods of time while searching for potential targets before attacking.

Kamikaze drones are incredibly agile and maneuverable, making pinpointing and intercepting them hard. They can also carry a variety of payloads, such as smoke grenades or flash-bang weapons as well as high-explosive warheads, fragmentation grenades, and even non-lethal payloads. Kamikaze drones can be used for reconnaissance and surveillance in addition to their offensive capabilities. They can be loaded with cameras, sensors, and other payloads to acquire information on adversary targets.

The employment of kamikaze drones has increased recently as a result of numerous nations developing and utilizing these systems for military operations. In the 2020 fight over Nagorno-Karabakh between Azerbaijan and Armenia, kamikaze drones were prominently used. According to reports, Azerbaijan attacked Armenian military targets, including tanks and defense systems, using loitering munitions made by the Israeli

company Harop. These drones proved to be quite effective at eliminating their targets, and Azerbaijan's victory in the fight was greatly influenced by their employment.

Another example is the Houthi rebels' deployment of kamikaze drones in Yemen. These drones have been employed by the Houthis to attack military and industrial targets in Saudi Arabia. These attacks have significantly damaged infrastructure and sparked worries about the danger that kamikaze drones pose.

Several parties to the conflicts have also employed kamikaze drones in Libya and Syria. The Russian-made Krasnopol loitering munition has been deployed by the Syrian military to assault rebel strongholds in Syria. Wing Loong drones, which are built in China, have been deployed by the Government of National Accord (GNA) and the Libyan National Army (LNA) to attack each other's positions in Libya.

In general, kamikaze drone use has grown recently, and they have shown to be very powerful in combat scenarios. They are useful instruments on the battlefield because they may be employed as both a weapon and a scouting tool. Yet, their use has also sparked worries about their potential to harm vital infrastructure and result in human casualties. As such, the use of kamikaze drones remains a contentious issue in modern warfare.

1.2 History

The term "kamikaze" refers to the Japanese tactic of using human-piloted aircraft to collide with enemy ships during World War Two. [1]

In the 1980s, Israel created the Harpy, an unmanned aircraft intended to strike adversary air defense systems, giving rise to the idea of kamikaze or suicide drones. The Harpy was a loitering munition, which means it could hover over the battlefield for a long time

until a target was found. The Harpy would fly straight at a target once it was located and detonate upon contact.

The MQ-9 Reaper and the RQ-7 Shadow are two of the suicide drones that the US developed in the early 2000s. These drones were made to conduct ongoing observation and launch precise attacks against enemy fighters.

The Turkish military started employing kamikaze drones in their conflict with Kurdish terrorists in southeast Turkey in 2015. The Turkish drones, known as Bayraktar TB2, could remain in the air for up to 24 hours and were equipped with precision-guided weapons. Other nations took notice and started working on creating their own kamikaze drone capabilities as a result of the Bayraktar TB2's effectiveness in Turkey's conflict with the Kurds.

Since then, kamikaze drones have been deployed by both the Ukrainian and Russian militaries in a number of conflicts, including the ongoing conflict in Ukraine. 2020 saw Azerbaijan's battle with Armenia over the disputed Nagorno-Karabakh territory involve the use of kamikaze drones, including the Israeli-made Harop.

Many contemporary suicide drones have been designed in recent years. The most well-known of these is the AeroVironment Switchblade 300.

1.3 Modern UAVs

1.3.1 AeroVironment Switchblade 300

The AeroVironment Switchblade is a loitering munition that was initially designed by the company to support American forces in Afghanistan against hostile ambushes. The UAV is employed by various US military branches and is tiny enough to fit into a backpack. The loitering munition has the convenience of being canister-launched, negating the need for any kind of complicated launching device. The Switchblade

shoots out of the canister, flies towards the intended target, and then slams into it, detonating the warhead.

The loitering munition is only 2.5 kg and up to 2 feet long. The Switchblade uses a canister-based launching system. The Switchblade 300 has a powerful yet compact battery that allows it to cruise at up to 101.38 km/h. [2]

Figure 1 Switchblade 300 [3]

1.3.2 Hero 30

Another lightweight portable loitering munition is UVision Air Ltd.'s Hero 30. An important NATO member assessed the astonishing capabilities of this high-precision munition, which was produced by the Israeli UAV manufacturer UVision. Due to its cutting-edge technology and extensive 30-year field experience with a qualified management team, UVision is well-liked among UAV manufacturers and consistently produces extremely distinctive aerodynamic systems.

Design-wise Hero 30 features foldable both main wings and tail in a cruciform configuration with a wingspan of 0.8m. The UAV launches from its pneumatic canister, unfolds its wings, and reaches a top speed of 115 mph. The UAV is small and lightweight, weighing around 3 kg, and it can carry a warhead weighing 0.5 kg. The

light weight of loitering ammunition is due to the use of a battery rather than an engine to drive the propeller at the drone's back, which produces the necessary propulsion. Unfortunately, this limits the UAV's endurance to 30 minutes, making it only useful for short-distance use. [4]

Figure 2 UVision Hero 30 [4]

1.3.3 Alpagut Loitering Munition

Two Turkish businesses, Roketstan and STM, created the loitering munition known as the ALPAGUT. Unmanned aerial systems can be used to launch the loitering munition. According to the firms, the suicide drone was created for target destruction and reconnaissance. Loitering weapons are both transportable and launchable from a variety of platforms. The ALPAGUT Loitering Munition can be fired from the ground, as well as from helicopters, unmanned aerial vehicles, and sea-based carriers.

Design-wise the ALPAGUT loitering munition measures 2.3 meters in length, weighs 45 kg, and contains an 11 kg warhead. The loitering munition has a 2.5-meter wingspan and a 60-kilometer range. The loitering munition has a fixed-wing design with an inverted V-tail and a pusher-style propeller. With a battery life of more than 60 minutes, the UAV is powered by batteries. Once launched the loitering munition enters into

target detection, tracking, and evaluation mode, and then hovers over the target at an altitude ranging from 300-1500m for a specified period of time. [5]

Figure 3 Alpagut Loitering Munition [6]

1.3.4 Raytheon Coyote

The Raytheon Coyote is a small and compact UAV manufactured by the Raytheon Company. A small and portable UAV made by the Raytheon Company is called the Coyote. The unmanned aircraft is equipped to fly in self-contained swarms (coordinating with multiple UAVs to execute tasks that would be otherwise difficult for a single drone). The UAV may carry different payloads at once. It has humanitarian and scientific qualities in addition to military utility. The National Oceanic and Atmospheric Administration (NOAA) uses the UAV to track hurricanes.

Small and weighing only 5.9 kg, the UAV can carry 1.8 kg of payload (which can vary in accordance with mission requirements). Either a sonobuoy canister or a pneumatic tube can be used to launch the aerial vehicle. The UAV uses a pusher-style, battery-operated, two-blade propeller that is positioned at the back of the aircraft. The aerial vehicle is appropriate for short-distance missions because of its endurance, which falls within a one-hour window.The Raytheon Coyote is capable of reaching a maximum speed of 80mph and a cruising speed of 63mph. [7]

Figure 4 Raytheon Coyote [7]

1.4 Motivation

Pakistan's rugged terrain and diverse geography pose a significant challenge for its military operations. With several regions being virtually inaccessible, terrorist hideouts have thrived, making it increasingly difficult for the military to track and respond effectively. To combat this issue, there is an urgent need for a highly advanced and precise attack drone that can operate in any terrain and effectively neutralize hidden targets. Fortunately, attack drones offer a highly efficient and effective solution to this problem. With their ability to attack targets from any angle, they can render any terrain-based cover useless. Therefore, a drone must be designed with ease of manufacturing and cost-effectiveness in mind, making it an accessible tool for Pakistan's military.

In addition to the benefits gained by the military, the project would certainly be very beneficial to the students participating in it. Due to complexity of the project, it builds teamwork skills and leadership skills. Moreover, addressing real-life problems and striving to develop a viable solution, builds problem-solving skills and also expands the vision of real-world of students.

1.5 Objectives

The main objective of the project titled ‘Design of Unmanned Aerial Vehicle for Kinetic Attack Applications’ was the design and fabrication of a UAV that must satisfy a certain set of criteria defined below:

- The Maximum Takeoff Weight (MTOW) must not exceed 10 kg.
- The UAV must be able to hit a target precisely.
- The UAV should be highly maneuverable.
- The UAV must be controllable during all phases of flight.
- The UAV must be economical and simple in relation to manufacturing.

Chapter 2: Literature Review

2.1 Classification of UAVs

UAVs have many sizes as well shapes and they can be classified into several categories based on their design and capabilities. Some common types of UAVs include fixed-wing, rotary-wing, and hybrid aircraft.

2.1.1 Fixed-Wing UAV

Fixed-wing UAV has a fixed wing, similar to a traditional airplane. Fixed-wing UAVs generate lift through the shape of their wings as they move forward through the air.

Fixed-wing UAVs have a longer flight time compared to other types of drones, because they require less energy to stay in the air due to their aerodynamic design. They are also able to cover larger distances and higher altitudes than other types of drones, making them ideal for tasks that require large area coverage.

However, fixed-wing UAVs require more space to take off and land than other types of drones due to their larger size and the need for a runway-like space. They also tend to be less maneuverable than other types of drones, which can make them less suitable for tasks that require precision or flexibility.

Overall, fixed-wing UAVs are a versatile tool for a range of applications, and their advantages in flight endurance and coverage make them an important option for many organizations and industries. Examples of fixed-wing UAVs include the Hero 30, Predator and the Global Hawk. [8], [9], [10]

Figure 5: Fixed wing UAV with V tail [11]

2.1.2 Rotary-Wing UAV

A rotary-wing UAV is a type of drone that uses rotating blades to generate lift and stay airborne, similar to a helicopter. These drones have at least one rotor, often two or more, that rotate around a central axis to create lift and control the drone's movement. Rotary-wing.

The main advantages that rotary-wing UAVs have is their ability to vertically take off and land, without requiring a runway or other takeoff and landing infrastructure. This makes them more flexible in terms of deployment and allows them to operate in areas where fixed-wing UAVs may not be able to go. Rotary-wing UAVs can also hover in place, which is useful for tasks that require precise positioning or stable imaging. They are more maneuverable than fixed-wing UAVs, making them more suitable for tasks that require agility and flexibility.

However, rotary-wing UAVs generally have a shorter flight time and range than fixed-wing UAVs due to their design, which requires more energy to stay in the air. They are also generally more complex to operate and maintain and can be more expensive than fixed-wing UAVs.

Overall, rotary-wing UAVs are a useful for a range of applications, particularly those that require vertical takeoff and landing, precision positioning, and maneuverability. Their unique capabilities and flexibility make them an important option for many industries and organizations. Examples of rotary-wing UAVs include the DJI Phantom and the RQ-11 Raven. [8], [9], [12]

Figure 6: Multi Rotor UAV [13]

2.1.3 Hybrid UAV

A hybrid UAV (Unmanned Aerial Vehicle) is a type of has features of both fixed-wing and rotary-wing UAVS. This type of drone typically has both a fixed wing for forward flight and a set of rotors for vertical takeoff and landing (VTOL). Hybrid UAVs are designed for a variety of tasks, such as aerial surveying, inspection, mapping, and transportation. They can be programmed to fly autonomously or controlled remotely by an operator on the ground using a radio controller or other communication devices.

The main advantage is that they can take off and land vertically, which makes them more flexible and adaptable than fixed-wing UAVs. They can also fly for more

distances and at greater speeds than rotary-wing UAVs, making them more efficient and effective for large area coverage. Hybrid UAVs can also hover in place, which is useful for tasks that require precise positioning or stable imaging. They are more maneuverable than fixed-wing UAVs, making them more suitable for tasks that require agility and flexibility.

However, hybrid UAVs tend to be more complex to operate and maintain.. They are also generally more expensive than either type of drone.

Overall, hybrid UAVs are a versatile and valuable tool for a range of applications, particularly those that require both VTOL capabilities and fixed-wing performance. Their unique capabilities and flexibility make them an important option for many industries and organizations. Examples of hybrid aircraft include the Bell V-280 Valor and the Quantix Recon. [8], [9], [14]

Figure 7: Hybrid UAV [15]

2.2 Categories of Fixed Wing UAVs

Each category of UAVs has its own set of advantages and limitations and are suitable for different types of missions and applications.

Table 1: Configuration Chart

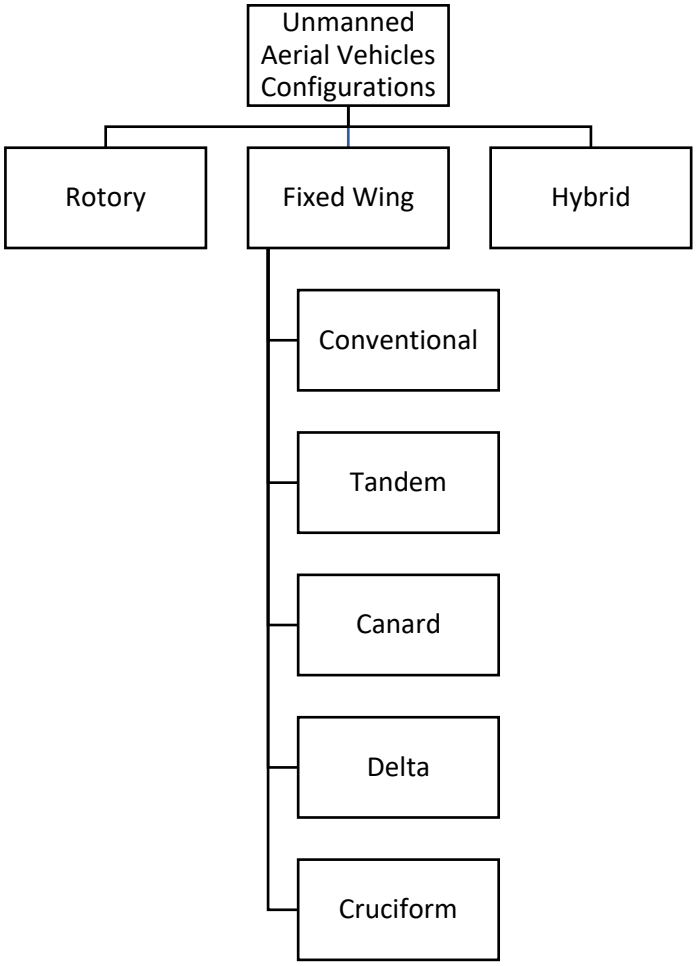

2.2.1 Conventional Configuration

A conventional configuration UAV follows the same basic design principles as a conventional manned aircraft. This type of UAV has a single wing in the middle of the fuselage, a tail section at the back of the aircraft, and a cockpit or payload section at the front of the aircraft.

One of the main advantages of conventional configuration UAVs is their stability and control. The wing provides lift and stability, while the tail section provides pitch and yaw control. This allows for more precise maneuvering and control, particularly in windy or turbulent conditions. Conventional configuration UAVs also typically have a longer endurance and range compared to other types of drones, due to their efficient

aerodynamic design. This makes them more effective for long-duration missions that require large area coverage.

However, conventional configuration UAVs typically require a runway or other take-off and landing infrastructure, which can limit their flexibility and deployment in some environments. They are also less maneuverable than other types of drones, which can make them less suitable for tasks that require agility and flexibility. [16]

2.2.2 Canard Configuration

A canard configuration UAV has a small wing which located ahead of the main wing. The canard provides lift and stability, while the main wing provides additional lift and controls the pitch of the aircraft.

One of the main advantages of canard configuration UAVs is their maneuverability and agility. The placement of the canard allows for greater control over the pitch and roll of the aircraft, making it more responsive to changes in flight conditions. This configuration is less common in UAVs but is known for its high-performance characteristics and its ability to perform at high speeds and high altitudes. Canard configuration UAVs are also typically more compact and lightweight than other types of drones, making them more suitable for operations in tight spaces or difficult terrain.

However, canard configuration UAVs can be more difficult to fly and require more skill to control, particularly in windy or turbulent conditions. They also typically have a shorter endurance and range compared to other types of drones, due to their less efficient aerodynamic design. [16]

2.2.3 Tandem Wing Configuration

A tandem configuration UAV has two or more wings arranged in a tandem, or fore-and-aft, configuration. In this design, the wings are positioned one behind the other, with the front wing typically smaller than the rear wing.

One of the main advantages of tandem configuration UAVs is their high degree of stability and control. The front wing provides lift, while the rear wing provides stability and control. This design allows for greater maneuverability and control. Tandem configuration UAVs also typically have a longer endurance and range, due to their efficient aerodynamic design. This makes them more effective for long-duration missions that require large area coverage.

However, tandem configuration UAVs tend to be more complex and expensive to manufacture and maintain than other types of drones. They also require more space to operate, as their longer wingspan can make them more difficult to store and transport. [16]

2.2.4 Delta Wing Configuration

A delta configuration UAV has a single, triangular wing that is mounted at the top of the aircraft's fuselage. This delta type wing provides both lift and control, and is designed to maximize stability and efficiency.

One of the main advantages of delta configuration UAVs is their high degree of stability and efficiency. The delta wing is designed to create a vortex of air that helps to stabilize the aircraft, while also reducing drag and increasing lift. Delta configuration UAVs are also typically very agile and responsive, allowing them to perform complex maneuvers and operate in tight spaces with different kinds of payloads. This configuration is known for its high-speed and low-altitude characteristics. However, delta configuration

UAVs tend to be less maneuverable, due to their triangular shape and limited control surfaces. They also tend to have a shorter endurance and range compared to other types of drones, which can limit their usefulness for long-duration missions. [16]

2.2.5 Cruciform Wing Configuration

A cruciform configuration UAV has four wings arranged in a cross or "plus" shape. The main wing in the center of the aircraft, while the remaining three wings are mounted at the front, back, and sides of the central wing. This configuration gives the drone a cross-shaped appearance, which is where the name "cruciform" comes from.

One of the main advantages of cruciform configuration UAVs is their stability and control. The multiple wings provide a high degree of stability and maneuverability, while the placement of the wings allows for precise control over the aircraft's pitch, roll, and yaw. Cruciform configuration UAVs are also typically very versatile and can be adapted to a wide range of applications.

However, cruciform configuration UAVs tend to be more complex and difficult to manufacture and maintain compared to other types of drones. They also require more space to operate, as their larger wingspan can make them more difficult to store and transport. [16]

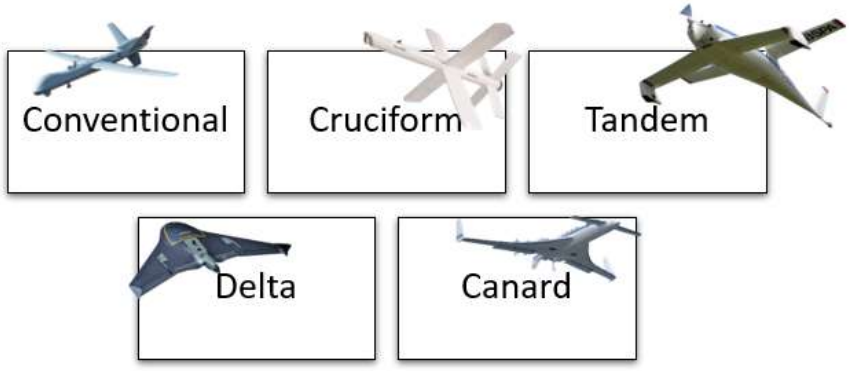

Figure 8: Different wing configurations of fixed wing UAVs

2.3 Classification based on Wing Location

2.3.1 Low-Wing UAVs

The wing is mounted on the bottom side . Low-wing UAVs have a higher wing loading which allows them to fly faster and have a higher roll rate. Low-wing UAVs also have a better performance in terms of speed and maneuverability, they are able to reach higher speeds and perform more complex maneuvers. Turbulence and ground can make them less stable during takeoff and landing. They also have a higher stall speed which means they require more power to maintain altitude and are less forgiving during takeoff and landing. The wing placement also makes them more sensitive to crosswinds and can be harder to control during gusty conditions. [8], [9], [17], [18]

2.3.2 Mid-Wing UAVs

The wing of a mid-wing UAV is mounted in the middle of the fuselage. Mid-wing UAVs provide stability and balance for the UAV. They are typically less susceptible to turbulence and ground effect than low-wing UAVs, making them more stable during take-off and landing. This wing placement also allows for better payload capacity, this is because the wing is located near the center of gravity making it easier to carry a heavier payload. Mid-wing UAVs may not be as fast or maneuverable as low-wing UAVs. They may also be more affected by wind, as the wing is not as high as high-wing UAVs. The wing placement also makes them more susceptible to wind gusts and can make them harder to control during turbulent conditions. [8], [9], [17], [18]

2.3.3 High-Wing UAVs

The wing of a high-wing UAV is mounted on the top of the fuselage. They are typically more stable than low-wing or mid-wing UAVs, as they are less susceptible to turbulence and ground effect. The wing placement also makes them less susceptible to

wind gusts and crosswinds. High-wing UAVs may not be as fast or maneuverable as other types of UAVs. They also have a higher stall speed and require more power to maintain altitude. [8], [9], [17], [18]

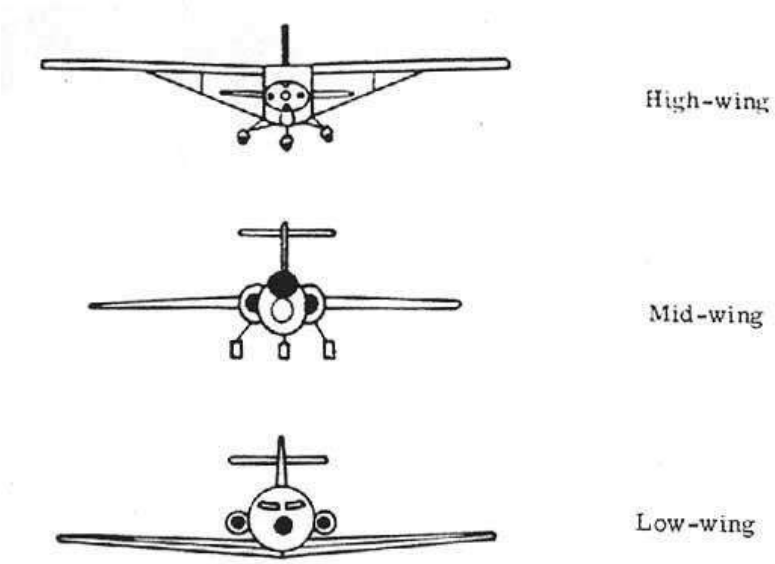

Figure 9: Different wing locations [19]

2.4 Aspect Ratio

Aspect ratio is the ratio of an aircraft's wingspan to its mean chord (average width) of the wing. In the context of aircraft design, aspect ratio is an important parameter that can affect the performance and handling characteristics of the aircraft.

2.4.1 High Aspect Ratio Wings

These wings are typically long and narrow, which allows them to generate lift at lower speeds. This makes them well-suited for long-endurance missions such as surveillance and reconnaissance, due to their ability to for longer periods of time in air using less power. They also have a lower induced drag, which means they use less energy to maintain a steady flight. This also gives them a more glider-like behavior and therefore they are able to fly at a higher altitude, with a more stable platform for sensors and cameras.

High aspect ratio wings are not as maneuverable as compared to low aspect ratio wings, as they have a low roll rate and responsiveness. This means that they are less agile and may have a slower reaction time to control inputs. They also have a lower maximum airspeed, as the long wings can create drag at high speeds. This can limit the UAV's ability to perform some specific tasks such as target tracking or close-range reconnaissance. [8], [9], [18], [20]

2.4.2 Low Aspect Ratio Wings

These wings are typically short and wide, which allows them to generate lift at higher speeds. This makes them well-suited for high-speed missions such as reconnaissance and target tracking, as they can reach higher speeds than high aspect ratio wings. They also have a higher roll rate and responsiveness, making them more maneuverable. This makes them more agile and have a faster reaction time to control inputs.

Low aspect ratio wings are not as efficient in terms of endurance, as they use more energy to maintain a steady flight due to their higher induced drag. They also have a lower maximum endurance, as they consume more energy at low speeds. This can limit the UAV's ability. [8], [9], [18], [20]

2.4.3 Mid-Aspect Ratio Wings

These wings are a balance between low and high aspect ratio wings. They tend to have a good balance between maneuverability, speed, and endurance. They also have a good balance between drag and lift, which allows them to maintain a steady flight at different speeds. This means that they have a good compromise of performance in terms of speed, endurance, and stability. They also have a better ability to handle wind and turbulence as compared to high aspect ratio wings.

These wing are a compromise between the low and high aspect ratio wing. They may not be as fast as low aspect ratio wings or as efficient in terms of endurance as high aspect ratio wings. They also require more power than low aspect ratio wings to maintain a steady flight and are more affected by wind and turbulence than low aspect ratio wings. [8], [9], [18], [20]

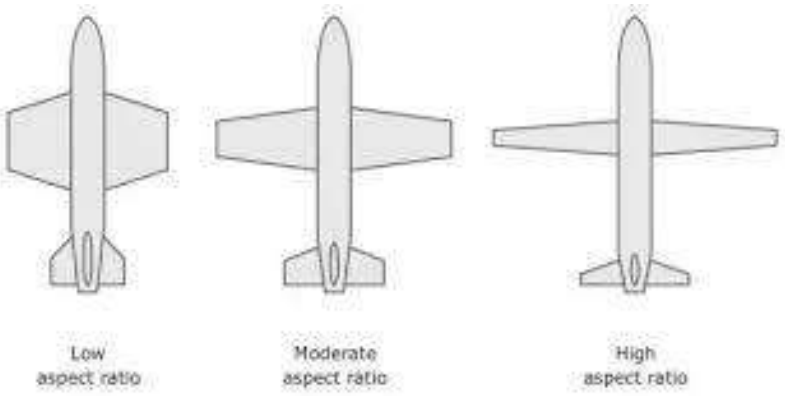

Figure 10 Different aspect ratio wings [20]

2.5 Tail Configurations

The tail is the section of the aircraft located at the rear, behind the main body or fuselage. It consists of one or more components, including a horizontal stabilizer, a vertical stabilizer, and control surfaces such as elevators, rudders, and ailerons. Tail assembly provides stability and control to the aircraft.

The size, shape, and location of the tail components can vary depending on the specific design and intended use of the aircraft. The tail design can also affect the overall performance and handling characteristics of the aircraft, including stability, maneuverability, and stall speed. [8], [9], [16], [21]

2.5.1 Conventional Tail

The conventional tail similar to the tail found on a traditional airplane and most commonly used in UAVs. It provides good stability and control at different speeds and is easy to manufacture and maintain.

The conventional tail increases the overall size and weight of the UAV, which can be an issue for smaller or more compact UAVs. Additionally, it can also create more drag, which can affect the UAV's performance and flight time. [8], [9], [16], [21]

2.5.2 V-Tail

The V-tail is a compact design that requires less space than a conventional tail. It is often used on smaller UAVs and can also reduce drag, which can improve the UAV's performance and flight time.

The V-tail can provide less stability and control than a conventional tail, which can make it less suitable for certain missions or flight conditions. Additionally, it may also be more difficult to manufacture and maintain. [8], [9], [16], [21]

2.5.3 T-Tail

The T-tail design allows for better control at high speeds and is often used on larger UAVs. Additionally, the T-tail design can reduce drag and improve the UAV's performance and flight time.

The T-tail can be more complex to manufacture and maintain than a conventional tail. Additionally, the T-tail design can make the UAV more susceptible to a stall, which can affect its stability and control. [8], [9], [16], [21]

2.5.4 Cruciform Tail

The cruciform tail provides additional stability and control, making it suitable for UAVs that are designed for specific missions such as surveillance or reconnaissance. It also provides redundancy in case of failure in any one of the control surfaces.

The cruciform tail is more complex to manufacture and maintain than a conventional tail. Additionally, it can increase the overall size and weight of the UAV, which can be an issue for smaller or more compact UAVs. [8], [9], [16], [21]

2.5.5 Canard Tail

Canard tail design provides additional lift and stability and is often used on UAVs that are designed for specific missions such as reconnaissance and surveillance. It also provides redundancy in case of failure in any one of the control surfaces.

Canard tail design is complex to manufacture and it increases the overall size and weight of the UAV, which can be an issue for smaller or more compact UAVs. [8], [9], [16], [21]

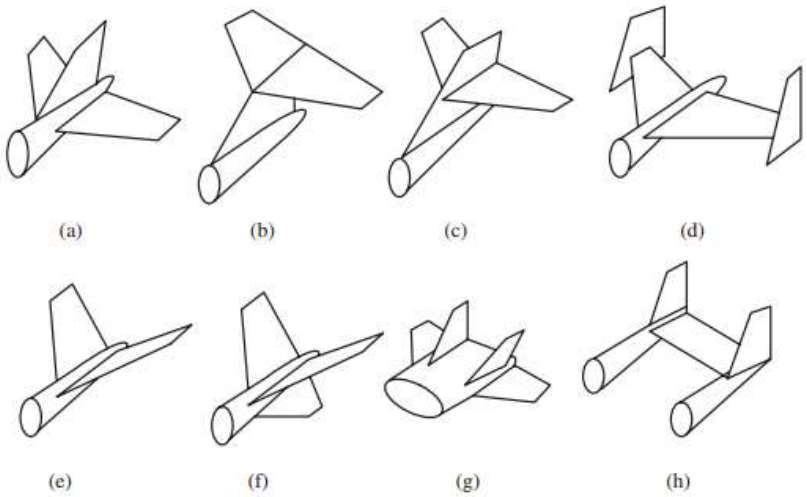

Figure 11: Different aircraft tails [8]

2.6 Propulsion System

In UAVs, propulsion system refers to the components and mechanisms that generate the thrust needed to propel the aircraft through the air. Common propulsion systems used in UAVs use electric motors power using batteries, and IC engines. Propellers or rotors are typically used to convert the energy from the propulsion system into thrust. [8], [9], [22]

2.6.1 Electric Motor Propulsion Systems

In electric motor propulsion system thrust is generated using battery powered electric motor. They are lightweight, efficient, and produce low noise levels. Electric motors are available in various sizes and power ratings, from small brushless DC motors to large induction motors. The components used in electric motor propulsion system include:

2.6.1.1 Electric Motor

The core components of electric propulsion system is electric motor. These motors can be: DC (Direct Current), AC (Alternating Current) and BLDC (Brushless DC). DC motors are usually cheaper, but have lower efficiency, less power density and shorter lifespan than AC and BLDC motors. AC motors are more efficient, but they are less common in UAVs because they require a complex power conversion system. BLDC motors have high efficiency, power density, and lifespan, which makes them the most popular choice for UAVs. [8]

2.6.1.2 Electronic Speed Controller

Electronic speed controller is used to control and regulate the speed of the electric motor. It receives a control signal from the flight controller and adjusts the power supplied to the motor. Speed controllers can be classified into two types: brushed and

brushless. Brushed controllers are less efficient and less reliable than brushless controllers. Brushless controllers are more efficient and more reliable, which makes them the most popular choice for UAVs. [23]

2.6.1.3 Propeller

The propeller or rotor converts the mechanical energy from the engine into thrust. Propellers are more common in fixed-wing UAVs because they provide more thrust and efficiency than rotors. Rotors are more common in rotorcraft UAVs because they provide more lift and maneuverability than propellers. [24]

2.6.1.4 Power Source

The power source provides the electrical energy needed to power the motor. The most commonly used power sources include batteries and fuel cells. Batteries are usually cheaper and have higher energy density than fuel cells, but they have a shorter lifespan and need to be replaced or recharged frequently. Fuel cells are more expensive and have lower energy density than batteries, but they have a longer lifespan and can be refilled or refueled.

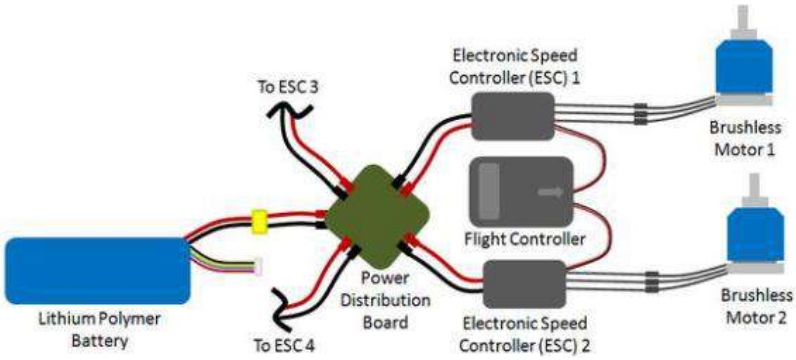

Figure 12 Electric propulsion system in a UAV [22]

2.6.1.5 Advantages

High efficiency: Electric motors are highly efficient, up to 90%. This means less energy is wasted as heat and more energy is used to generate thrust.

Low noise levels: Electric motors produce very little noise, making them ideal for stealth operations or applications where noise levels need to be kept to a minimum. This makes them suitable for reconnaissance, surveillance and monitoring missions.

Low emissions: Electric motors produce no emissions, making them environmentally friendly. This makes them suitable for indoor and outdoor applications. [22], [25]

2.6.1.6 Disadvantages

Limited flight duration: Electric motors are limited by the energy stored in the batteries or fuel cells, which typically provides a flight duration of 20 to 30 minutes for most UAVs. This means that they need to be recharged or replaced frequently.

Limited payload capacity: Electric motors are relatively lightweight, which limits the payload capacity of the UAV. This means that they can't carry heavy payloads such as sensors, cameras, or weapons.

Limited operational range: Due to limited energy storage, this system typically provides a flight range of a few miles. This means that they have limited range of operation. [22], [25]

2.6.2 Internal Combustion Engine Propulsion Systems

Internal combustion engine propulsion systems use small internal combustion engines (ICE) powered by gasoline, diesel, or jet fuel to generate thrust. They are more powerful and provide longer flight durations than electric motor propulsion systems. The main components of an internal combustion engine propulsion system include:

2.6.2.1 Engine

The core components of the propulsion system is IC engine. It converts the chemical energy stored in the fuel into mechanical energy. Internal combustion engines can be: reciprocating and rotary.

The Reciprocating engines have a linear movement of the pistons, while rotary engines have a rotary movement of the rotor. Reciprocating engines are more common in UAVs because they are more efficient and reliable than rotary engines. [26]

2.6.2.2 Fuel Tank

The purpose of fuel tank is to store fuel to power the engine. Fuel tanks can be made of various materials, such as aluminum, steel, or composite materials. They need to be designed to withstand the pressure, temperature and vibration of the UAV. [27]

2.6.2.3 Propeller

The propeller or rotor converts the mechanical energy from the engine into thrust. Propellers are more common in fixed-wing UAVs because they provide more thrust and efficiency than rotors. Rotors are more common in rotorcraft UAVs because they provide more lift and maneuverability than propellers. [24]

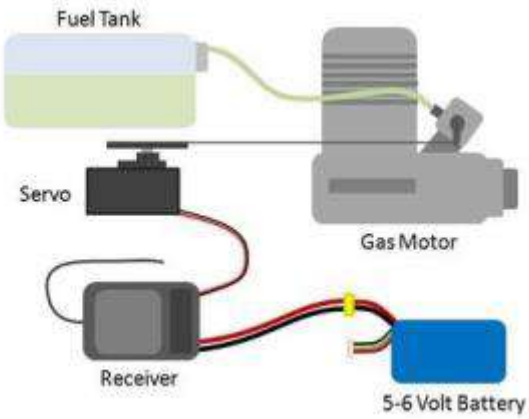

Figure 13: Fuel propulsion system in a UAV [22]

2.6.2.4 Advantages

Longer flight duration: Internal combustion engines can provide flight durations of several hours, depending on the size of the fuel tank. This means that their air stay time is longer than electric motor propulsion systems.

Greater payload capacity: Internal combustion engines are more powerful than electric motors, which allows for larger payloads to be carried by the UAV. This means that they can carry heavy payloads such as sensors, cameras, or weapons.

Greater operational range: Internal combustion engines can provide ranges of several hundred miles, depending on the size of the fuel tank. This means that they can cover a larger area of operation than electric motor propulsion systems. [22]

2.6.2.5 Disadvantages

Lower efficiency: Internal combustion engines are less efficient than electric motors, converting only 20% to 30% of the energy stored in the fuel into propulsion power. This means that more energy is wasted as heat and less energy is used to generate thrust.

High noise levels: Internal combustion engines produce significant noise levels, making them less suitable for stealth operations or applications where noise levels need to be kept to a minimum.

High emissions: Internal combustion engines produce emissions that are harmful to the environment. This means that they are not suitable for indoor or sensitive outdoor applications.

In conclusion, both electric motor and internal combustion engine propulsion systems have their own advantages and disadvantages. The choice of propulsion system depends on the specific mission requirements, including flight duration, payload capacity, operational range, noise levels and emissions. Electric motor propulsion systems are more efficient, quieter and greener but with limited flight duration and range, while internal combustion engine propulsion systems are more powerful, have longer flight duration and range but less efficient, noisier and polluting. [22]

2.7 Control System

Control system refers to the set of hardware and software components that allow the UAV to fly autonomously or to be operated remotely. The control system typically includes sensors (such as GPS, accelerometers, and gyroscopes) for navigation and stabilization, actuators (such as motors and servos) for controlling the movement of the UAV, and a flight controller that uses input from the sensors and operator commands to control the actuators. Some UAVs also have additional systems, such as cameras or payloads, that are controlled by the main control system. The control system is a key component of a UAV, as it allows the vehicle to fly and perform its intended mission. [8], [9], [28]

2.7.1 Fixed Wing Drone Control System

Fixed wing movement control are usually controlled by the movement of their control surfaces. Control surfaces are defined as the surfaces which are moveable and are usually on the plane's tail and wings, which create a difference of air pressure to produce positive and negative lift to maneuver the plane. These control surfaces include:

Ailerons: To control the aircraft roll, ailerons are used which are located on the trailing edge of the wings.

Elevators: To control the aircraft pitch, elevators are used which are located on the horizontal tail.

Rudder: To control the aircraft yaw, rudders are used which are located on the vertical tail.

Flaps: to increase the lift during landing and take, flaps are used which located at the upper side the wings,

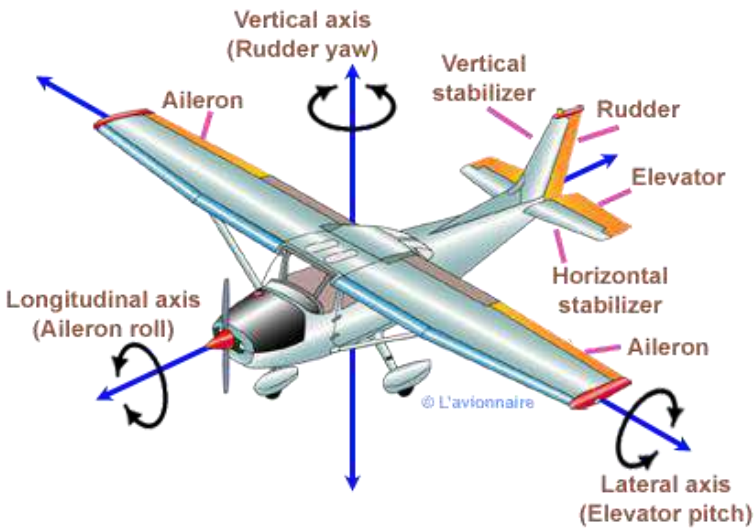

Figure 14: Aircraft flight controls system rotation axes among other movements. [28]

2.7.2 Rotary Wing Control System

Rotary wing drones such as quadcopters do not have any specific surface to control the motion of drone. Instead of depending of moving surfaces for maneuverability, quadcopters rely on speed of thrust motor. Hence by varying the speed of motors, quadcopters can do motion about all three axis with great precision. In the figure, motion schematic of quadcopter is shown. It is clear from diagram how just by using varying combination of motor speeds, quadcopter motion about all axis can be controlled. [8], [9]

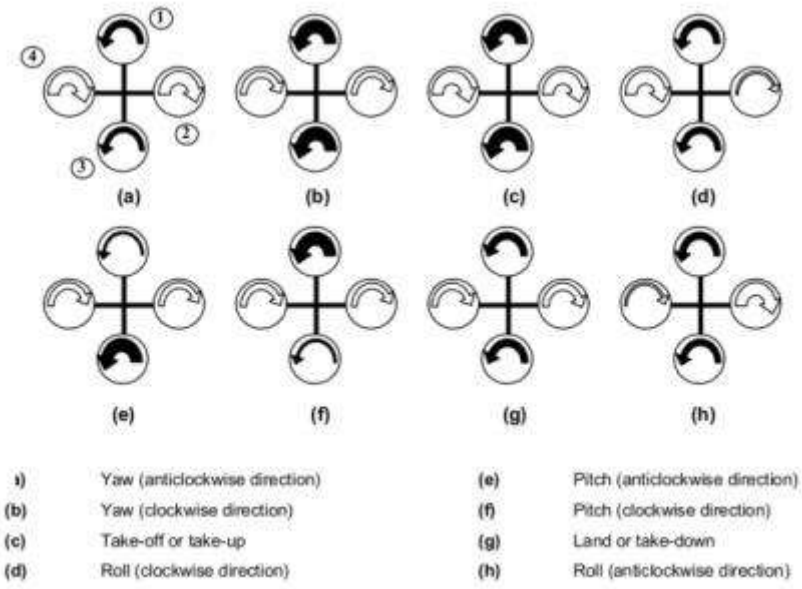

Figure 15: Quad copter movement description [29]

Each control surface is connected to an actuator, controlled by the control system. Inputs coming from sensors like GPS, accelerometers, and gyroscopes are used by control system to determine the aircraft's position and orientation by sending output commands to actuators. The pilot or the autonomous system can adjust the position of the control surfaces to change the aircraft's direction and altitude.

2.8 Sensors

GPS (Global Positioning System) sensor: used to determine the aircraft's location and ground speed. [30]

Accelerometer: aircraft acceleration and tilt are measured using accelerometer. [30]

Gyroscopes: aircraft's angular velocity and orientation are measured using gyroscope. [30]

Barometer: used to measure the aircraft's altitude above sea level. [30]

Pitot tube: aircraft's airspeed and altitude are measured using pitot tube. [30]

Electronic Speed Controller (ESC): Electronic speed controller is used to control and regulate the speed of the electric motor. It receives a control signal from the flight controller and adjusts the power supplied to the motor. [30]

Flight Controller: micro-controller responsible for controlling the flight of the drone by processing data from various sensors and adjusting the motors' speed and direction to maintain aircraft’s stability and control. [30]

Motors and servos: used to control the movement of the control surfaces and change the aircraft's direction and altitude. [30]

Cameras: used to capture images or video of the aircraft's environment. [30]

LIDAR: Light Detection and Ranging used for navigation and obstacle detection. [30]

RADAR: Radio Detection and Ranging used for navigation and obstacle detection. [30]

LEDs: used for signaling and communication. [30]

All these sensors are connected to the flight controller, which after processing sensor data give commands to the actuators to control the aircraft's movement. The flight controller also monitors the aircraft's status and can take corrective action if necessary, such as returning to a safe altitude if the aircraft encounters an obstacle or malfunctions.

2.9 Common Terminologies

Lift: The upward force that an airfoil generates when it moves through a fluid. [31]

Drag: The force opposing the motion of a body when it moves through a fluid. [31]

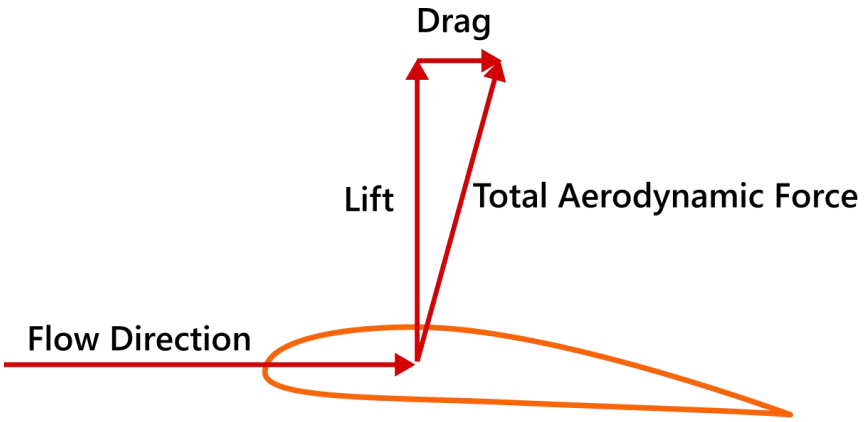

Figure 16: Aerodynamic forces [32]

Induced drag: This drag is due to the production of lift by the airfoils. Vortices are produced when airfoil generates lift which creates this drag. [31]

Parasitic Drag: This drag caused by the friction and resistance that the object encounters as it moves through the fluid. [31]

Thrust: The force required to overcome drag and propel aircraft forward. [31]

Weight: The force exerted on an aircraft by gravity. [31]

Stall: The condition in which an airfoil stops producing lift when the angle of attack is too high. [31]

Lift Coefficient (CL): The ratio of the lift to the dynamic pressure of the air. [31]

Drag Coefficient (CD): The ratio of the drag force to the dynamic pressure of the air. [31]

Moment Coefficient (CM): The ratio of the pitching moment the dynamic pressure of the air. [31]

Lift-to-Drag Ratio (L/D): The ratio of the lift force to the drag force The lift-to-drag ratio is an important measure of the UAV's efficiency, as higher values indicate that the aircraft can fly farther or for longer on a given amount of fuel or battery power. [31]

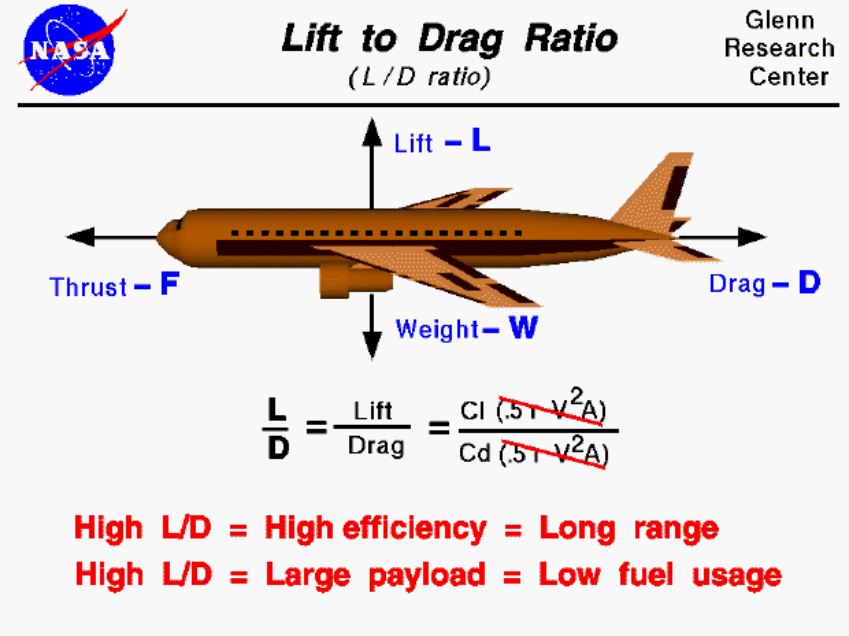

Figure 17: Lift to drag ratio [33]

Side Force Coefficient (CY): The ratio of the side force to the dynamic pressure of the air. [31]

Rolling Moment Coefficient (Cl): The ratio of the rolling moment to the dynamic pressure of the air. [31]

Yawing Moment Coefficient (Cn): The ratio of the yawing moment to the dynamic pressure of the air. [31]

Span: Distance from one wingtip to another wingtip of main wing. [31]

Chord: The perpendicular distance from the leading edge to the trailing edge of the wing. [31]

Leading edge: Wing's forward edge . [31]

Trailing edge: Wing's rear edge. [31]

Angle of Attack: The angle between the chord line of an airfoil and the relative wind, which is the direction of the airflow around the airfoil. [31]

Camber: The curvature of the wing surface. A cambered wing is curved, while a flat wing has no curvature. [31]

Aspect ratio: Aspect ratio is the ratio of an aircraft's wingspan to its mean chord (average width) of the wing. [31]

Wing loading: Ratio of aircraft weight to the wing area. Higher wing loading means more weight per unit area, which can impact the aircraft's performance and stability. [8]

Sweep: The angle of the wing relative to the fuselage. [8]

Taper Ratio: Ratio root chord to the tip chord. It describes the change in the shape of a wing from its root to its tip. [8]

Dihedral angle: The angle between the wing and the horizontal plane. [8]

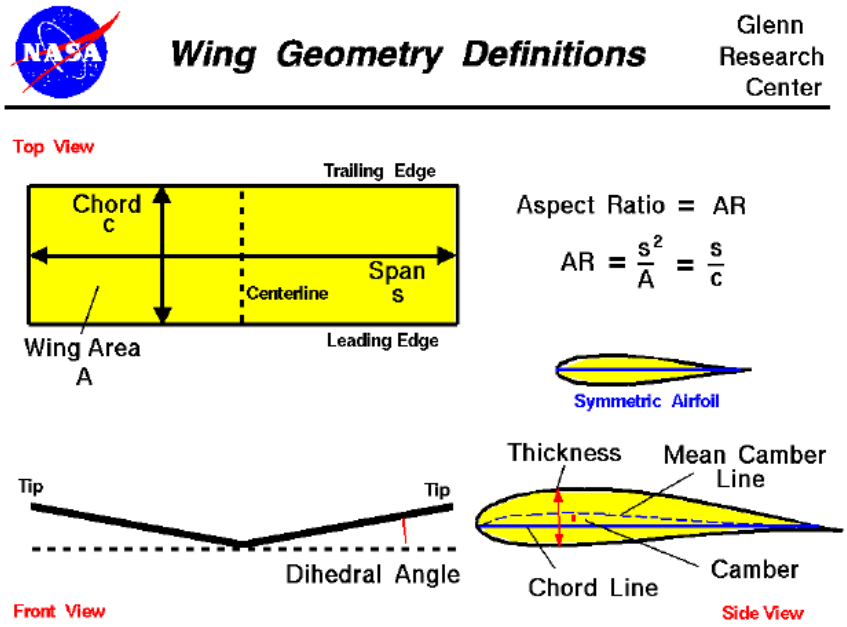

Figure 18: Wing geometry definitions [34]

Wing incidence: The angle of the wing relative to the horizontal plane. Positive wing incidence angles result in a nose-up attitude, while negative angles result in a nose-down attitude. [8]

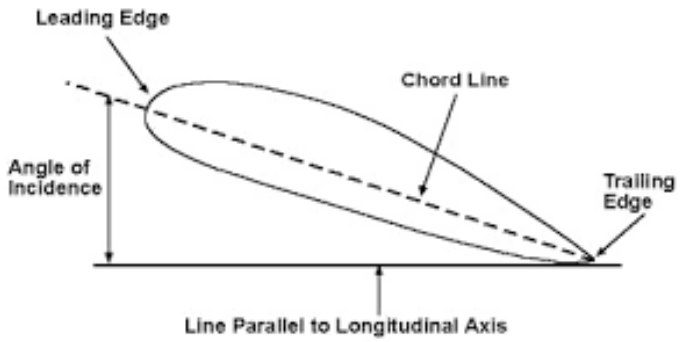

Figure 19: Angle of incidence [35]

Center of Pressure: The point where the total aerodynamic force on an airfoil can be considered to act. This point can move along the airfoil as angle of attack changes and is a key parameter for determining the control effectiveness of an aircraft. [31]

Neutral Point: The point where the pitching moment coefficient is zero. [31]

Power Loading: Power loading is a ratio that is used to express how much weight an aircraft can carry for each unit of engine power it generates. It is calculated by dividing the weight of the aircraft by the power output of its engine. [8]

Static Stability: The ability of an aircraft to return to its original state after being disturbed. There are three types of static stability: positive, neutral, and negative. [36]

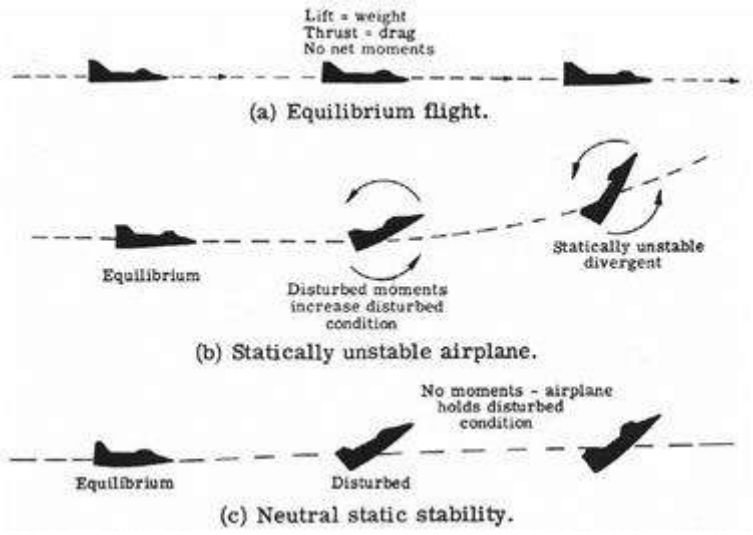

Figure 20: Static stability description [36]

Dynamic Stability: Aircraft's ability to remain stable in response to ongoing disturbances, such as turbulence or pilot inputs. [36]

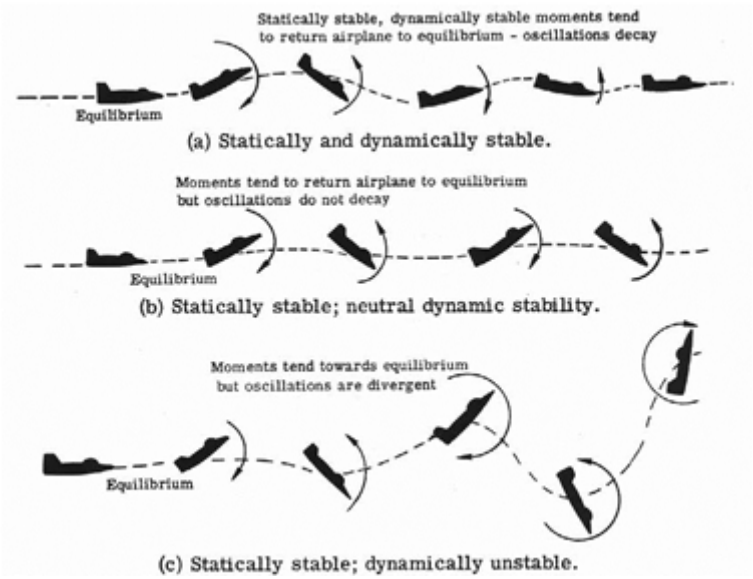

Figure 21: Dynamic stability description [36]

Chapter 3: Design Methodology

In this design phase, a structured approach was developed to design a drone that fulfils our mission requirements. Design methodology involves the identification of design requirements, selection of drone configuration, and propulsion system.

3.1 Design Requirements

Objective of this project is to design an autonomous aerial vehicle for kinetic attack applications. Firstly, UAV requirements are defined based on the objective for which unmanned aerial vehicle must be designed. The basic UAV requirement defined are the capability of a UAV to be able to be launched without much infrastructure requirement, easy to transport, ability to track the target, lock on to the target and detonate on target with impact. Secondly, since these drones are for one time use only, hence cost effectiveness is also a major design requirement.

3.2 Drone Configuration Selection

In this design phase, based on the literature review and keeping in view our design requirements, a configuration is selected which best suits to our case. For configuration selection, different designed UAVs effect of each configuration on UAV performance is studied. To select a configuration which best suits to our case, a decision matrix is made based on following factors. In decision matrix, weighted average is assigned to each factor according to its importance and at last a configuration is selected which showed highest weighed average.

- Maneuverability
- Manufacturing Cost
- Ease of Manufacturing

- Terminal Speed
- Weight

3.2.1 Propulsion System Selection

To decide between electric and motor propulsion system, decision matrix methodology is used. Keeping in view design requirements and data collected from literature, factors were selected, and weighted average is assigned to each factor. List of the selected factors is given below:

- Noise
- Thrust controllability
- Reliability
- Simple in Design
- Cost effectiveness
- Availability
- Moving components

Results of decision matrix table shows electric propulsion system is better to use in our case.

3.2.2 Parameter Selection

Predictive analysis is used to select performance and design parameters. Literature review is done of previously design UAVs for attack applications and their design and performance parameters were studied. Based on visual inspection of the data of more than 80 UAVs, Top Speed, Span, MTOW, Range, Payload weight, Endurance and other design parameters of the under-development UAV is decided. Detail of all these selected parameters is given in following chapters.

3.2.3 Design Calculations

For design calculations, engineering approach as described by Sadarey and Raymer is used instead of empirical approach. Advantage of using engineering approach is that we know exactly what performance constrains of designed UAV are. Another advantage is that we can easily improve UAV in single area such as control by simply assigning a larger safety factor during calculations of control surfaces.

Design calculation phase is subdivided into three phases:

- Conceptual Design
- Preliminary Design
- Detail Design

In conceptual design phase, configuration selection, propulsion system and parameter selection is done. In preliminary design phase, payload carrying capacity, endurance and thrust to weight ratio of UAV is fixed and later based these parameters battery and motor is selected. This knowledge is then used to calculate MTOW of the drone assuming structure weight as 36% of the total weight. After establishing basics, top speed and stall speed (these parameters were using predictive analysis as described in previous section) are used to draw matching plot between wing loading and power requirements and optimum design point is selected. This design point latter helped in calculation of wingspan and hence the main wing.

In conceptual design phase, aircraft wing, tail and control surfaces are designed. For airfoil selection of main wing, NACA, Eppler, Clark-YM and MH airfoils database is accessed, and best suitable airfoil is selected based on design requirements. Moreover, cruising angle of main wing is adjusted to the angle of attack where airfoil drag is minimum.

Static equations are then used to find static margin of plane assuming plane is in longitudinal trim position and no lift is required from tail for plane to fly stably while also ensuring pitching moment coefficient derivative is negative. Then tail arm and tail sizing is done such that drag is minimum. At last, control surfaces are designed considering maneuverability and control requirements of UAV. Tail setting angle is calculated based on downwash of the main wing. In theoretical calculations, lift line theory is used to calculated lift and moment coefficient of 3D wing and tail.

MATLAB is used to perform all calculations all the calculation because once all the formulae are encoded in it, it proves very helpful to iterate over theoretical calculations hence making the design optimization process faster. Another software used for designing is XFLR5. XFLR5 has capability to simulate wing and tail combination hence, it proved helpful to us to validate our design and inspect whether designed UAV configuration do have the expected capability of steady state flight and maneuverability.

After the end of each design phase, a design review is done to ensure that design fulfills the defined quantitative and qualitative requirements. Performing review after each design phase not only increased our understanding about UAVs but also increased reliability of the project.

Four main design reviews are conducted during the project:

- Conceptual Design Review (CDR)
- Preliminary Design Review (PDR)
- Evaluation and Test Review (ETR)
- Final Design Review (FDR)

Overall flow of the project design phase is shown below:

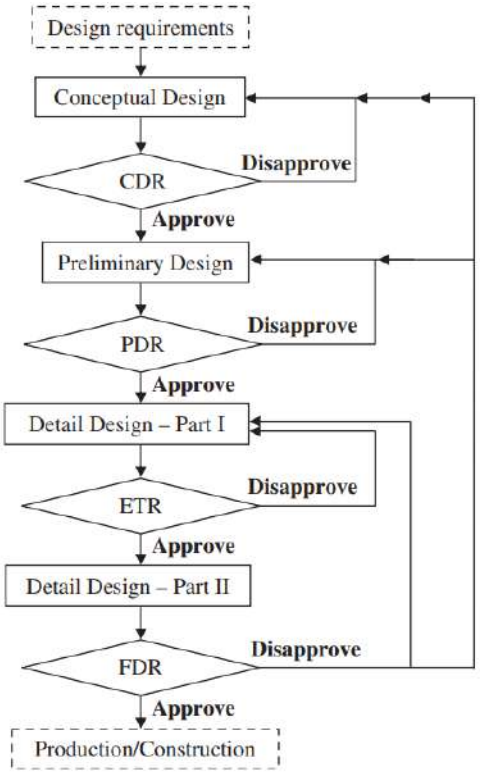

Figure 22: Design Methodology

Chapter 4: Conceptual Design

In this chapter, a potential path is selected by determining all the factors that will lead to a design that will fulfill the design requirements. As it will be evident later, this design phase is more aligned with the design requirements and concepts, rather than calculations and derivations. The design process initiates with the identification of the parameters required for the design. It is very crucial to have a statement that encompasses all the design requirements, so it is convenient to progress toward the next step in the design phase. After identification of the requirements, a suitable selection is made for various aircraft systems for instance wings, tail, propulsion systems, etc. The figure below shows a detailed flow chart that breaks down the various design phases of conceptual design.

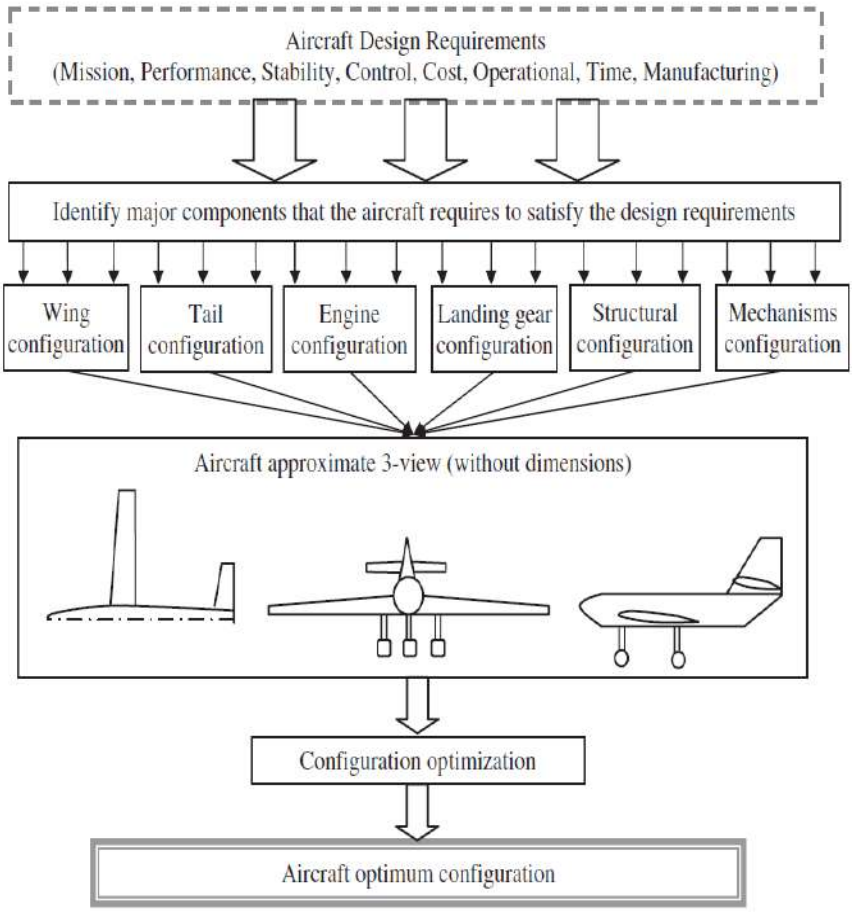

Figure 23: Conceptual design flow

4.1 Drone Configuration

As evident from the flowchart above, the first task in the design is to select the wing configuration that matches the requirements of the design and by first going through the three configurations for the UAVs by pitting them against each other, we can select a suitable configuration that fulfills our requirements. The following table depicts the pros and cons of the three basic UAV configurations.

Table 2: Aircraft Configuration Comparison

<table>
<tr><th colspan="3">Type</th><th>Pros</th><th>Cons</th></tr>
<tr><td colspan="3">Fixed Wing</td><td></td><td></td></tr>
<tr><td>Type</td><td>Pros</td><td>Cons</td><td></td><td></td></tr>
<tr><td>Conventional</td><td>Low Wing loading
High endurance
Less take-off distance.
Generate less noise</td><td>Low maneuverability</td><td rowspan="4">Low Cost

Launched via hand/catapult.

High Endurance

High maximum speed

High payload capacity

High Stability</td><td rowspan="4">Low Maneuverability</td></tr>
<tr><td>Tandem</td><td>High Stability
Moderate Payload Capacity
Good Resistance to wind gusts
Good endurance</td><td>Low maneuverability
Complex design
Heavier UAV</td></tr>
<tr><td>Delta</td><td>High Stability
High Payload Capacity
Easy to manufacture.
Efficient gliding</td><td>Low maneuverability
Vulnerable to wind gusts
Greater take-off distance</td></tr>
<tr><td>Cruciform</td><td>High maneuverability</td><td>Low endurance</td></tr>
</table>

	High Stability High lift generated	Low Speed Low Payload Capacity		
Canard	High lift to drag Ratio High Stability Good maneuverability Resistant to stall	Complex Design Costly design Less efficient at high speeds		
Multi Rotor			High maneuverability Low Cost Compact	Low endurance Low altitude of flight Prone to crosswinds Low payload capacity
Hybrid			High Endurance High Stability Runway not Required High Maximum Speed	Low Pay load Capacity Expensive technology

After conducting a thorough examination of the benefits and practicality of the three possible configurations, it was determined that the Fixed Wing configuration was the most advantageous choice. This decision was reached because the advantages of this configuration far exceeded its disadvantages. Additionally, the objective was to construct a low-cost unmanned aerial vehicle (UAV), and the fixed-wing configuration fit the bill in terms of meeting this requirement.

4.2 Fixed Wing Configuration

Having selected the fixed-wing configuration, the next step was to evaluate the different configurations that fall under this category as outlined in chapter 2. This involved

comparing the pros and cons of the various fixed-wing configurations to determine which one would be the most suitable for our needs. A comprehensive table was created to aid in this evaluation, which succinctly compares the strengths and weaknesses of each configuration.

Table 3: Wing configuration selection matrix

Configuration	**Conventional fixed wing**	**Canard**	**Cruciform**	**Delta (with longitudinal tail)**	**Tandem**	**Conventional main wing with cruciform tail**
Loitering Endurance (10)	9	7	7	6	7	9
Gust effect (10)	8	7	6	9	7	8
Controllability (10)	7	8	9	8	8	8
Attack Velocity (5)	4	4	3	5	4	4
Total Points	28	26	25	28	26	29

After conducting a thorough evaluation of the pros and cons of the various configurations available under the category of fixed wing, conventional configuration was selected. For the tail, the cruciform wing configuration was selected. The reasons for choosing the conventional configuration were twofold. Firstly, it had a low wing loading which directly affected the stall speed, meaning a slower speed was required for takeoff. This was particularly advantageous as it enabled the plane to be launched

by hand. Secondly, the conventional configuration offered high endurance for the UAV, which was deemed necessary to achieve the goal of locking onto a target and loitering for an extended period of time.

With the configurations selected, the next step was to choose the desired aspects from among the several wing configuration alternatives. This involved evaluating the various options available and selecting those that best suit the needs of the UAV project.

4.3 Number of Wings

The first objective was to determine the number of wings for the Unmanned Aerial Vehicle (UAV). There were three options available for selection: a monoplane, a biplane, or a triplane. Among these options, monoplane UAVs tend to be lighter in weight and possess superior aerodynamics due to lower drag resistance. This advantage is crucial for the design of a low-weight and cost-effective UAV that must meet specific performance criteria. For these reasons, it was ultimately decided to choose a monoplane UAV for the project.

4.4 Wing Location

As previously noted in Chapter 2, Unmanned Aerial Vehicles (UAVs) can be broadly classified into three main categories based on the positioning of the wings relative to the fuselage. This categorization is an essential aspect of understanding the design and capabilities of UAVs, and provides a useful framework for comparing and contrasting different types of UAVs. By taking into account the arrangement of the wings on the fuselage, it is possible to distinguish between UAVs that are optimized for specific applications and to identify the unique features and characteristics of each type of UAV. This categorization serves as a starting point for further analysis and investigation into the design, performance, and capabilities of UAVs. These categories are:

1. High Wing
2. Mid Wing
3. Low Wing

After a comprehensive review of the pros and cons of each wing position, it was ultimately concluded that the high wing configuration was best suited to achieve the design and performance goals of the UAV. The selection of the high wing position was based on several key factors, including its greater stability and robustness against gusts of wind.

The high wing configuration provides several advantages over other wing positions in terms of the overall design and performance of the UAV. For example, the higher positioning of the wings enhances the stability of the UAV, making it less prone to roll, pitch, and yaw, even in adverse weather conditions. Furthermore, the high wing configuration makes the UAV less vulnerable to wind gusts, which can cause significant fluctuations in altitude and attitude. This is particularly important for UAVs that must operate in environments with strong wind currents, as it helps to ensure that the UAV can maintain stable and consistent flight characteristics.

In conclusion, after careful consideration of the various options, it was determined that the high wing configuration was the best choice for meeting the design and performance goals of the UAV. The high wing position offers a combination of stability, robustness, and safety, making it an ideal solution for the desired application.

4.5 Wing Type

In the process of determining the wing type for this category, there were several options to choose from, including tapered, rectangular, swept back, swept forward, and elliptical. Ultimately, rectangular wings were selected as they were easier to

manufacture and simpler in design. Additionally, they provide a larger surface area which contributes to improved lift and stability, as well as greater payload capacity compared to the other options.

For the tail of the UAV, the cruciform wings in a cross configuration were selected. This decision was based on the desire to increase the maneuverability of the UAV, as indicated in the data table, the cruciform wings provide greater maneuverability than other options. In comparison, using a conventional wing as the main wing was not providing the desired level of maneuverability, so the cruciform configuration was chosen as a solution. Another factor contributing to the selection of the cruciform configuration was it less weight, as the span of the tail is smaller. The smaller span also results in reduced bending moments on the tail, thus requiring less reinforcement.

4.6 Propulsion System

For the selection of a suitable propulsion system for the UAV, a thorough literature review was conducted. After conducting an extensive review of available literature and conducting a thorough analysis of the weighted matrix, electric propulsion system was selected. This decision was based on two primary factors. Firstly, electric propulsion systems are significantly lighter in weight compared to engine propulsion systems, which allows for more payload to be added to the UAV. Secondly, electric propulsion systems are easier to integrate with the UAV as they are less complex and require less maintenance and operation costs in comparison to engine propulsion systems.

The results of which were in the form of the table below:

Table 4: Propulsion system selection matrix

		Electric Propulsion		**Engine Propulsion**	
	Weightage	**Rating (10)**	**W. Rating**	**Rating (10)**	**W. Rating**
Ease of Control	20	9	18	7	14
Reliability	10	9	9	8	8
Cost	15	10	15	6	9
Safety	10	9	9	8	8
Availability of components locally	15	8	12	5	7.5
System Weight for light weight UAVs	10	10	10	7	7
Response to Variable input	20	10	20	6	12
Total	**100**		**94**		**65.5**

It was concluded through the examination of the literature that for low-end UAVs, the use of an electric propulsion system is more economical and efficient than an engine propulsion system. This is because the lower weight of the electric propulsion system enhances the overall performance of the UAV and the simpler integration process which reduces operational costs and maintenance requirements. Furthermore, electric propulsion systems are more environmentally friendly and have a smaller carbon footprint than engine propulsion systems.

4.7 Materials and Structure configuration

The next major step in conceptual design is to select the appropriate materials for the structure of the UAV. Here there are usually four options for the structure:

1. Metal (often aluminum)
2. Wood and fabric
3. Composite materials
4. Metal and composite materials

Analyzing the properties of the different materials and checking with the requirement criteria, balsa wood was finalized as the structure for the manufacture of the stringers, ribs, and skin of the aircraft. There were a few reasons that helped to make the choice of using Balsa wood for the aforementioned structural elements.

1. Lightweight: Balsa wood has a low density which makes it an ideal material for UAV structures as it minimizes the weight of the aircraft. This results in improved flight performance, longer flight time, and the ability to carry more payload.

2. Strong: Despite its lightweight, balsa wood has a high strength-to-weight ratio, making it suitable for use in lightweight structures that need to withstand the loads of flight.
3. Workability: Balsa wood is easy to work with and can be machined, sanded, and finished to achieve a desired shape and surface finish.
4. Cost-effective: Balsa wood is widely available and relatively inexpensive, making it a cost-effective option for UAV structures. [37]

Spars are the primary structural elements of an aircraft that support the wings and provide stability and strength. [38]

The materials used for spars in UAVs can vary depending on the specific requirements and constraints of the design. Similarly, for the spars there were a few choices:

1. Carbon fiber composites
2. Aluminum alloys
3. Fiberglass composites
4. Wood
5. Magnesium alloys

After thoroughly studying the properties and feasibility of all the materials noted above Carbon fiber was selected as the most appropriate material for spars due to several reasons:

1. Lightweight: Carbon fiber rods have a high strength-to-weight ratio and are significantly lighter than other materials such as aluminum or wood, making them ideal for UAVs where reducing weight is a critical factor.

2. High Strength: Carbon fiber has high tensile strength, compressive strength, and bending strength, making it an ideal material for UAV spars that need to withstand loads of flight.
3. Stiffness: Carbon fiber rods have high stiffness, which means that they can resist deformation and bending moments and maintain their shape. This is crucial for UAV spars that need to maintain their geometry during flight.
4. Durability: Carbon fiber composites are resistant to fatigue, corrosion, and moisture, making them a durable option for UAV spars.
5. Design Flexibility: Carbon fiber composites can be molded into complex shapes and sizes, giving designers greater flexibility in designing UAV spars that meet specific requirements. [38], [39]

Chapter 5: Design Parameters

5.1 Drones Study

Data of more than 80 attack drones and some commercial aircrafts is used as a starting point to select design parameters considering design requirements, manufacturing cost and availability of local components. In parameter selection process, best attack drones in low weight range (based demand and number of militaries around the world using that drone) are specially considered. List of these drones are:

1. Switchblade 300
2. Hero 30
3. Raytheon Coyote
4. Alpagut

5.1.1 Switchblade 300

Following are a few features of the Switchblade 300:

Table 5: Switchblade 300 data

Features	Values
M_{TOW}	2.5 kg
Weight	2.5 kg
Payload	0.23 kg
Range	10 km
Endurance	15 min
Propulsion system	Battery powered
Max speed	100 mph
Configuration	Tandem (Monoplane, low mounted, straight)

Cruise	63 mph
Wingspan	0.686m
Fuselage	2 ft

5.1.2 Hero 30

Following are a few features of the Hero 30:

Table 6: UVision Hero 30 data

Features	**Values**
M_{TOW}	3 kg
Weight	3 kg
Payload	0.5 kg
Range	40 km
Endurance	30 min
Propulsion system	Battery powered
Max speed	100 knots or 185 kph
Configuration	Cruciform with missile-like rear (Monoplane)
Cruise	
Wingspan	0.8 m
Fuselage	0.78 m

5.1.3 Raytheon Coyote

Following are a few features of the Raytheon Coyote:

Table 7: Raytheon Coyote data

Features	Values
M_{TOW}	5.9kg
Weight	5.9 kg
Payload	1kg+ (can vary depending on mission)
Range	200km
Endurance	More than 1 hour
Propulsion system	Battery powered
Max speed	102km/h
Configuration	Tandem
Cruise	102km/h
Wingspan	1.5m
Fuselage	0.91m

5.1.4 Alpagut

Following are a few features of the Alpagut:

Table 8: ALPAGUT loitering munition data

Features	Values
M_{TOW}	45kg
Weight	45kg
Payload	11kg
Range	60km
Endurance	More than 1 hour

Propulsion system	Battery powered
Max speed	100km/h (Cruise) 400km/h (Diving)
Configuration	Fixed Wing with inverted V-tail
Cruise	102km/h
Wingspan	2.5m
Fuselage	2.3m

5.2 Parameter Selection of Drones

5.2.1 Performance Parameters

Using the data of attack drones as described above, following performance parameters are selected:

Table 9: Performance parameters of UAV

Parameter	**Value**
M_{TOW}	2kg
$Payload\ Weight$	0.3kg + (can vary depending on mission)
Range	18 km
Endurance	16 minutes
Top Speed	90 kph
Cruising Speed	72 kph
Terminal Speed	190 kph
Climbing Rate	2 m/s
Cruising Height	400 ft

5.2.2 Wing Parameters

Table 10: Wing parameters

Parameter	Value
Aspect Ratio	$A.R_w = 7$
Configuration	Fixed Wing
Position	High Wing

5.2.3 Tail Parameters

Table 11: Tail parameters

Parameter	Value
Aspect Ratio	$A.R_t = \frac{2}{3} A.R_w = 4.7$
Configuration	Cross tail
Dihedral Angle	45 degrees
Horizontal tail volume coefficient	0.45
Vertical tail volume coefficient	0.07

5.2.4 Fuselage Parameters

Table 12: Fuselage parameters

Parameter	Value
Slenderness Ratio	13
Tail moment Arm to Fuselage Ratio	0.6
Nose Shape	Parabolic
Payload Position	In nose

5.2.5 Propulsion and Control System Parameters

Table 13: Propulsion and control system parameters

Parameter	Value
Propulsion System	*Battery Powered Electric Motor*
Motor Position	Aft
Controller	Pixhawk 6C
GPS	External
Communication with GCS	Telemetry

Chapter 6: Chapter 6: Preliminary Design

After conceptual design and parameter selection of drone, preliminary design of drone was made. In this design phase, following necessary parameters are determined:

- Required Motor Thrust
- Required Battery Capacity
- MTOW
- Wing Span
- Wing Chord

6.1 Methodology

Weight estimation is done by estimating weight of each component to be carried on plane such as:

- Avionics component weight
- Battery weight
- Payload weight
- Structure weight of the airframe structure itself.

Weight estimation is an iterative process, first weight of motor and battery is estimated by defining assuming a weight and drag to lift ratios in cruise and climbing. After initial sizing of battery and motor based on assumed weight, MTOW is calculated. Based on calculated MTOW, motor and battery sizing steps were repeated. These iterations were done until solution was converged. [8], [9]

6.2 Initial Motor Selection:

From design point for fixed wing, maximum thrust required during climb:

$$\frac{T}{W} = 0.44$$

Assuming 23 N of weight:

$$T = 10.12\ N$$

Assuming motor is throttled to 40 percent during climb:

$$T_{motor\ thrust\ @\ 40\%} = 10.12\ N = 1.03\ kg$$

$$T_{total} = 25.3\ N = 2.57\ kg$$

Hence, EMAX GT2826/04 1090KV Thrust 3100 gram was selected which give 1 kg of thrust at 40 percent throttle and has weight of 175 grams. [40]

6.3 Battery Selection

For Cruise:

Ratio of drag to lift was assumed to be 10 empirically from data of previously designed UAVs:

$$\frac{W}{T} = 10$$

$$W = 23\ N$$

$$T = 2.3\ N$$

For Climb:

$$\frac{T}{W} = 0.44$$

$$T = 10.12\ N$$

Power Requirement:

$$P_{motor} = \frac{VT}{\eta_{propeller}}$$

Assuming 50 % propeller efficiency and climb velocity same as cruise:

$$P_{cruise} = \frac{20 \times 2.3}{0.5} = 92\ W$$

$$P_{climb} = \frac{20 \times 10.12}{0.5} = 404.8\ W$$

Assuming cruise flight of 30 minutes and 1 minute of climb,

$$E_{required} = P_{cruise} \times \frac{15}{60} + P_{climb} \times \frac{1}{60} = 29.8\ Wh$$

Motor supports 4S LIPO battery, using 6S power source:

$$Battery\ Capacity \geq 37.4 \times \frac{1000}{14.7}$$

$$Battery\ Capacity \geq 2020\ mAh$$

Hence, TATTU 4S 14.7V 2300 mAh Li-Po Battery is selected which weighs 224 g.

6.4 MTOW Estimation

Weight of each component is calculated as tabulated below:

Table 14: MTOW Estimation

Component	Quantity	Weight
Brushless Motor	1	0.175 kg
TATTU 4S 14.7V 2300 mAh Li-Po Battery	1	0.224 kg
Payload Weight	1	0.3 kg
ESC	1	0.109 kg
Camera	1	0.5 kg
Telemetry	1	0.006 kg
Flight Controller	1	0.120 kg
Servos	6	0.013 kg
GPS Module	1	0.068 kg
Propeller Mass	1	0.0279 kg
Safety Factor	-	0.2 fraction of whole component weight
Weight Fraction of Wires	-	0.05 fraction of whole weight
Weight fraction of structure	-	0.38 fraction of whole weight

Using above data and following equation, MTOW is calculated using MATLAB code:

$$MTOW = W_c \times 1.2 + W_c \times 0.05 + W_c \times 0.35$$

$$MTOW = 2.25\ kg$$

Where:

$$W_c\ is\ sum\ of\ weight\ of\ avionics\ components, battery\ and\ motor$$

6.5 Main Wingspan and Chord

Now, using above estimated weight as input, matching plots is drawn between power loading and wing loading based on:

$$Stall\ speed\ power\ loading$$

$$Rate\ of\ Climb\ power\ loading$$

$$Maximum\ Speed\ power\ loading$$

$$Absolute\ Ceiling\ power\ loading$$

Matching plots is drawn by taking following parameters as input. These parameter values were estimated be using specifications data of previously designed attack drones.

$$Cl_{max,w_{2D}} = 1.2$$

$$V_{cruise(min)} = 20\ m/s$$

$$V_{stall} = 12\ m/s$$

$$V_{loiter} = 1.3 \times V_{stall}$$

$$V_{max} = 1.3 \times V_{cruise}$$

$$\frac{Cl}{Cd} = 10$$

$$CD_o = 0.04$$

$$Ceiling\ height = 500\ m$$

$$Propeller\ efficiency = 0.6$$

$$Aspect\ Ratio = 7$$

Based on these design requirements, matching plots is drawing using MATLAB code between Power loading and wing loading. Based on calculated parameters at design point in MATLAB, airfoil is selected. Using, value of maximum cl/cd ration for airfoil and already calculated wing area new cruise velocity is calculated using XFLR5 as follows:

$$V_{cruise} = 21.4\frac{m}{s} = 77\frac{km}{h} > 72\frac{km}{h}\ (req)$$

$$V_{max} = 27.8\frac{m}{s} = \ 100\frac{km}{h} > 90\frac{km}{h}(req)$$

Now, updating the V cruise in the given data, matching plot was again plotted, and maximum power required, and other span was calculated at design point:

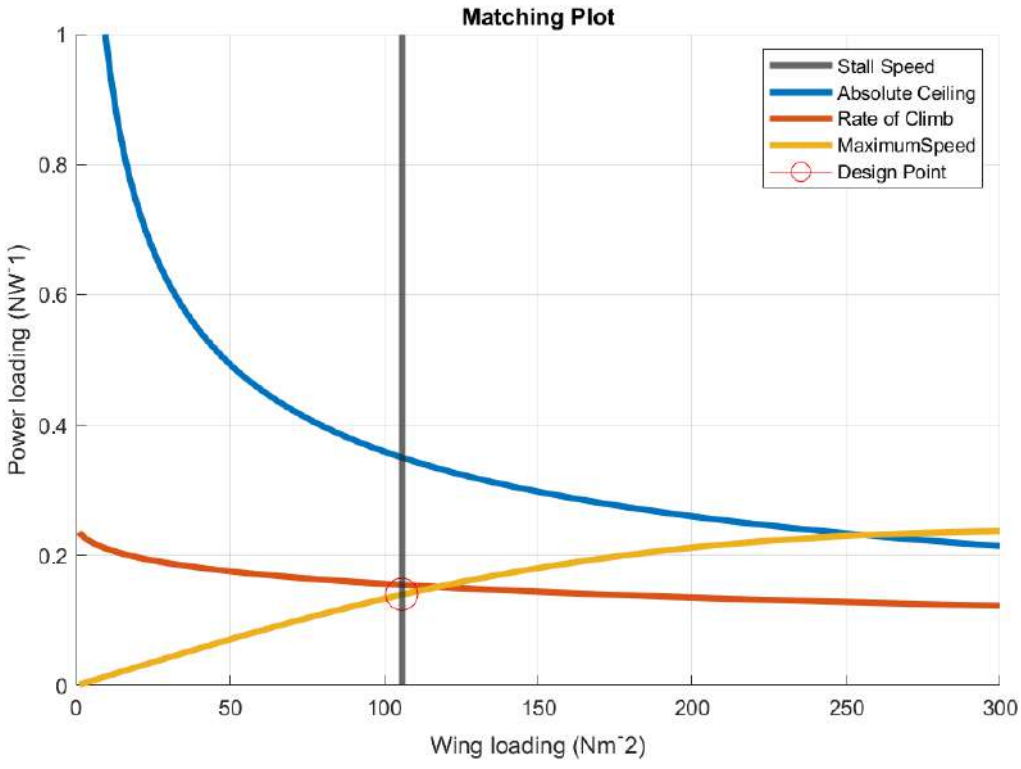

Figure 24: Matching plot

At design point:

$$Maximum\ Power\ Required = 158\ Watt$$

$$Wing\ Area\ Required = 0.209\ m^2$$

$$Wing\ Span = 1.2\ m$$

$$Wing\ Chord = 0.173\ m$$

Battery Resizing

Now since, since maximum power required at any point is less than initially estimated value (404 Watt) and also actual Cl/Cd of selected airfoil (next section) is greater than 10, so no battery resizing is required.

Motor Resizing:

Also, from matching plot at design point:

$$\frac{P}{W} = \frac{1}{0.15} = 6.7$$

$$P = \frac{V_{climb}T}{\eta_{propeller}}$$

$$\Rightarrow \frac{T}{W} = 6.7 \times \frac{0.6}{(12 \times 1.1)} = \ 0.3 < 0.44\ (initially\ assumed)$$

Hence, no need of motor resizing.

Chapter 7: Detailed Design

The next step in the design process is the detail design, in this phase all the major aircraft components like wing, tail, fuselage and control surfaces are designed.

7.1 Wing Design

Wing is the most important and critical component in the fixed-wing UAV as it affects the design of all other components of the aircraft. Wing produces lift for flying but also generate drag force and nose down pitching moment. During wing design the aim is to maximize the lift force and minimize the drag force and nose down pitching moment [8], [9]

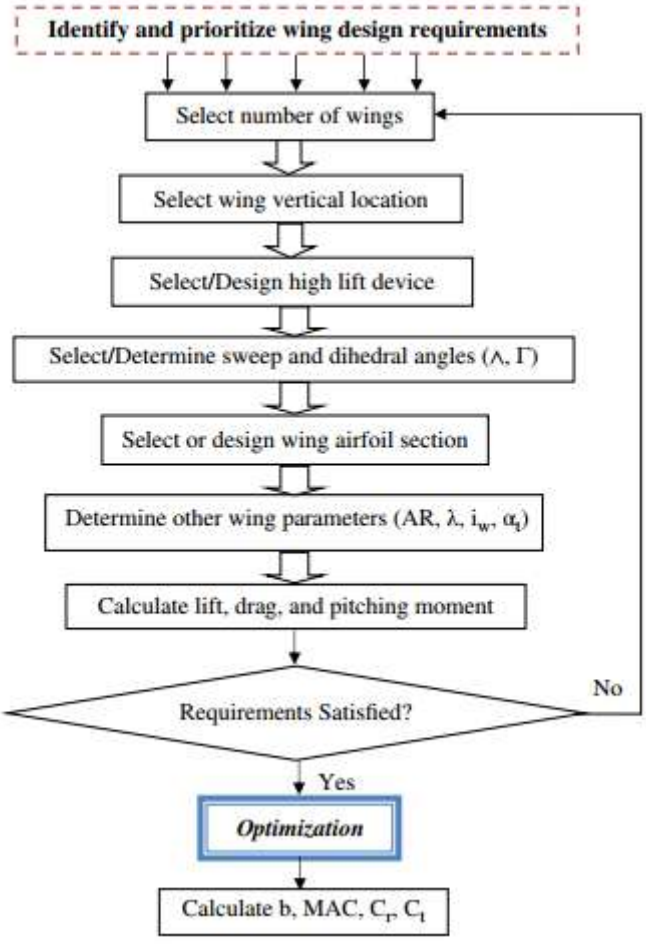

Figure 25: Wing design flowchart [9]

During wing design we have taken many factors into consideration such as performance, stability and control, manufacturability etc. Performance requirements include parameters such as cruise speed, top speed, stall speed, range and endurance. Stability and control requirements include parameters like lateral and direction stability. There are several parameters that have to determine during wing design.

To ensure a systematic and organized approach to our design, it is essential to establish a step-by-step design process that can be followed in a chronological order and facilitate the optimization process later on. A design flowchart, as depicted in Figure serves this purpose. However, it is crucial to acknowledge that every design process is iterative. Therefore, it is imperative to develop our design programs or MATLAB scripts with flexibility to do modifications later on.

7.1.1 Number of Wings

Now, nearly all aircraft have a monoplane, while only a few still use a biplane configuration. There are currently no modern aircraft designs that employ three wings. In the past, using multiple wings was primarily due to limitations in manufacturing technology. However, with advancements in manufacturing technologies and the use of stronger aerospace materials, this reason is no longer valid. Monoplane UAVs tend to be lighter in weight and possess superior aerodynamics due to lower drag resistance. So, a monoplane is chosen for the uav. [8], [9]

7.1.2 Wing Location

Wing location has a direct impact on the design of other aircraft components which include tail and center of gravity. There are three common options to consider for the vertical location of the wing. Mid wing, Low wing and High wing.

Every wing location has its own pros and cons discussed earlier. The most effective method for selecting the wing location is to create a weightage tabl. It is typically necessary to assign weight to each design objective, such that the total equals 100%. By comparing the total weights for each option, the designer can determine the optimal configuration.

7.1.3 Airfoil Section

One of the critical wing parameters is airfoil selection. The airfoil section plays a significant role producing optimal lift with optimal pressure distribution at lowest possible aerodynamic cost.

There are countless types of airfoils available, each with unique geometry and properties, the selection process can be overwhelming. However, since we are selecting an airfoil and not designing one, a decision matrix can be employed to assist in the process once the ideal requirements for the drone have been identified.

During the selection of an airfoil, various parameters are associated with importance. However, it is necessary to maintain a compromise, as no airfoil can provide the best results in all parameters simultaneously. Seven of the most crucial parameters have been identified for the drone, and by weighing them into a decision matrix, we can effectively select the most suitable airfoil for the wing. [8], [9]

The parameters are briefly described below:

Cl_{max}: The maximum lift coefficient is a crucial parameter that affects the drone's lifting capability. A higher maximum lift coefficient allows us to generate more lift with a smaller wing, resulting in lower drag. [9]

Cd_{min}: The minimum drag coefficient is a critical parameter that affects the battery life and power requirements of the drone. Minimizing this parameter can increase the drone's endurance. [9]

C_{m_o}: The coefficient of moment is an important consideration during the design of the drone's tail. A higher coefficient of moment requires a larger tail, resulting in a bulkier drone. [9]

$\frac{Cl}{Cd_{max}}$ **:** The ratio of lift to drag is a key parameter that complements both the maximum takeoff weight and endurance requirements of the drone. However, optimizing this ratio requires a compromise between maximizing MTOW and minimizing drag. [9]

α_s: It is the maximum angle at which the wing will stall called stall angle. The value should be optimal to prevent the drone from stalling during climbing. [9]

Cl_α: The lifting-curve slope of an airfoil determines the rate of change of lift coefficient with respect to the angle of attack. A higher slope allows us to generate more lift at lower angles of attack. [9]

Stall quality: This parameter indicates the type of stalling behavior when the wing reaches the stall angle. A gentle stalling behavior is always preferred. [9]

By weighing these parameters in a decision matrix, we can effectively choose the most suitable airfoil for our drone.

Table 15: Airfoil Selection Matrix

Airfoil	Stall Angle	C_{mo}	C_L (max)	C_D (min)	$\frac{C_L}{C_D}$ (max)	Thickness (max)	Camber (max)
NACA 2412	15.25^o	-0.0505	1.407	0.0063	87.2826	12.00%	2.00%
CLARK-YM-18	15.75^o	-0.0746	1.5159	0.00831	77.64081	18.00%	3.60%
EPPLER E1212	17.25^o	-0.0577	1.6443	0.01079	84.74872	17.70%	3.20%
MH102	15.5^o	-0.0581	1.4771	0.00941	94.17069	17.00%	2.80%
NACA 23012	14.25^o	-0.0041	1.4299	0.00647	77.12995	12.00%	1.80%
SM701	17.5^o	-0.1236	1.6533	0.00809	95.88362	16.00%	3.00%

7.1.4 Wing Incidence

The wing incidence angle is the angle between the chord line of the wing (a straight line joining the leading and trailing edges) and the longitudinal axis of the aircraft (a straight line running from the nose to the tail of the aircraft). The wing incidence angle affects the lift and drag characteristics of the wing.

The lift to drag is a measure of the efficiency of a wing. The wing incidence angle should be set to the angle that gives the highest L/D ratio for the expected flight conditions; in our case it is cruise flight. Following requirements must be satisfied to determine the optimal wing incidence angle:

1) During cruising, the must generate the required lift. [9]
2) Minimum drag is produced during cruise. [9]

3) During takeoff the wing setting angle should allow safe variation of angle of attack. [9]
4) During cruising, there should be minimum drag on fuselage at the setting angle. [9]

The angle at which the lift to drag ratio is highest results in optimum wing incident angle as the wing is most efficient at that angle. In our case the maximum cl/cd ratio is obtained at angle of incident of 2.5 degrees which is obtained by analyzing the airfoil in xflr5.

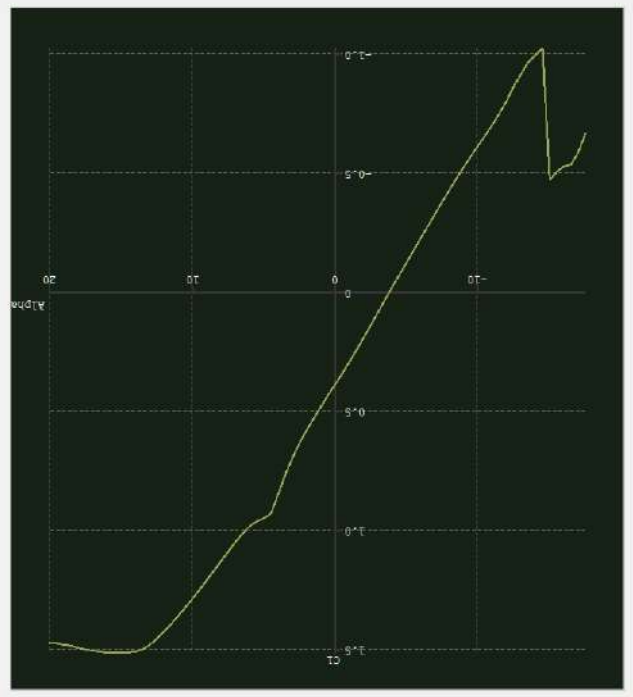

Figure 26: Variation of lift with angle of attack of Clark YM-18

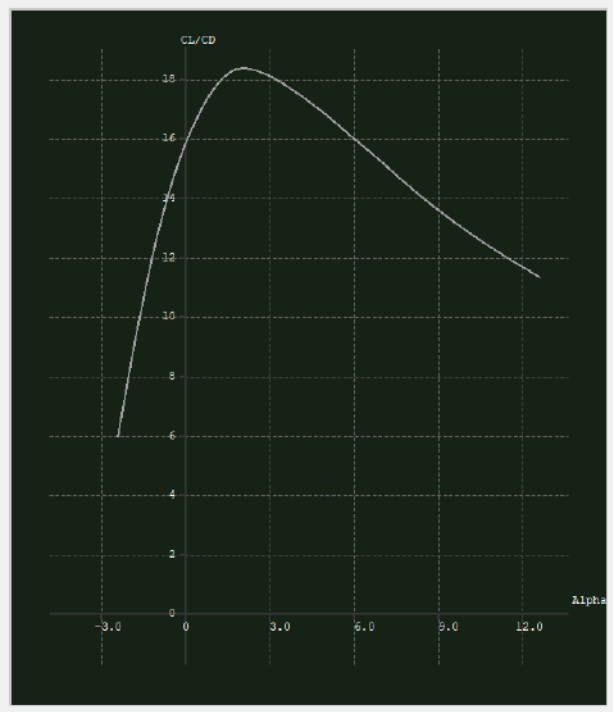

Figure 27: Variation of Cl/Cd with angle of attack of Clark YM-18

7.1.5 Aspect Ratio

Choosing an optimum value of the aspect ratio is crucial for good aircraft performance as it directly impacts induced drag and weight.

Higher aspect ratios generate more lift with less induced drag, they become more flexible and susceptible to structural deformations and flutter. In contrast, lower aspect ratios are more structurally sound but generate more drag due to less span and more chord. Mid aspect ratio wings offer a compromise between these two extremes, providing a balance between structural integrity, lift-to-drag ratio, and overall efficiency. They are lighter in weight and easier to manufacture than high aspect ratio wings, making them a good choice as they provide a balance between various design trade-offs. So, aspect ratio of 7 is used.

$$AR_w = 7$$

No.	Aircraft type	Aspect ratio
1	Hang glider	4–8
2	Glider (sailplane)	20–40
3	Home-built	4–7
4	General aviation	5–9
5	Jet trainer	4–8
6	Low-subsonic transport	6–9
7	High-subsonic transport	8–12
8	Supersonic fighter	2–4
9	Tactical missile	0.3–1
10	Hypersonic aircraft	1–3

Figure 28:Typical aspect ratio of different aircraft types

7.1.6 Taper Ratio

One of the aim of wing design is to have a elliptical wing lift distribution. Taper ratio is useful in achieving an elliptical lift distribution. The benefits include improved flight safety during stall conditions, as the root of the wing generates less lift than the tip, allowing more time for spin recovery. Additionally, an elliptical lift distribution results in lower bending moments, leading to a lighter yet stronger wing structure, since the load distribution is proportional to the lift distribution. [8], [9]

Wing analysis in xlfr5 suggests that taper ratio 1 produces elliptical wing lift distribution and it is also backed by lifting line theory analysis as shown in figures.

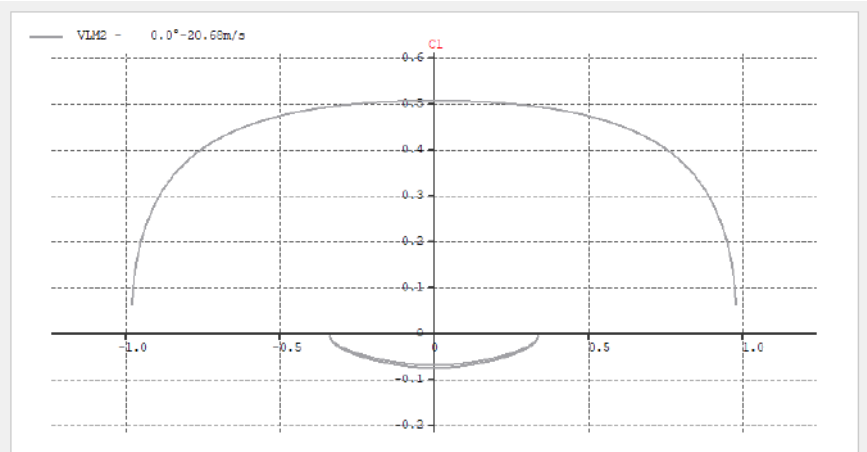

Figure 29: Elliptical wing distribution

7.1.7 Sweep Angle

The sweep angle of wing is crucial design parameter that affects the aerodynamic performance. It can provide benefits such as reducing drag, delaying the onset of shock waves, and improving stability and control. However, at low Mach numbers (less than 0.3), the advantages of sweep angle may not outweigh the disadvantages, such as increased weight, decreased lift, and reduced fuel efficiency. Therefore, the sweep was kept zero. [8], [9]

7.1.8 Twist Angle

The twist angle of a wing is important in determining its lift distribution and drag characteristics. By increasing the angle of twist towards the wingtip, the lift distribution can be made more elliptical, which enhances the safety during stall and results in a lighter and stronger wing structure. However, there are trade-offs, as excessive twist can cause additional drag and lead to a reduction in maximum lift coefficient. These effects are particularly relevant for low-speed flight conditions, such as those at Mach 0.3 or below. Also, manufacturability of a twisted wing is difficult and complex. Therefore, the twist angle is kept zero. [8], [9]

7.1.9 Dihedral Angle

The dihedral angle has two main effects on the wing:

1) Formation of moment of roll which tends to restore the level flight condition.
2) It increases lateral stability of the aircraft.

Giving dihedral angle to wing causes the wing effective planform area (*S*eff) to reduce which results in loss of lift. It can also increase the aircraft's drag and reduce its maneuverability. In our design, we have used a high wing position, high-wing aircraft already have inherent lateral stability due to the wing's position. Therefore, dihedral angle is kept zero.

7.2 Tail Design

Tail primary function is to provide trim and stability to aircraft and secondarily the control. Several design parameters associated with tails and wing are similar. The wing is optimized for maximum lift and efficiency, while the tail is optimized for trim, stability, and control. The tail design flow is given in figure below which include several parameters [8], [9]

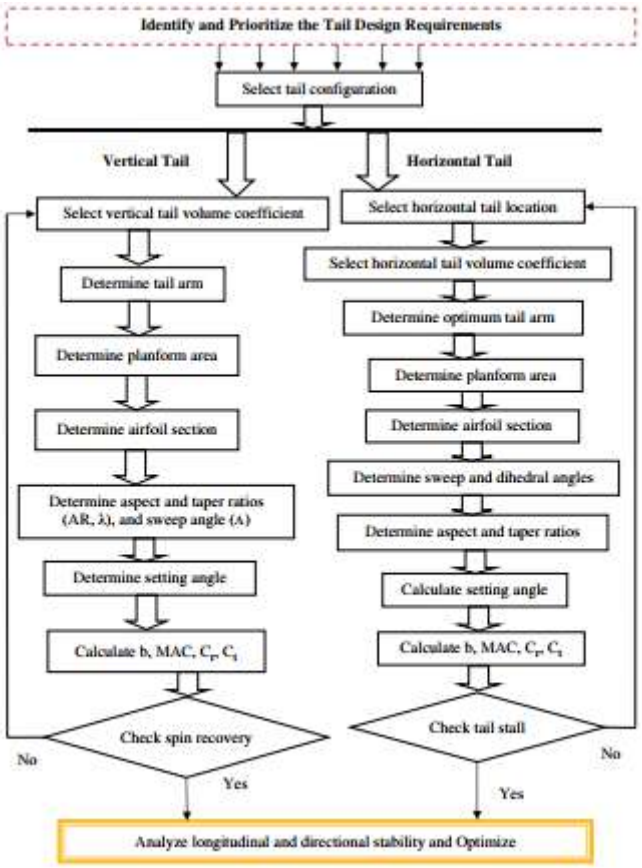

Figure 30: Tail desgin flowchart [9]

Both horizontal and vertical tail have same parameters and can be performed in parallel. According to the mission profile, the UAV is in cruise position for most of the time and we require good endurance as well maneuverability, so the aim is to design a tail with less possible drag and good control capabilities. Most parameters are determined using technical calculations, although some parameters are chosen using an engineering selection method. The design process is iterative and is repeated several times to achieve optimum tail. [8], [9]

7.2.1 Tail Configuration

Selection of tail configuration is first step in the process. There are mainly two configurations of tail based on its position.

1. Aft Tail
2. Canard

Mostly aft tail configuration (85%)is used by designers. The aft tail can provide good stability and control capabilities so, aft tail is used.

Moreover, the aft tail has many sub-configurations after conducting literature review and using design matrix (shown in table 3.1) cruciform aft tail configuration is selected.

7.2.2 Horizontal Tail

Determining horizontal tail volume coefficient, $\bar{V}_H$, is next step in tail design, It is primarily based on the longitudinal stability requirements of the aircraft. Increasing $\bar{V}_H$ will result in a small wing but longer fuselage or a larger tail. This will make the aircraft longitudinally more stable but less controllable. Conversely, decreasing $\bar{V}_H$ will make the aircraft less stable but more controllable in longitudinal direction. The appropriate value for $\bar{V}_H$ is selected based on the data from previously made UAVs that closely match our stability and control requirements. [8], [9]

7.2.3 Horizontal Tail Volume Coefficient

It is a dimensionless parameter. This parameter is used for sizing of tail. Higher value means larger size of tail and vice versa. Literature review showed most of the aircraft have volume coefficient in the range of 0.4-0.45. Hence, for horizontal tail design:

$$V_h = 0.45$$

7.2.4 Tail Arm and Planform Area

Tail arm is the distance between the aircraft center of gravity and the tail aerodynamic center. The tail arm affects the longitudinal trim and tail pitching moment. Tail arm and planform area inter-related. The objective is to find optimum value of Tail Arm and planform area of tail such that the drag is minimum. Both tail arm and planform relates to each other through tail volume coefficient as follows:

$$l_{h_{opt}} = K_c \sqrt{\frac{4C_w S_w V_h}{\pi D_F}}$$

$$S_h = \frac{(S.F)V_h C_w S_w}{l_{h_{opt}}}$$

Here value of fudge factor (K_c) depends upon the shape of the fuselage.

K_c
$= 1$ $for\ cylindrical\ fuselage\ and\ increases\ as\ aft\ fuselage\ taper\ angle\ increases$

Cylindrical aft fuselage is selected because:

1. It is easier to manufacture.
2. Offers more resistance towards bending compared tapered fuselage at slight cost of increased drag.
3. Manufacturing constrains.

Calculated value of tail arm and planform area from above equation are:

$$l_{h\_opt} = 0.475\ m$$

$$S_h = 0.2088\ m^2$$

7.2.5 Airfoil Selection

In the selection of the airfoil for the tail, the aim is to maximize the lift curve slope (Cl_{α_t}) for wide useable range of angle of attack. The airfoil must be able to generate both positive and negative lift to generate required moment during pitching up and pitching down of aircraft.

Another essential requirement for the tail is that it must not be affected by compressibility effects. To achieve this, the tail's lift coefficient should be lower than that of the wing, ensuring that the horizontal tail remains free of compressibility effects.

It is important to ensure that the horizontal tail never stalls before the wing. Therefore, the stall characteristics of the airfoil section used in the tail whether sharp or docile are not of significant importance. [8], [9]

Based on all these observations and literature review **NACA 0015** is selected for tail because Symmetric category of NACA airfoils has higher stall angles.

NACA0015 has maximum thickness of 15% of chord (25 mm) which is good enough to ensure tail is drag resistant (deduced from simulations).

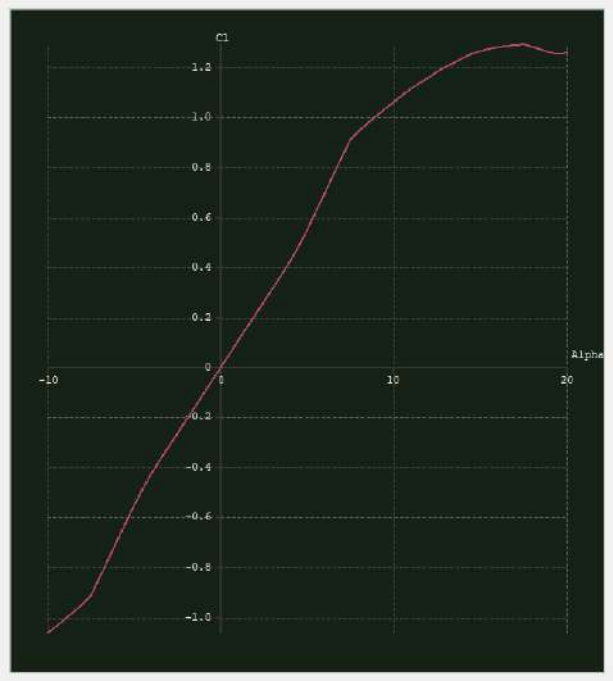

Figure 31: Variation of lift with angle of attack of NACA 0015

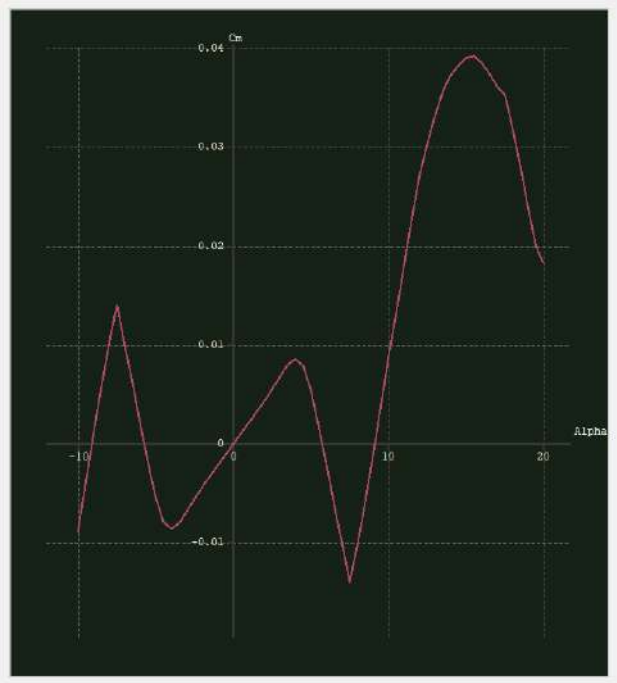

Figure 32: Variation of pitching moment with angle of attack of NACA 0015

7.2.6 Wing/fuselage Aerodynamic Pitching Moment Coefficient

The UAV experiences two major moments along the y-axis, wing pitching moment and lift relative to the center of gravity. To maintain equilibrium, a tail moment is required to balance these moments out. This is achieved by applying the total moment equation at the center of gravity along the x-axis and calculating the coefficient of moment for the tail in the longitudinal direction. Based on this calculation, the most suitable airfoil is selected from a database of airfoil data that matches the requirements for the tail's coefficient of moment at equilibrium. [8], [9]

7.2.7 Tail Setting Configuration

The aircraft has several flight conditions, to satisfy longitudinal trim conditions in flight condition, tail must produce positive or negative lift by changing the angle of attach. As the tail is fixed and has fixed planform area as well as airfoil, to achieve trim, there are three different tail setting configurations that can be used to change the angle of attack.

1. Fixed Tail

2. All Moving Tail

3. Adjustable Tail

Fixed tail is much easy to design, cheap and light, Hence fixed tail with control surfaces is used for trimming and increases maneuverability of drone. [8], [9]

7.2.8 Sweep Angle and Dihedral Angle

The sweep angle of tail is an important design parameter that affects the aerodynamic performance of an aircraft. It can provide benefits such as reducing drag, delaying the onset of shock waves, and improving stability and control. However, at low Mach numbers (less than 0.3), the advantages of sweep angle may not outweigh the disadvantages, such as increased weight, decreased lift, and reduced fuel efficiency. Therefore, the sweep angle was kept zero. [8], [9]

7.2.9 Dihedral Angle

Dihedral Angle is also an important parameter. Dihedral angle in tail not only decides the configuration but also has serious effects on working of control surfaces. Since, X tail configuration is selected for tail which has dihedral angle of 45°. Dihedral angle of horizontal tail is kept 45°.

7.2.10 Aspect Ratio

For the tail of an aircraft, it is preferable to have a low aspect ratio which is lower than wing aspect ratio. The rationale behind this is that when the elevator is deflected, it creates a bending moment at the tail root. By opting for a lower aspect ratio, the bending moment is reduced. Also tail has influence on several other parameters like center of gravity, stability and control.

A typical way of calculating aspect ratio of tail is: [8], [9]

$$AR_h = \frac{2}{3} AR_w$$

$$AR_h = 4.7$$

Hence, Aspect Ratio of horizontal tail is kept 4.7.

7.2.11 Taper Ratio

Taper ratio can be useful in achieving an elliptical lift distribution. Another motivation behind using tapered tail is to lower bending moment in tail but since tail has small span (0.8 m) added advantage of using taper ratio do not outweigh the complexity it adds in manufacturing. Hence, taper ratio for tail is kept one. [8], [9]

7.2.12 Tail Span, Root Chord, Tip Chord, MAC

Using calculated horizontal tail area and AR of 4, horizontal tail span, tip chord, root chord and MAC are calculated as follows:

$$b_h = \sqrt{AR_h(S_h)} = 0.4078\ m$$

$$C_{root_h} = \frac{b_h}{AR_h} = 0.0874\ m$$

$$C_{tip_h} = \lambda\left(C_{root_h}\right) = 0.0874\ m$$

$$C_h = \frac{\frac{2}{3}\left(C_{tip_h}\right)(1 + \lambda^2 + \lambda)}{1 + \lambda} = 0.0874\ m$$

7.2.13 Stability Check

After selecting airfoil and evaluating all 3D and 2D parameters using LLT (shown in MATLAB code in Appendix 1), it is easier to calculate the C_{m_α} of the plane. $C_{m_\alpha}$is pitching moment coefficient and the greater the value of C_{m_α} is in negative, the more stable the aircraft is. For maneuverable aircraft, its value should be between -0.35 and -0.8.

C_{m_α} relates with center of gravity, tail arm and tail span as follows:

$$C_{m_\alpha} = Cl_{\alpha_{w,3D}}(h - h_o) - Cl_{\alpha_{h,3D}}\eta_h\left(\frac{S_t}{S_w}\right)\left(\frac{l_{h_{opt}}}{C_h} - h\right)(1 - \varepsilon_o)$$

Literature review showed, conventionally it is safe to consider horizontal tail as 75 % effective in pusher configuration. Hence by selecting:

$$\eta_h = 0.75$$

$$C_{m_\alpha} = -0.35$$

Hence plane is stable, and its values lies with in desirable range of -0.35 − -0.8.

7.3 Vertical Tail

7.3.1 Vertical Tail Volume Coefficient

It is a dimensionless parameter. This parameter is used for sizing of tail. Higher value means larger size of tail and vice versa. Literature review showed most of the aircrafts has volume coefficient in the range of 0.06-0.09. Hence, for horizontal tail design, horizontal tail volume coefficient is selected to be:

$$V_h = 0.07$$

7.3.2 Tail Arm

Since object is to design X-tail where same plane act as both horizontal and vertical tail, tail arm of vertical tail cannot be changed.

$$l_{h_{opt}} = l_{v_{opt}}$$

7.3.3 Planform Area

Knowing the value of tail arm, it is easy to calculate planform area of vertical tail following the procedure described in horizontal tail design:

$$S_v = \frac{(S.F)V_v C_w S_w}{l_{v_{opt}}} = 0.0356\ m^2$$

7.3.4 Airfoil Selection, Sweep Angle and Aspect Ratio

It is necessary to keep all these parameters for vertical tail the same as those in horizontal tail for X-tail configuration because in X-tail same planform acts both as

vertical and horizontal tail and these parameters cannot be different for the same platform. Hence, same values are selected for vertical tail for these parameters as are selected in horizontal tail design in pervious section.

7.3.5 Tail Span, Root Chord, Tip Chord, MAC

Using calculated horizontal tail area and AR of 4, horizontal tail span, tip chord, root chord and MAC are calculated as follows:

$$b_v = \sqrt{AR_v(S_v)} = 0.4078m$$

$$C_{root_v} = \frac{b_v}{AR_v} = 0.08\ m$$

$$C_{tip_v} = \lambda\left(C_{root_v}\right) = 0.08\ m$$

$$C_v = \frac{\frac{2}{3}\left(C_{tip_v}\right)(1+\lambda^2+\lambda)}{1+\lambda} = 0.08\ m$$

7.3.6 Stability Check

After selecting airfoil and evaluating all 3D and 2D parameters using LLT (shown in MATLAB code in Appendix 1), it is easier to calculate the C_{n_β} of the plane. C_{n_β} is yaw moment coefficient and the higher the value of $C_{n_\beta} is$, the more stable the aircraft is. For maneuverable aircraft, its value should be between 0.2 and 0.4.

C_{n_β} relates with center of gravity, tail arm and tail span as follows:

$$C_{n_\beta} = \frac{K_f C l_{\alpha_{v,3D}} \left(1 - \frac{d\sigma}{d\beta}\right) \eta_v l_{v_{opt}} S_v}{b_w S_w}$$

Literature review showed, conventionally it is safe to consider vertical tail as 75 % effective in pusher configuration. Hence by selecting:

$$\eta_h = 0.75$$

$$C_{n_\beta} = 0.5525$$

7.4 Tail Design

Comparison of C_h, C_v and b_h, b_v showed horizontal tail of larger planform area is required compared to the vertical tail to meet design requirements. In other words, horizontal tail parameters are limiting parameters and X-tail has to be designed based on horizontal tail parameters to meet both horizontal and vertical tail design requirements. Hence,

$$S_t = \frac{S_h}{\cos(45°)} \times \frac{1}{2}$$

$$b_t = \sqrt{AR_h(S_t)} = 0.3429m$$

$$C_{root_t} = \frac{b_t}{AR_h} = 0.0735\ m$$

$$C_{tip_t} = \lambda\left(C_{root_t}\right) = 0.0735\ m$$

$$C_t = \frac{\frac{2}{3}\left(C_{tip_t}\right)(1 + \lambda^2 + \lambda)}{1 + \lambda} = 0.0735\ m$$

7.4.1 Check

Now it is desirable to check the volume coefficient of vertical tail to ensure its value lies within the recommended range of 0.06 to 0.09. Hence using following equation

$$S_{v_{new}} = S_t \times \cos(45°) \times 2 = 0.0356$$

$$b_{v_{new}} = \sqrt{AR_v\left(S_{v_{new}}\right)} = 0.4078m$$

$$V_{v_{new}} = \frac{S_{v_{new}} l_{v_{opt}}}{b_w S_w} = 0.0836$$

New value of vertical volume tail coefficient is calculated to be $\mathbf{0.0836} > \mathbf{0.07}$ ($\boldsymbol{required}$) which is in the recommended design range. Hence, design is good.

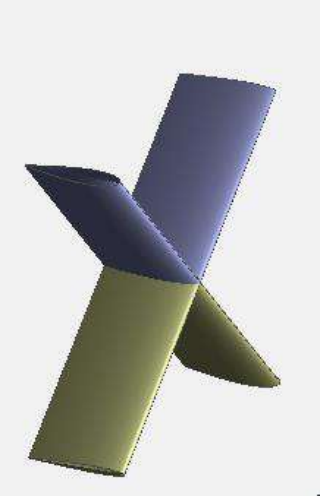

Figure 33: Final X tail

7.4.2 Tail Incidence at Trim Position

To ensure proper longitudinal trim during cruising flight, it is necessary to determine the horizontal tail incidence or i_t . The aim is to cancel out the effect of pitching moment generated by generating required positive or negative lift from tail. To meet the trim design requirement, the tail incidence is determined without any control surface being deflected.

To calculate pitching moment of plane at different angle of cruciform tail Vortex Latex method is used using XFLR5, instead of conventional LLT theory xflr5 results because Vortex Lattice method generates more accurate results compared to LLT theory. Based on the xflr5 simulation results shown in table, 0.9 degree is selected as tail incidence angle because at this tail angle:

1. Pitching moment is zero in trim position (0 degree of AOA)
2. Slope of the graph (C_{m_α}) is -0.79 which shows aircraft is stable.

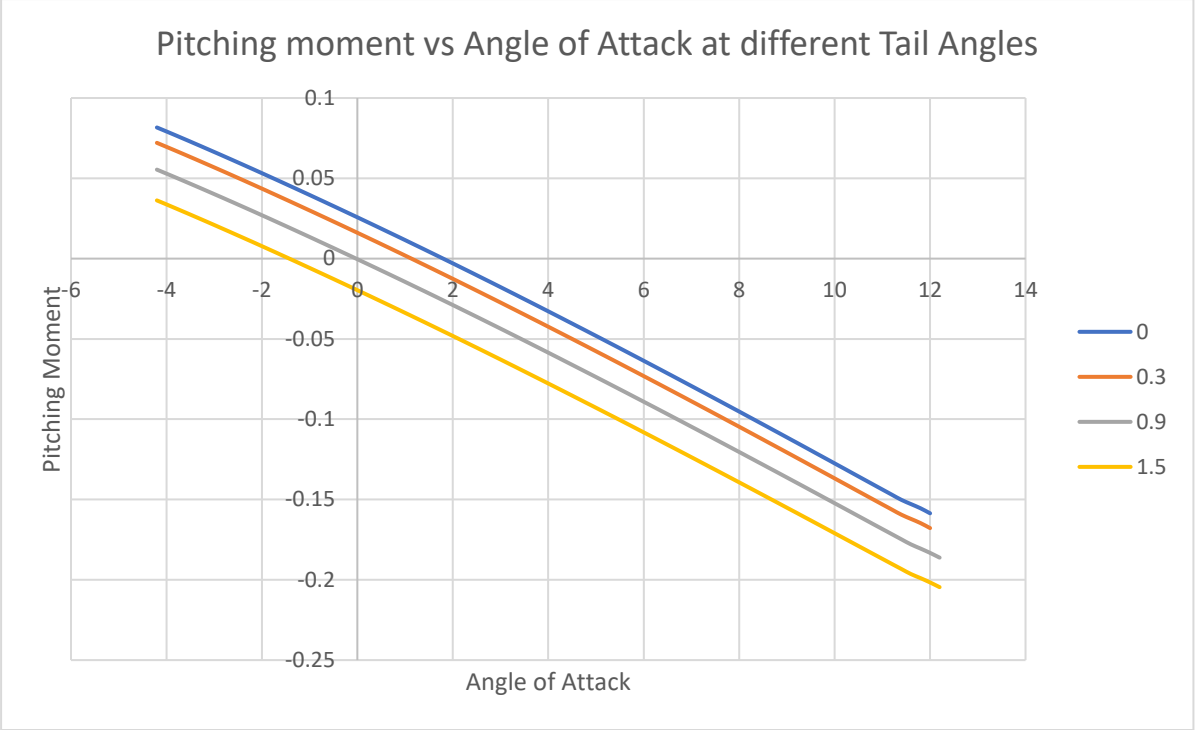

Chart 1: Pitching moment vs angle of attack at different tail angles

7.5 Fuselage Design

After design of wings and tail next crucial step is the design of fuselage. Fuselage not only act as the base structure on which all other components are attached but it also encapsulates all the electronic equipment and payload. Fuselage has major contribution in the total zero lift drag Cd_o of drone which needs to be minimized. So, in the design of fuselage following parameters are considered:

1. Minimum diameter required based on size of components to be placed inside fuselage.
2. Ratio of length of fuselage in front of main wing to total fuselage length (l/L)
3. Fineness ratio of fuselage
4. Manufacturability
5. Ability to act as base structure and carry load.

7.5.1 Minimum Required Diameter

Minimum required diameter can be determined by listing dimensions of all the components to be placed inside the fuselage. Following is the list of components that are to be placed inside fuselage along with its dimensions:

Table 16: Components Dimensions

Component	Dimension
Flight Controller	$50 \times 15.5 \times 81.5\ mm$
Telemetry	$51 \times 30 \times 10\ mm$
Battery	$106 \times\ 36 \times\ 31mm$
Pitot	$117 \times 8 \times 22.3$ mm

Since Pixhawk has highest width, minimum square shaped empty space required inside fuselage is 50 mm. Since height is small, we can say, 57 mm is enough.

Since some space will be covered by structure too, structural analysis of fuselage (shown in chapter 7) shows formers annular radius has to be 6 mm to maintain safety factor of 2 for fuselage. Since skin of fuselage is to be made of balsa wood 3mm thick sheet minimum required diameter can be calculated as follows:

$$D_{min} = thickness\ of\ skin \times 2 + annular\ radius\ of\ former \times 2 + 57\ mm$$

$$D_{min} = 6 \times 2 + 6 \times 2 + 57\ mm$$

$$D_{min} =\ 75\ mm$$

7.5.2 Fuselage Front to Total Fuselage Length Ratio

One important factor in design of fuselage is the ratio of fuselage length in front of main wing and total length of fuselage. This factor help to decide what should be the total length of fuselage based on the fact that in latter stage during mass distribution and

adjustment of center of gravity, one had enough space in fuselage to place objects to adjust center of gravity of plane as per requirement. For aft tail and push configuration, its recommended value is 0.45.

No.	Aircraft configuration/type	l/L
1	An aircraft whose engine is installed at the nose and has an aft tail	0.6
2	An aircraft whose engine(s) are installed above the wing and has an aft tail	0.55
3	An aircraft whose engine is installed at the aft fuselage and has an aft tail	0.45
4	An aircraft whose engine is installed under the wing and has an aft tail	0.5
5	Glider (with an aft tail)	0.65
6	Canard aircraft	0.4
7	An aircraft whose engine is inside the fuselage (e.g., fighter) and has an aft tail	0.3

Figure 34: Values of l/L for different aircrafts [8]

Hence,

$$\frac{l_{h_{opt}}}{Total\ fuselage\ lenght} = 0.45$$

$$\frac{l_{h_{opt}}}{l_{h_{opt}} + l} = 0.45$$

$$\Rightarrow\ l_{h_{opt}} = 0.45 \times l_{h_{opt}} + 0.45l$$

$$\Rightarrow l = 0.58\ m$$

$$or\ L = \ 1.05\ m$$

7.5.3 Fineness Ratio and Structural Deflection

Fineness ratio of aircraft is the ratio of total fuselage length to its diameter. If one keeps on decreasing the diameter of fuselage, drag will not keep on decreasing. Optimal value for fineness ratio of fuselage is 16.4 as shown in graph if only drag is considered. But with decrease in diameter of fuselage, bending moment stress in structure increases which in turn increases the deflection in fuselage during flight. To counter bending

moment cross-sectional area such as stringer diameter and skin sheet thickness has to increase which increase overall weight of the structure. [8]

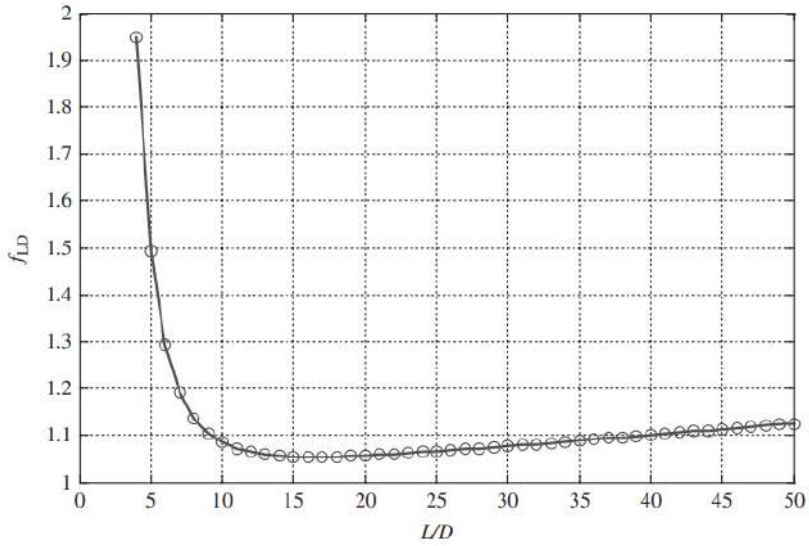

Figure 35:Fuselage Friction coefficient vs length to diameter ratio [8]

Above figure shows there is small change in drag coefficient value over the 13 to 18 fineness ratio hence it **sweet spot** for the design of fuselage.

Structural analysis of fuselage (shown in chapter 7) showed if diameter of fuselage is kept 75 mm, fuselage deflect by only 3 mm (in cantilever beam arrangement when 25 N is applied at the end of fuselage and support is provided at main wing attachment) when only 4 stringers are used. Hence, 75 mm is recommended diameter because:

1. Fineness lies in sweet spot.
2. Deflection in fuselage is minimal (3 mm)
3. Diameter is larger then D_{min}
4. Only 4 stringers of 5X3 mm are to be used hence structural weight of the fuselage is minimal.

Final Fuselage parameters

$$Fuselage\ length = L = 1050\ m$$

$$Fuselage\ Diameter\ = 75\ mm$$

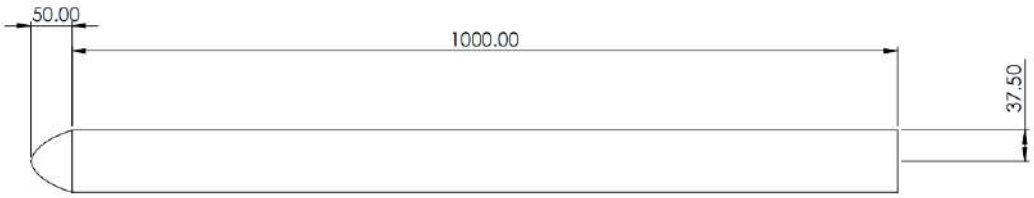

Figure 36: Fuselage

Chapter 8: Design of Control Surfaces

The control surfaces of a UAV are moveable components on the wings and tail of a UAV which allow the UAV's movements to be controlled and contribute to its stability. There are three primary control surfaces that allow for control of UAV's movements. These surfaces include: Ailerons, Elevators and Rudder.

Designing the control surfaces of a UAV form a very critical part of UAV design as the control surfaces are responsible for controlling the movements of a UAV and stability of a UAV. A poorly designed control surface can negatively impact the drone's stability, maneuverability, and responsiveness, and potentially leading to a crash. It can also result in excessive drag, which can reduce the drone's overall performance and endurance, limiting its ability to complete a mission.

Conversely, a well-designed control surface can improve the drone's stability, maneuverability, and responsiveness, allowing the user to control the drone with greater precision and accuracy. It can also reduce drag and increase the drone's range and endurance, enhancing its effectiveness in a variety of missions. In the case of Attack Drones, controllability is a very crucial factor, and hence, the need to design a drone that has a greater level of controllability than the rest arises. [8], [9]

8.1 Aileron Design

An important part of an airplane's control system that gives the user control over the rolling motion of the craft is the aileron. Ailerons cause the aircraft to roll by deflecting airflow over the wings, which creates lift.

Because it directly influences the aircraft's handling characteristics and overall performance, the aileron's design is of highest significance. The aircraft's

responsiveness to pilot inputs, its ability to roll swiftly, and its stability while in flight can all be affected by the size, shape, and location of the aileron.

For instance, a larger aileron can provide the user more control authority and allow for quicker roll rates, but it can also make the plane more susceptible to user inputs, thereby raising the possibility of overcontrolling or stalling the plane. A smaller aileron, on the other hand, might be less sensitive, but it might also result in a smoother, more stable flying.

Category	Examples of flight operation
A	(i) Air-to-air combat (CO); (ii) ground attack (GA); (iii) weapon delivery/launch (WD); (iv) aerial recovery (AR); (v) reconnaissance (RC); (vi) in-flight refueling (receiver) (RR); (vii) terrain following (TR); (viii) anti-submarine search (AS); (xi) close formation flying (FF); and (x) low-altitude parachute extraction system (LAPES) delivery.
B	(i) Climb (CL); (ii) cruise (CR); (iii) loiter (LO); (iv) in-flight refueling in which the aircraft acts as a tanker (RT); (v) descent (D); (vi) emergency descent (ED); (vii) emergency deceleration (DE); and (viii) aerial delivery (AD).
C	(i) Take-off (TO); (ii) catapult take-off (CT); (iii) powered approach (PA); (iv) wave-off/go-around (WO); and (v) landing (L).

Figure 37: Examples of flight operation [8]

Aileron placement on the wing is also crucial. It may not provide enough roll control or may result in undesirable pitch or yaw movements if not placed at right distance. The airflow across the wing and the overall aerodynamic effectiveness of the aircraft can be impacted by the shape of the aileron, especially its trailing edge profile and degree of curvature. [8], [9]

8.2 Design Requirements

8.2.1 Roll Surface Configuration

Due to the nature of the aircraft configuration, and the need for low cost and simplicity in design (for the sake of ease of manufacturing), aileron, a conventional roll surface configuration is selected. [8], [9]

8.2.2 Aircraft class and Critical Flight Phase

Referring to Sadraey's Aircraft design and observing how aircrafts are categorized based on their characteristics, the aircraft class 1 was selected due to the maximum take-off mass less than 6000kg. [8], [9]

Class	Aircraft characteristics
I	Small, light aircraft (maximum take-off mass less than 6000 kg) with low maneuverability
II	Aircraft of medium weight and low-to-medium maneuverability (maximum take-off mass between 6000 and 30 000 kg)
III	Large, heavy, and low-to-medium maneuverability aircraft (maximum take-off mass more than 30 000 kg)
IV	Highly maneuverable aircraft, no weight limit (e.g., acrobatic, missile, and fighter)

Figure 38: Aircraft classes [8]

Now for the flight phase since the drone needs to loiter over the target, category B was selected. The examples of the flight phases are shown below in the figure taken from Sadraey's Aircraft Design.

The third thing to be considered while designing the control surfaces is the level of acceptability in handling requirements. After careful consideration a level of acceptability of 3 was selected. The following figure (taken from Sadraey's Aircraft Design) defines the three levels of acceptability.

8.2.3 Handling Quality Design Requirements

Since the aircraft falls in class I, with flight phase B and 3 as a level of acceptability, the roll control handling qualities of aircraft require it to achieve a bank angle of 45° in 3.4 seconds.

Level	Definition
1	Flying qualities clearly adequate for the mission flight phase.
2	Flying qualities adequate to accomplish the mission flight phase, but some increase in pilot workload or degradation in mission effectiveness, or both, exists.
3	Flying qualities such that the airplane can be controlled safely, but pilot workload is excessive or mission effectiveness is inadequate, or both. Category A flight phases can be terminated safely, and Category B and C flight phases can be completed.

Figure 39: Handling Qualities Classification [8]

8.2.4 Aileron Position

The position of Aileron is very critical to stability and control of the UAV, and in turn influences the performance of the UAV. The position of the Aileron is defined as a function of wingspan. There are three parameters that need to be described before proceeding with the design (i.e., b_{ai}/b, b_{ao}/b, and b_a/b). From literature, we discovered that these value for b_{ai}/b should lie in the range of 0.6-0.8 and for b_{ao}/b it should not be lesser than b_{ai}/b and should not be greater than 1, for the b_a/b the range is 0.2-0.3. These parameters are clearly explained in reference to the wing in the figure below taken from Sadraey's aircraft design.

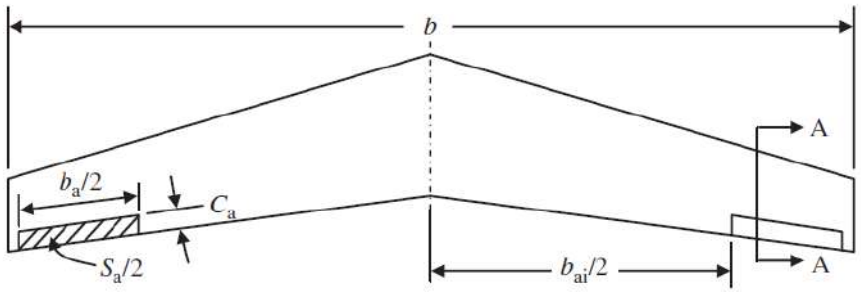

Figure 40: Aileron Parameters [8]

The values for these parameters were selected as follows:

$$\frac{b_{ai}}{b} = 0.6\ (Inward\ aileron\ span\ location\ to\ wing\ span\ ratio)$$

$$\frac{b_{ao}}{b} = 1.0\ (Outward\ aileron\ span\ location\ to\ wing\ span\ ratio)$$

$$\frac{b_a}{b} = 0.3\ (Aileron\ span\ to\ wing\ span\ ratio)$$

8.2.5 **Aileron Chord to Wing Chord Ratio**

After consulting Sadraey's aircraft design it was found that the recommended range for aileron chord to wing chord ratio was 0.15 – 0.25. Hence Aileron chord to wing chord ratio was selected to be 0.2.

8.2.6 **Aileron Effectiveness**

The capacity of the ailerons to produce the sufficient lift to begin and maintain a roll is referred to as aileron effectiveness. The ailerons' size, form, and placement on the wing all play a role in this. The effectiveness of a roll is boosted by the larger the aileron, which may generate more lift. Yet larger ailerons can also result in more drag, which reduces the UAV's overall speed and effectiveness.

For the calculation of aileron effectiveness parameter τ_a the graph from Sadraey's aircraft design was consulted. The graph's equation was used to find the effectiveness at the selected aileron chord to wing ratio. The equation for finding the aileron effectiveness is only valid for Aileron chord to wing chord ratio up to 0.7.

$$\tau_a = -6.108\left(\frac{C_a}{c}\right)^4 + 11.59(\frac{C_a}{C})^3 - 8.2457(\frac{C_a}{C})^2 + 3.225(\frac{C_a}{C})$$

Using this equation, the value for τ_a came out to be 0.4182.

8.2.7 **Aileron Rolling Moment Coefficient Derivative**

For the rolling moment coefficient derivatives, the following equation was utilized:

$$C_{l_\delta} = \frac{2(C_{l_{w3d}}\tau_a C_r)}{S_w b_w} \times \frac{{y_o}^2}{2} + \frac{2}{3}\left(\frac{\lambda_w - 1}{b_w}\right) \times y_o^3 - \left(\frac{y_i^2}{2} + \frac{2}{3}\left(\frac{\lambda_w - 1}{b_w}\right) \times y_i^3\right)$$

Where:

$$y_i = \frac{b_{ai}}{b} \times \frac{b_w}{2}$$

$$y_o = \frac{b_{ao}}{b} \times \frac{b_w}{2}$$

$$C_r = 1.5 \times MAC \times \left(\frac{1 + \lambda_w}{1 + \lambda_w + \lambda_w^2}\right)$$

The results obtained from the equations above yield a value of 0.1901 for Aileron Rolling Moment Coefficient Derivative.

8.2.8 **Maximum Aileron Deflection**

The maximum value for the deflection was selected as 20°. The typical values for maximum aileron deflection are ±25°.

8.2.9 **Aircraft Rolling Moment Coefficient**

This coefficient is represented in a symmetric aircraft with no sideslip and no rudder deflection as:

$$C_l = C_{l_\delta} \times \delta_{A_{max}} \times \frac{\pi}{180}$$

The parameter C_{l_δ} is known as the aircraft rolling moment coefficient..

MATLAB Script Aileron Design calculates the aircraft rolling moment coefficient when the aileron is deflected with the maximum deflection:

$$C_l = 0.0644$$

8.2.10 Aircraft Rolling Moment

Rolling moment of the aircraft (LA) is calculated when the aileron is deflected to its fullest extent. The average approach velocity is between 1.1 and 1.3 times the stall speed; hence the aircraft is said to be approaching at 1.3 Vs. For the approach flight operation, the sea-level altitude is also taken into account. We have the following using MATLAB Script Aileron Design:

$$V_T = 1.3V_s$$

$$L_A = \frac{1}{2}\rho_s(V_T^2)(S_w C_l b_w)$$

Using the above equations, we get $L_A = 4.015$

8.2.11 Steady-State Roll Rate

A transient state and a steady state can be distinguished in the aircraft's rate of roll response to aileron deflection. The roll rate (P) integral limit ranges from the beginning trim point of zero roll rate to the roll rate's steady-state value. The deflection of the aileron will eventually produce a steady-state roll rate since it is used as a rate control.

The steady-state roll rate is determined using MATLAB Script Aileron Design:

$$y_D = 0.4 \times \frac{b_w}{2}$$

$$C_{D_R} = 1$$

$$P_{ss} = \left(\frac{2L_A}{(\rho_s(S_w + 2P_{h_{area}})C_{D_R}(y_D^3)} \right)^{0.5}$$

Using the above equations, we find the value of $P_{ss} = 21.3200$

8.2.12 **Bank Angle**

Now the bank angle needs to be calculated at which the aircraft reaches steady-state roll rate using the following equation:

$$\phi_l = \frac{(I_{xx} \times \log P_{ss}^2)}{(\rho_s(S_w + 2P_{h_{area}}) \times C_{D_R} \times (y_D^3)}$$

Using the above equation, we get $\phi_l = 68.9581°$

8.2.13 **Aircraft Roll Rate**

Next, we have to calculate the aircraft roll rate that is produced by the aileron rolling moment until the aircraft reaches the steady-state roll rate using the following equation:

$$\dot{P} = \frac{P_{ss}^2}{2\phi_l}$$

$$\dot{P} = 3.2958$$

8.2.14 **Aileron Area Calculation**

After an extensive code for Aileron parameters, we obtained the following Aileron parameters:

Table 17: Aileron Parameters

Parameter	Value
b_a	0.2418 m
S_a	0.0167 m^2
MAC_a	0.0345 m
δ_{Amax}	20°

8.3 Elevator Design

Elevators are a crucial part of an aircraft's control system because they give the pilot control over the aircraft's pitch, or ability to move up and down. The elevator design is equally as significant for a UAV.

The size, weight, and planned usage of a UAV are a few of the variables that affect the elevator's construction. The elevator surfaces move up or down, respectively, when the pilot moves the control stick forward or backward, which causes the UAV to pitch up or down. [9]

The elevator surfaces' range of motion is yet another crucial factor. The elevator's range of motion should be sufficient to offer proper pitch control, but not excessive enough to make the UAV unsteady or challenging to control. The weight and speed of the UAV, among other things, determine how much elevator deflection is necessary to produce a specific pitch shift.

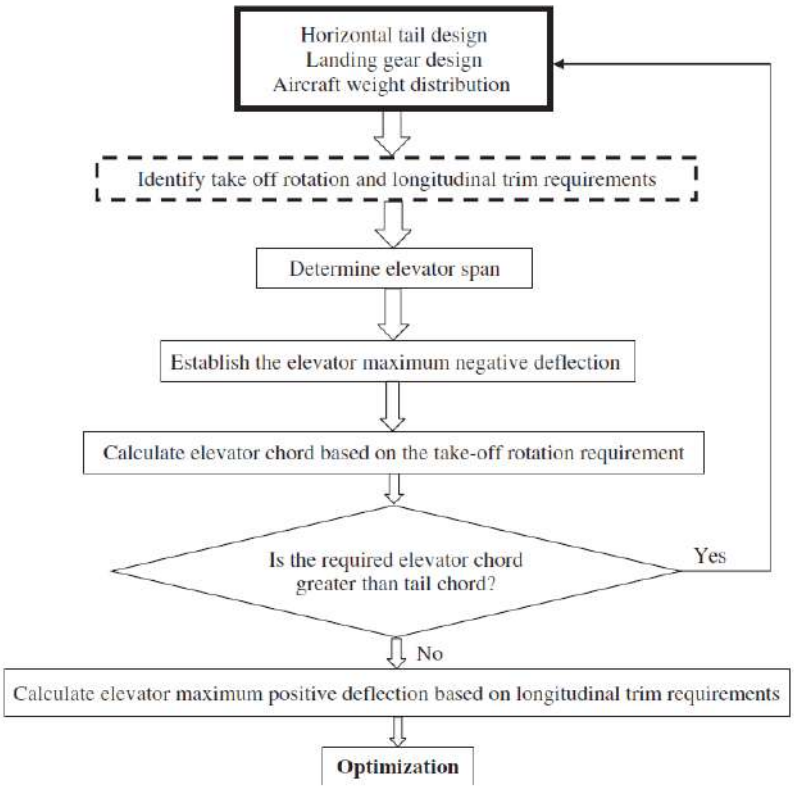

Figure 41: Elevator design flowchart [9]

The effectiveness of the elevator surfaces can also be impacted by their form and design. Both symmetrical and asymmetrical designs are possible for elevator surfaces, and each has advantages and problems of its own. Symmetrical elevators can offer good pitch control over a wide range of airspeeds and are often simpler in design. On the other side, asymmetrical elevators may be more challenging to design and make, but they can offer more precise control at high speeds. Designing the elevator requires the calculation of four main parameters that are elevator planform area, elevator chord, elevator span, and maximum elevator deflection. The following chart depicts how the elevator design is broken down into steps that yield the required dimensions for suitable elevator. [8], [9]

8.3.1 Elevator Requirements

The first step is to enlist the requirements for the elevator that needs to be designed. The main requirement for the elevator is that it should have low cost and must be easy to manufacture.

8.3.2 Elevator Span

The value of elevator span is usually expressed as the percentage of the control surface and the typical values for the elevator span range from 0.8 – 1.0. The ratio of elevator span to lifting surface span was selected as 0.83

$$\frac{b_E}{b_h} = 0.83$$

The following table contains typical values for various parameters that are throughout elevator design:

Control surface	Elevator	Aileron	Rudder
Control surface area/lifting surface area	$S_E/S_h = 0.15–0.4$	$S_A/S = 0.03–0.12$	$S_R/S_V = 0.15–0.35$
Control surface span/lifting surface span	$b_E/b_h = 0.8–1$	$b_A/b = 0.2–0.40$	$b_R/b_V = 0.7–1$
Control surface chord/lifting surface chord	$C_E/C_h = 0.2–0.4$	$C_A/C = 0.15–0.3$	$C_R/C_V = 0.15–0.4$
Control surface maximum deflection (negative)	−25 deg (up)	25 deg (up)	−30 deg (right)
Control surface maximum deflection (positive)	+20 deg (down)	20 deg (down)	+30 deg (left)

Figure 42: Elevator design parameters [8]

8.3.3 Maximum Elevator Deflection

Just as with the Aileron design, first four parameters needed to be selected, the same is the case with the elevator design and now the maximum elevator deflection needs to be determined. The elevator must be able to fulfil the required pitch control magnitude while also preventing the tail from stall. The table above provides some

typical values for maximum elevator deflection and hence a maximum deflection of 15 degrees was selected for the Elevator. [9]

8.3.4 Desired Tail Lift Coefficient

To validate the elevator design, an appropriate tail lift coefficient must be first specified. Its lift coefficient is often the same as that of a horizontal tail.

8.3.5 Elevator angle of Attack Effectiveness

An elevator's ability to adjust an aircraft's angle of attack, is referred to as its angle of attack effectiveness. The elevator's usefulness is based on its capacity to alter the lift force and pitching moment of the aircraft. The parameter 'τ_e' is used to denote the elevator angle of attack effectiveness and it can be calculated via the following equation:

$$\boldsymbol{\tau_e = \frac{\frac{C_{l_h}}{C_{l_{\alpha 3D}}} - \alpha_h}{\delta_e}}$$

Using the above equation,

$$\tau_e = 0.58$$

8.3.6 Elevator Chord Ratio

The effectiveness obtained in the previous step is then utilized for the calculation of the chord ratio which can be obtained by using the governing equation for the graph between effectiveness and chord ratio. The value for chord ratio at effectiveness of 1.0 turns out to be 1.0.

$$Chord\ Ratio = \frac{C_E}{C_h} = 0.38$$

8.3.7 Elevator Planform Area

Once the value of chord ratio and span is known, the elevator planform area can be calculated using the following equation:

$$S_E = b_E \times C_E$$

8.3.8 Validation of Elevator Parameters

In this step, CFD techniques are employed to calculate the tail coefficient at the maximum negative elevator deflection. Once calculated this value is compared with the required tail coefficient. If the two values are equal then the design is valid, if not the flowchart should be consulted again.

8.3.9 Non-Dimensional Derivatives

The next step, once the design is validated, is the calculation of the three non-dimensional derivatives that are the measure of longitudinal control power.

8.3.10 Longitudinal Control Power Derivative

The rate of change of the aircraft pitching moment coefficient with respect to elevator deflection is the non-dimensional derivative, which represents the longitudinal control power derivative, and it can be determined using the equation below:

$$C_{m_{\delta E}} = \frac{\partial C_m}{\partial \delta_E} = -\frac{C_{L_{\alpha_{h3D}}} \eta_h V_h b_E \tau_e}{b_h}$$

8.3.11 Contribution of Elevator to Aircraft Lift

It is the rate of change of aircraft lift with respect to elevator deflection and can be determined using the following equation:

$$C_{L_{\delta E}} = \frac{\partial C_L}{\delta_E} = -\frac{C_{L_{\alpha_{h3D}}} \eta_h S_h b_E \tau_e}{S_w b_h}$$

8.3.12 Contribution of Elevator to Tail Lift Coefficient Derivative

It is the rate of change of the tail lift coefficient with respect to the elevator deflection and can be determined using the following equation:

$$C_{L_{h_{\delta E}}} = \frac{\partial C_{L_h}}{\partial \delta_E}$$

8.3.13 Calculation of Elevator Deflection for Required Longitudinal Trim

In order to get the necessary elevator deflection, we must first determine the angle of attack at which the highest deflection is required. The following equations are used to calculate the deflection and angle of attack required.

$$\alpha = \frac{(C_{L_1} - C_{L_0})C_{m_{\delta E}} + (C_{m_o})C_{L_{\delta E}}}{C_{L_\alpha} C_{m_{\delta E}} - C_{m_\alpha} C_{L_{\delta E}}}$$

$$\delta_E = \frac{(C_{L_1} - C_{L_0})C_{m_\alpha} + (C_{m_o})C_{L_{\delta E}}}{C_{L_\alpha} C_{m_{\delta E}} - C_{m_\alpha} C_{L_{\delta E}}}$$

8.3.14 Final Elevator parameters

Table 18: Elevator Parameters

Parameter	Value
S_E	0.0112 m^2
b_E	0.3385 m
C_E	0.0332 m
δ_{Emax}	±15°

8.4 Rudder Design

A major flight control surface on an aircraft called a rudder. The yaw, or the side-to-side movement of the aircraft around its vertical axis, is managed by the rudder. Rudders are crucial for directing the aircraft and preserving flight stability in unmanned aerial vehicles (UAVs). A UAV's rudder design plays a key role in determining how precisely and safely the aircraft can fly. A side force acts on it when it is deflected on either side, creating a yawing moment of the aircraft's center of gravity. Because most rudders are located above the aircraft's center of gravity, this yaw is accompanied by a brief rolling moment. The following figure represents rudder deflection and

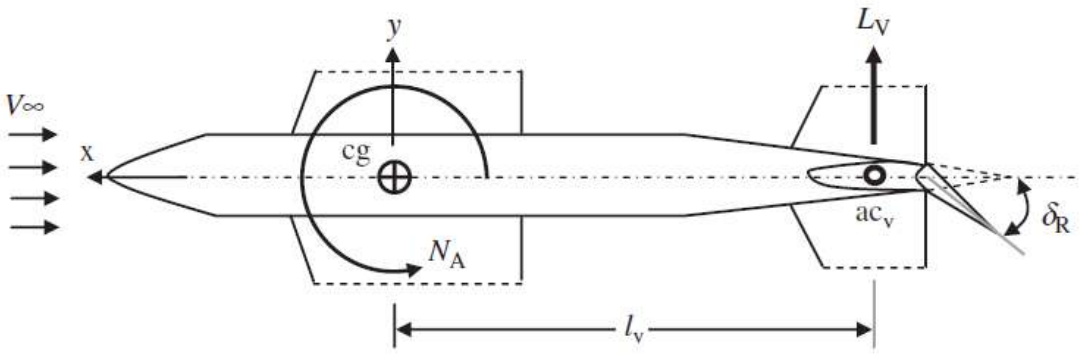

Figure 43: Free body diagram of Elevator Deflection [8]

how the forces bring about the change in direction of the aircraft. [8], [41]

Rudder deflection to the left is typically regarded as positive, and any deflection will result in a yawing moment near the center of gravity in the exact opposite direction. The following flowchart represents the stages in rudder design:

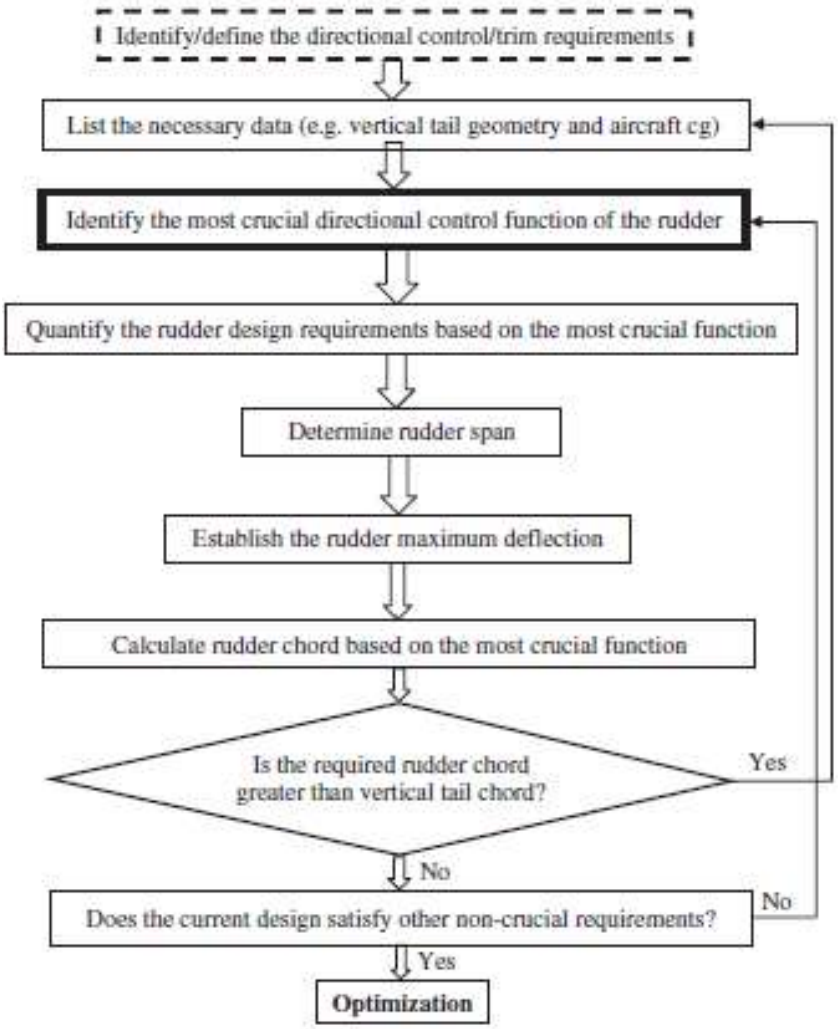

Figure 44: Rudder design flowchart [9]

8.4.1 **Vertical Tail Geometry**

Before starting with the dimensional and performance related parameters, it is essential to restate the relevant parameters of the vertical tail. The table below encapsulates the relevant vertical tail parameters.

Table 19: Effective vertical tail parameter

Parameter	Value
Planform area Sv	0.0356 m^2
Span bv	0.4078 m
Chord Cv	0.087 m
Aspect Ratio ARv	4

8.4.2 Spin Recovery

The spin recovery, which necessitates that the UAV be quick enough to exit the spin once it has entered it, is the most crucial design factor for Rudder. A spin is a self-sustaining rotation of an aircraft around its vertical (z) axis when its mean angle of attack of wings is greater than its stall angle. The aircraft can be brought out of spin with the help of a strong rudder.

In addition to the rudder, the geometry of the fuselage and the aircraft mass moments of inertia in various axes both significantly influence the spin recovery characteristics.

8.4.3 Angle of Attack During Spin Maneuver

Experimental measurements reveal that the angle of attack during a spinning motion often ranges between 30 and 60 degrees, depending on the kind of aircraft.

$$\alpha_{spin} = 40°$$

8.4.4 Mass Moments of Inertia

With a spin-recovery rudder, it's crucial to calculate the mass moments of inertia known as rolling inertia (I_{xx}), yawing inertia (I_{zz}), and the product of inertia (I_{xz}). FEA of the model was used to calculate these moments of inertia in the body-axis coordinate

system, and after that, a transformation matrix based on the spin angle of attack will be used to calculate them in the wind-axis coordinate system:

$$\begin{bmatrix} I_{xx_w} \\ I_{zz_w} \\ I_{xz_w} \end{bmatrix} = \begin{bmatrix} \cos^2 \alpha_{spin} & \sin^2 \alpha_{spin} & -\sin 2\alpha_{spin} \\ \sin^2 \alpha_{spin} & \cos^2 \alpha_{spin} & \sin 2\alpha_{spin} \\ \frac{1}{2}\sin 2\alpha_{spin} & -\frac{1}{2}\sin 2\alpha_{spin} & \cos 2\alpha_{spin} \end{bmatrix} \begin{bmatrix} I_{xx_B} \\ I_{zz_B} \\ I_{xz_B} \end{bmatrix}$$

The moments of inertia about the body-axes and wind-axes are indicated by the subscripts "B" and "w," respectively. During a spin, the aircraft is no longer revolving along its own axis but is instead being rotated by the wind, necessitating this transformation. Using the FEA model, the values obtained were:

$$\begin{bmatrix} I_{xx_B} \\ I_{zz_B} \\ I_{xz_B} \end{bmatrix} = \begin{bmatrix} 0.0509 \\ 0.213 \\ -0.0029 \end{bmatrix}$$

Now using the transformation matrix, moments of inertia about the wind axis can be obtained:

$$\begin{bmatrix} I_{xx_B} \\ I_{zz_W} \\ I_{xz_W} \end{bmatrix} = \begin{bmatrix} 0.1207 \\ 0.1432 \\ -0.0803 \end{bmatrix}$$

8.4.5 Desirable Rate of Spin Recovery

The majority of general aviation aircraft must recover from a one-turn spin in less than three seconds, which necessitates the following spin recovery rate:

$$\dot{R_{SR}} = 1.4 \frac{Rad}{s^2} = 80 \frac{degrees}{s^2}$$

This value was taken from Sadraey's Aircraft Design and is recommended as the desirable rate of recovery.

8.4.6 Required Counteracting Yawing Moment

The rudder deflection creates the counteracting moment of yaw that is required to quickly cease the spinning motion. The value for the required counteracting yawing moment can be calculated using the following equation:

$$N_{SR} = \left(\frac{I_{xx}I_{zz} - I_{xz}^2}{I_{xx}}\right)_w R_{SR}$$

Substituting the values, the required counteracting yawing moment comes out:

$$N_{SR} = 0.1256\ Nm$$

8.4.7 Effective Vertical Tail Area and Volume Ratio

A UAV with a traditional aft tail will suffer wake from the horizontal tail during a spin maneuver, which will affect the performance of the vertical tail and the rudder. As a result, the volume coefficient and effective vertical tail area will be lower than the actual values.

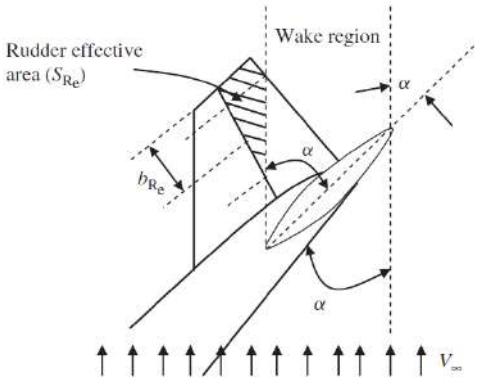

Figure 45: Effective Vertical tail area at alpha AOA [8]

The effective rudder tail volume ratio is calculated using:

$$\bar{V}_{V_e} = \frac{l_V S_{V_e}}{bS}$$

Where S_{Ve} is the effective vertical tail area,

$$\bar{V}_{V_e} = 0.18$$

8.4.8 Rudder- Vertical Tail Span Ratio

The ratio of rudder span to span of vertical tail is an important parameter that needs to be determined. The values for this ratio are between 0.7 and 1.0 (both limits included). Hence, the value of the span ratio was selected as:

$$\frac{b_R}{b_V} = 0.83$$

8.4.9 Effective Rudder Span

$$b_{R_E} = b_R$$

8.4.10 Maximum Rudder Deflection

To prevent flow separation and its detrimental effects, the maximum deflection a rudder is permitted to have must be restricted. Consulting Sadraey's aircraft design, the selection of maximum rudder deflection was made easier and hence the following value was selected for rudder deflection:

$$\delta_R = \pm 15°$$

It is customary to interpret rudder deflection to the left as positive and to the right as negative. We utilize this value as a benchmark to improve the performance of our rudder design. The rudder needs to be redesigned if the calculated maximum deflection is greater than this value.

8.4.11 Rudder to Vertical Tail Chord Ratio

Just like with the span ratio, the typical values for the rudder chord ratio are between 0.15-0.4. However, if the calculated chord ratio exceeds 0.5 then that means the design

calls for an all moving tail. The chord ratio was selected to be 1.0 since the intention was to have an all moving tail for greater maneuverability.

$$\frac{C_R}{C_V} = 0.38$$

8.4.12 Rudder Angle of Attack Effectiveness

This metric, which assesses the effect of rudder size on rudder control efficacy, is a function of the rudder-tail chord ratio. A graph of observed values between the angle of attack effectiveness and the chord ratio is used to determine it.

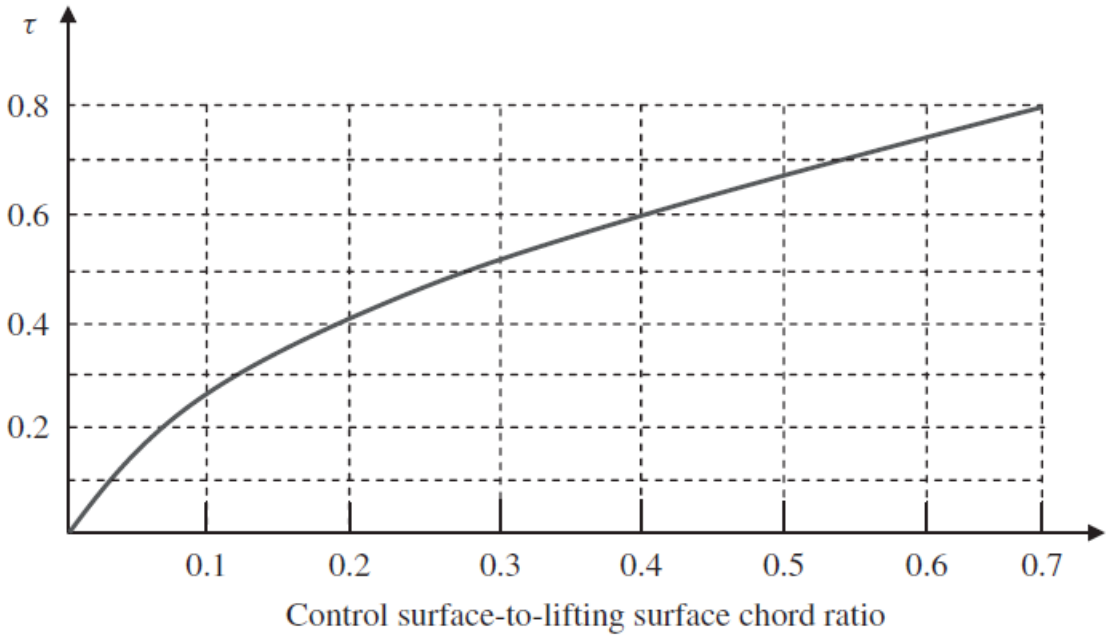

Figure 46: Angle of Attack Effectiveness vs Control Surface to Lifting Surface Chord Ratio [8]

By approximation, the angle of attack effectiveness was determined and the value came out to be

$$\tau_R = 0.5816$$

8.4.13 Rudder Control Derivative

It is the derivative of directional control, often known as the yawing moment coefficient resulting from rudder deflection. It is also known as the power to control yaw. This

derivative essentially tells us how the yawing rate will change in response to changing the rudder deflection either increasing or decreasing. The rudder control derivative can be calculated using the following equation:

$$C_{n_{\delta R}} = -\frac{C_{L_{\alpha_{v_{3D}}}} \bar{V}_v \eta_v \tau_R b_R}{b_v} = -0.0317 \frac{1}{rad}$$

8.4.14 Verification

To ensure that our design is acceptable, we will now determine the maximum rudder deflection from other equations. The following also provides the required counteracting yawing moment (already found):

$$N_{SR} = \frac{1}{2} \rho V_s^2 S_w b_w C_{n_{\delta R}} \delta R$$

Rearranging the above equation to find the rudder deflection:

$$\delta R = \frac{2N_{SR}}{\rho V_s^2 S_w b_w C_{n_{\delta R}}} = -10.87\ °$$

There is no need to modify the rudder design because the value falls well within the previously set maximum deflection.

8.4.15 Final Rudder Design Parameters

Table 20: Rudder Parameters

Parameter	**Value**
b_R	0.4078 m
C_R	0.08 m
S_R	0.0326 m^2
δ_{Rmax}	±15°
Required δ_R	±10.87°

Chapter 9: Mission Profile

CFD simulation

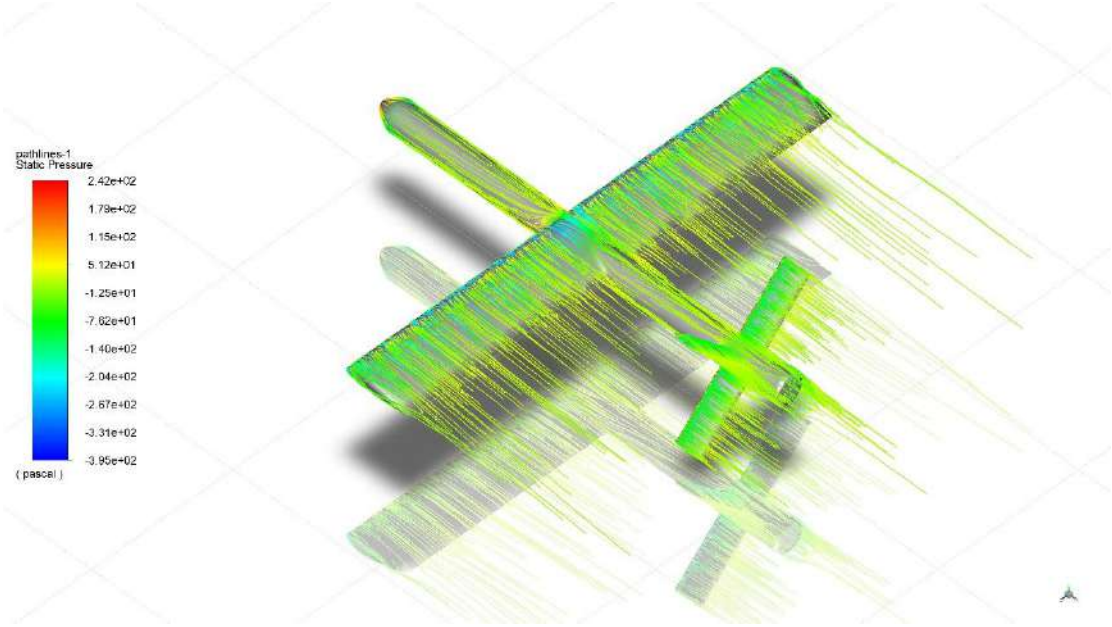

Table 21 Drag Coefficients at different flight modes

Flight Mode	Drag Coefficient
During Cruise	0.0105
During Loitering	0.0213
During Climbing	0.0345

Hence, exact mission profile time can be calculated as follows:

$$\rho_{air} = 1.225\ kg/m^3$$

$$S_{ref} = 1\ m^2$$

$$V_c = 21.4\frac{m}{s}$$

$$V_{climb} = 13\frac{m}{s}\ at\ \alpha = 9\ degree$$

$$V_{loiter} = 15.3\ m/s\ at\ \alpha = 9\ degree$$

9.1 Mission Profile Calculation

For Cruise:

Thrust during cruise

$$T = \frac{1}{2} \times \rho_{air} \times S_{ref} \times V_c^2 \times C_{D_{cruise}}$$

$$T = \frac{1}{2} \times 1.225 \times 21.4^2 \times 0.0105$$

$$T = 2.94\ N$$

For Climb:

Thrust during cruise

$$T = \frac{1}{2} \times \rho_{air} \times S_{ref} \times V_{climb}^2 \times C_{D_{climb}}$$

$$T = \frac{1}{2} \times 1.225 \times 13^2 \times 0.0213$$

$$T = 2.2\ N$$

For Loiter:

Thrust during cruise

$$T = \frac{1}{2} \times \rho_{air} \times S_{ref} \times V_c^2 \times C_{D_{loiter}}$$

$$T = \frac{1}{2} \times 1.225 \times 15.3^2 \times 0.0345$$

$$T = 0.32\ N$$

Power Requirement:

$$P_{motor} = \frac{VT}{\eta_{propeller}}$$

Assuming 50 % propeller efficiency and climb velocity same as cruise:

$$P_{cruise} = \frac{21.4 \times 2.94}{0.5} = 125\ W$$

$$P_{climb} = \frac{13 \times 2.2}{0.5} = 57.2\ W$$

$$P_{loiter} = \frac{15.3 \times 0.32}{0.5} = 9.79\ W$$

Since, TATTU 4S 14.7V 2300 mAh Li-Po Battery is selected which weighs 224 g.

$$Battery\ Capacity = E_{required} \times \frac{1000}{14.7}$$

$$E_{required} = 33.81\ Wh$$

Assuming cruise flight of 30 minutes and 1 minute of climb,

$$E_{required} = P_{cruise} \times \frac{x}{60} + P_{loiter} \times \frac{x \times 0.3}{60} + P_{climb} \times \frac{1}{60}$$

$$33.81 = 125 \times \frac{x}{60} + 9.79 \times \frac{x \times 0.3}{60} + 57.2 \times \frac{1}{60}$$

$$x = 16.6\ minutes$$

$$Endurance = x + 0.3 \times x + 1 = 22.58\ minutes$$

Maximum Attack Speed

To maintain controllability during attack, attack angle is selected as 15 degree hence,

$$Maximum\ Motor\ Thrust = \ 3.1\ kg = 30.4\ N$$

$$P_{max}\ \eta_{prop} = TV_{ter}$$

$$Drag\ Power\ Losses = 0.5C_D\rho S$$

$$Drag\ Power\ Losses = 0.5(0.14)(1.225)(1) = \ 0.0857\ W.\frac{m}{s}$$

$$W\sin(\gamma) = 2 \times 9.81 \times (\sin(15)) = 49\ W$$

Power Equation

$$P_{max}\ \eta_{prop}V_{ter} - 0.5C_D\rho SV_{ter}^3 + W\sin(\gamma)\,V_{ter} = 0$$

$$T(V_{ter})^2 - 0.5C_D\rho SV_{ter}^3 + W\sin(\gamma)\,V_{ter} = 0$$

$$V_{ter} = 72\ m/s$$

Chapter 10: Analysis

10.1 Fuselage Structure Analysis

10.1.1 Stress in Former

In aircraft design, a former refers to a structural element that provides shape and support to the fuselage. Formers are placed perpendicular to the longitudinal axis of the airplane and are spaced at regular intervals to provide structural stability and rigidity to the fuselage.

Stress analysis of formers is essential in aircraft design because it helps ensure that the fuselage structure can withstand the various stresses and forces that it will experience during flight. Structural analysis was performed by applying 30 N load at wing connecting position and fixing each end of the fuselage. Stress contours of formers as a result of previous boundary conditions are shown.

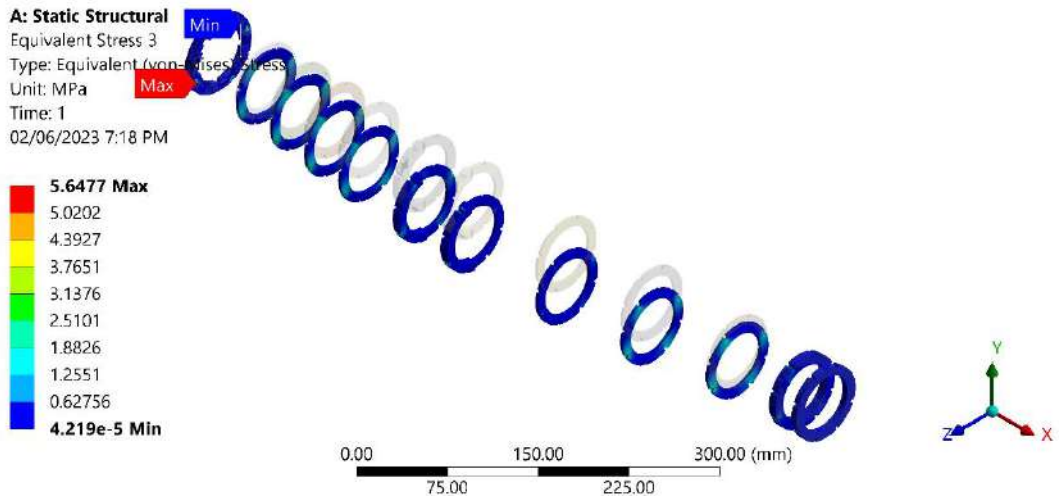

Figure 47: Stress in formers

$$maximum\ von-misses\ stress\ in\ formers = 5.64\ MPa$$

Since PLA material has strength of more than 30 MPa, hence it is safe to use PLA to manufacture formers of fuselage.

10.1.2 Stress in Stringers

In aircraft design, a stringer is a longitudinal structural element that runs parallel to the fuselage's longitudinal axis. Stringers are typically placed between the formers and help distribute the loads and stresses over a larger area.

Stress analysis of stringers is necessary in aircraft design because it helps ensure that the structure can withstand the various stresses and forces that it will experience during flight. Structural analysis was performed by applying 80 N load at wing connecting position and fixing each end of the fuselage. Stress contours of formers as a result of previous boundary conditions are shown.

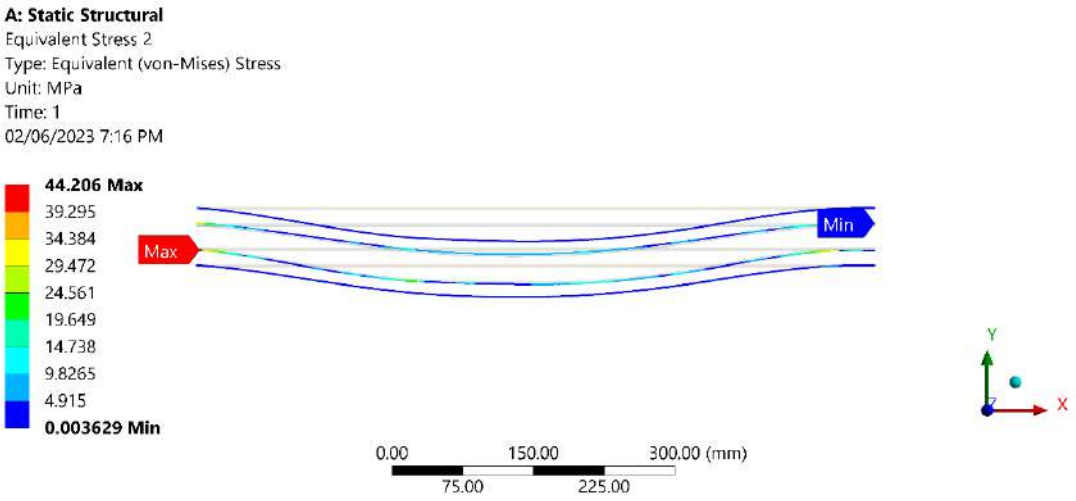

Figure 48: Stress in stringers

$$maximum\ von-misses\ stress\ in\ Stringers = 44.2\ MPa$$

Since carbon fiber has strength of more than 600 MPa, hence it is safe to use carbon rods as stringers of fuselage. Since carbon fiber is light weight and since it has high young modulus value, deflection in fuselage will be small during flight which is important for efficient flight performance.

10.1.3 Stress in full Structure

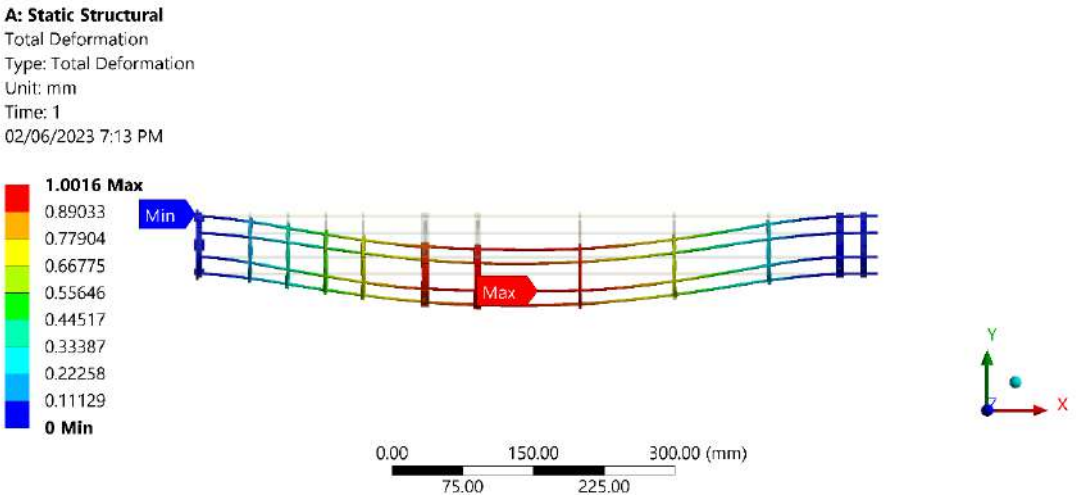

Figure 49: Stress in structure

10.1.4 Stress in fuselage shell

Stress analysis of fuselage body is performed to see stress in fuselage shell due to small deflection in fuselage structure. The maximum stress is only 1.1085 which is quite below both longitudinal (17 MPa) and lateral strength (2MPa) of balsa wood. Hence, from structural analysis it can be concluded that using balsa wood for fuselage shell is safe since minimum S.F is 1.81

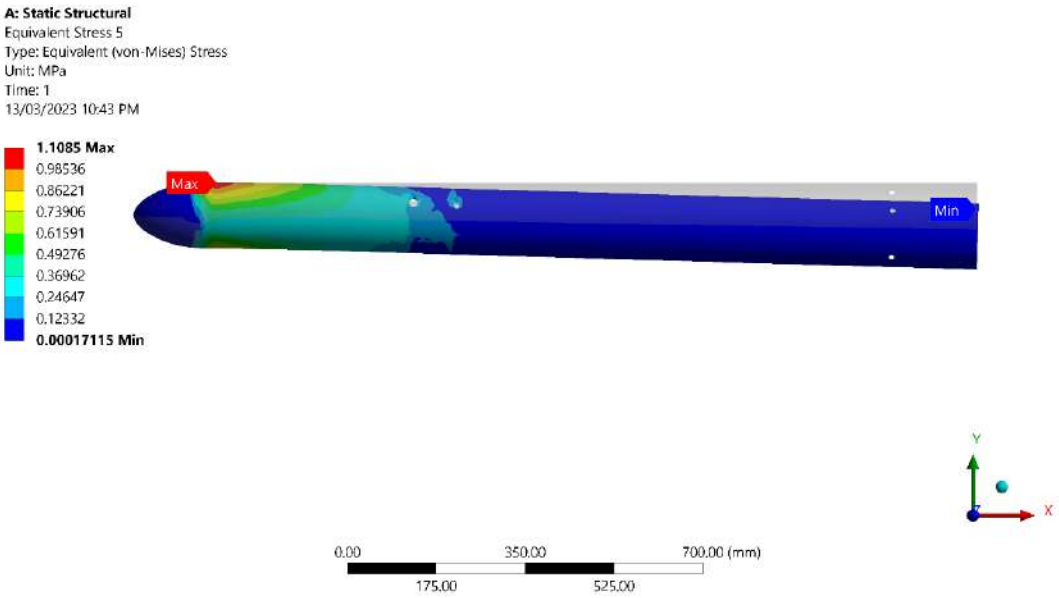

Figure 50: Stress in fuselage shell

10.2 Wing Structural Analysis

10.2.1 Stress in Wing

A wing must be able to withstand many kinds of of loads, like its own weight, lift force, drag force etc. Structural analysis helps to determine the appropriate materials and design for the wing, as well as the size and placement of structural members such as spars, ribs, and stringers. This ensures that the wing is able to support the weight of the aircraft and generate the lift required for flight.

In this analysis, 13 N distributed upward load, which is half of MTOW, is applied on wing and 10 N backward load along longitudinal axis applied to compensate drag force on wings during flight. Resultant stress contours on wing structure are shown.

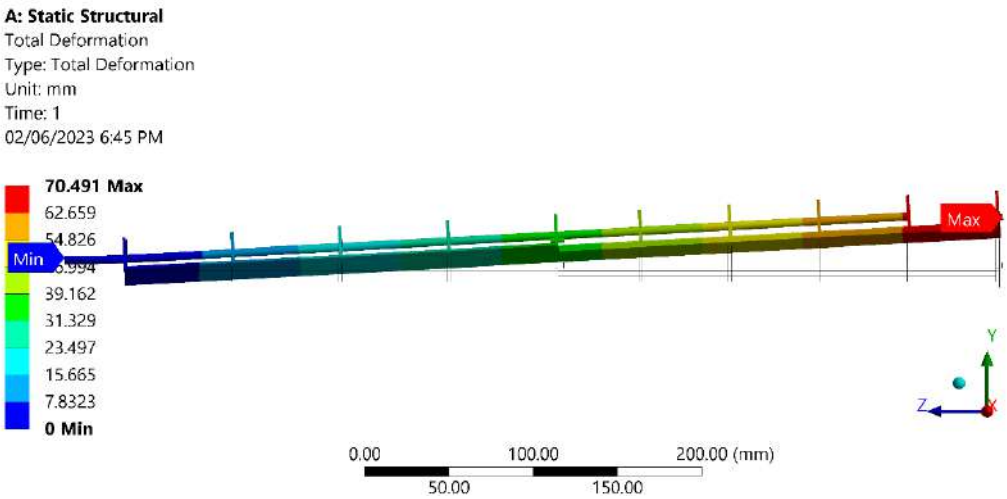

Figure 51: Stress in wing structure

$$Maximum\ von-mises\ stress\ on\ wing\ spar = 189.88\ MPa$$

$$Maximum\ von-mises\ stress\ on\ leading\ ribs = \ 17.5\ MPa$$

$$Maximum\ von-misses\ stress\ in\ other\ ribs = 4.2\ MPa$$

To ensure optimal strength and safety, usage of a carbon fiber spar with a tensile strength of 600 MPa, PLA for the leading rib with a tensile strength of 37 MPa, and balsa wood for additional support with a tensile strength of 17 MPa is recommended. Implementing this combination of materials will result in a safety factor of 7.5 for the carbon fiber spar, and 2.1 and 2.4 for the leading rib and rest of the ribs, respectively.

10.2.2 Stress in Wing Spar

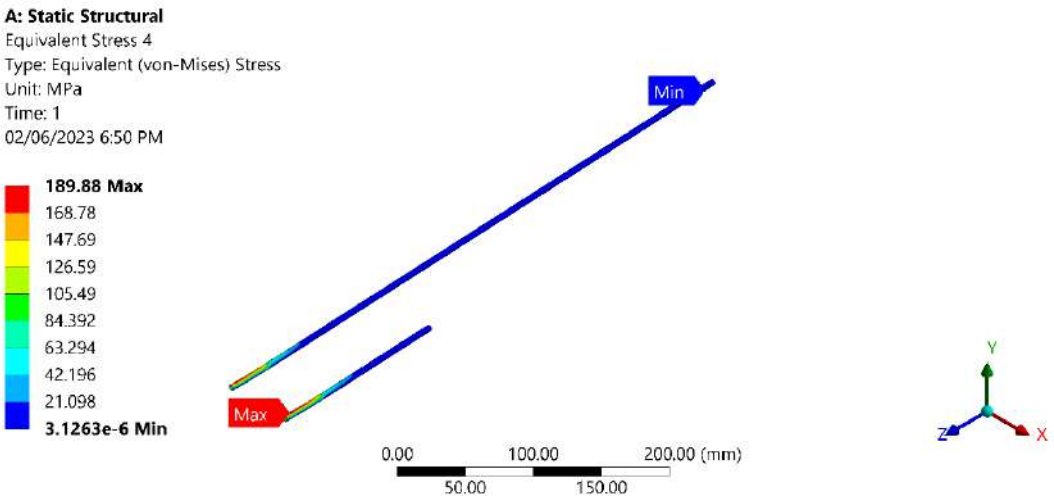

Figure 52: Stress in wing spar

10.2.3 Stress in Rib

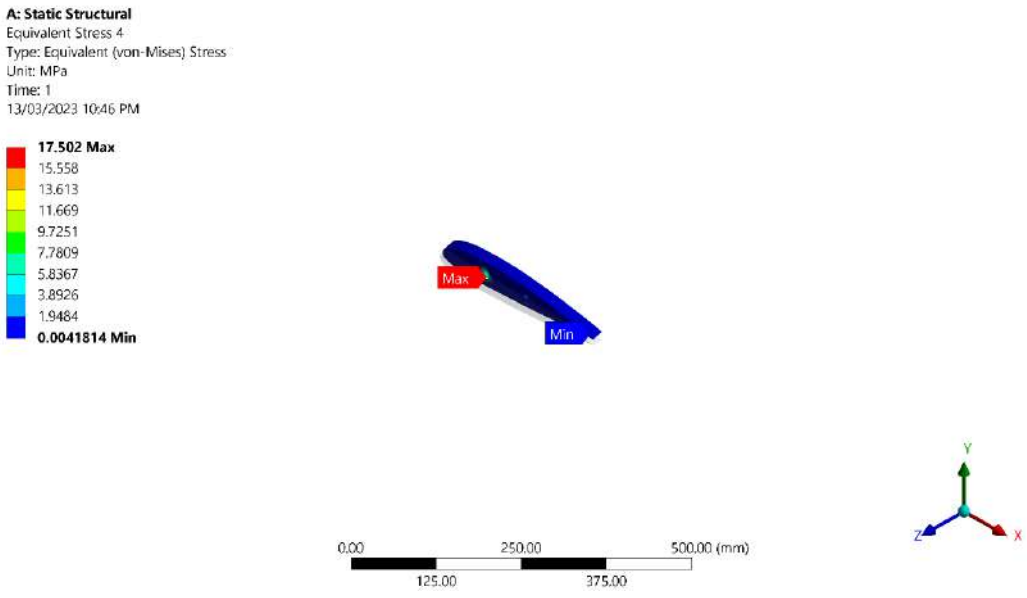

Figure 53: Stress in leading rib

10.2.4 Total Stress in Wing

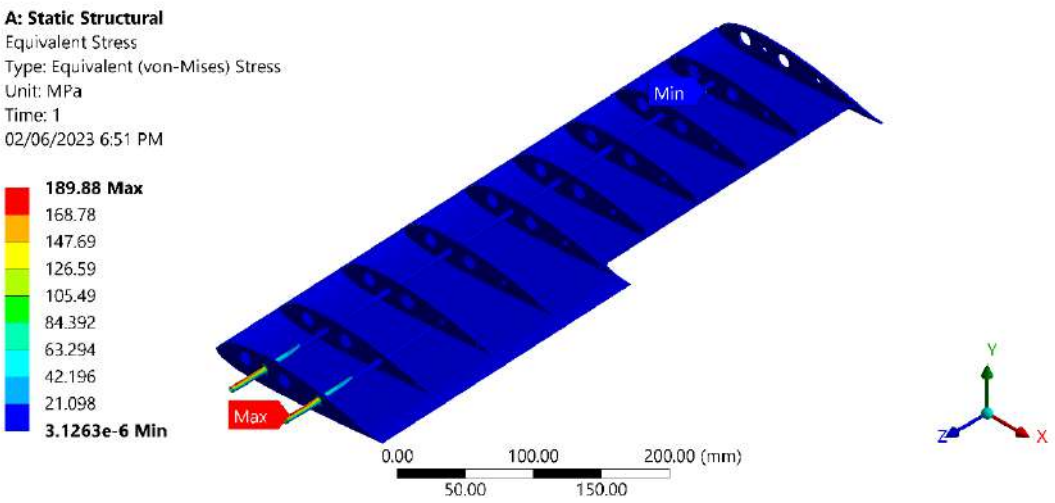

Figure 54: Stress in wings

10.3 Aerodynamic Stability Analysis

It is also important to validate the stability of the aircraft in its primary axes of freedom. The UAV must have sufficient lateral and longitudinal stability to sustain level flight in cruise mode.

For aerodynamic stability analysis it important that we have location of point mass of each component of UAV whether it is avionics components or structural components. These point masses are given as data to XFLR5 software with respect to leading edge. The software determines the CG location and stability of the UAV by using the point masses data. The points masses are shown in figure and table also the CG location in shown in figure

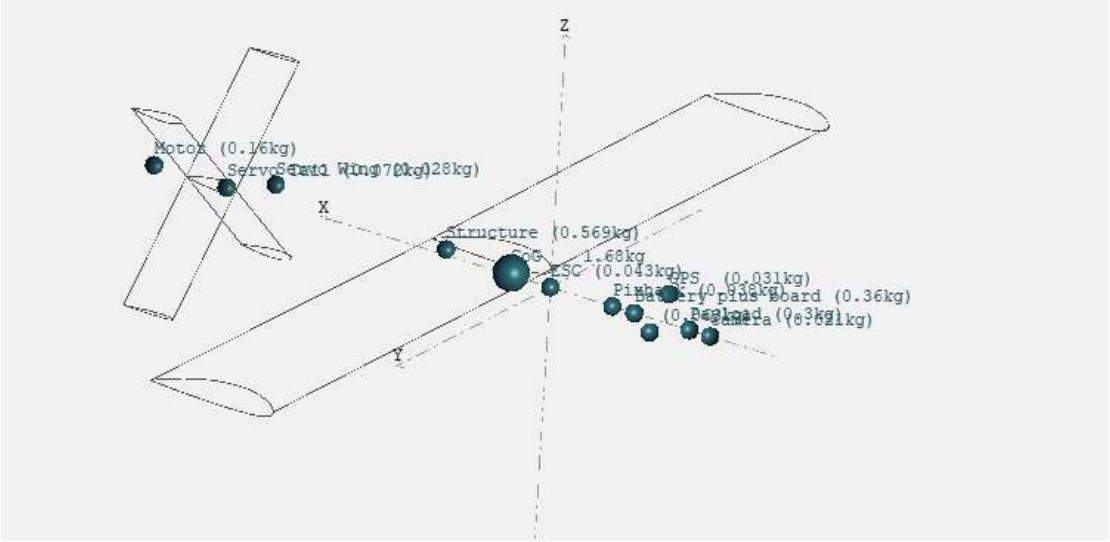

Figure 55: Mass distribution of UAV in XFLR5

Table 22: Mass distribution with position

Mass (kg)	X (m)	Y (m)	Z (m)	Description
0.67	0.1	0	0	Structure
0.25	-0.45	0	0	Payload
0.36	-0.410	0	0	Battery plus Board
0.068	-0.13	0	0	Pixhawk 6C
0.180	0.585	0	0	Motor
0.063	0.380	0	0	ESC
0.1	0.5	0	0	Servo Tails
0.02	0.1	0.5	0.023	Servo Wing 1
0.1	0	0	0.038	GPs
0.02	0.1	-0.5	0.023	Servo Wing 2
0.1	0.3	0	0	Wires

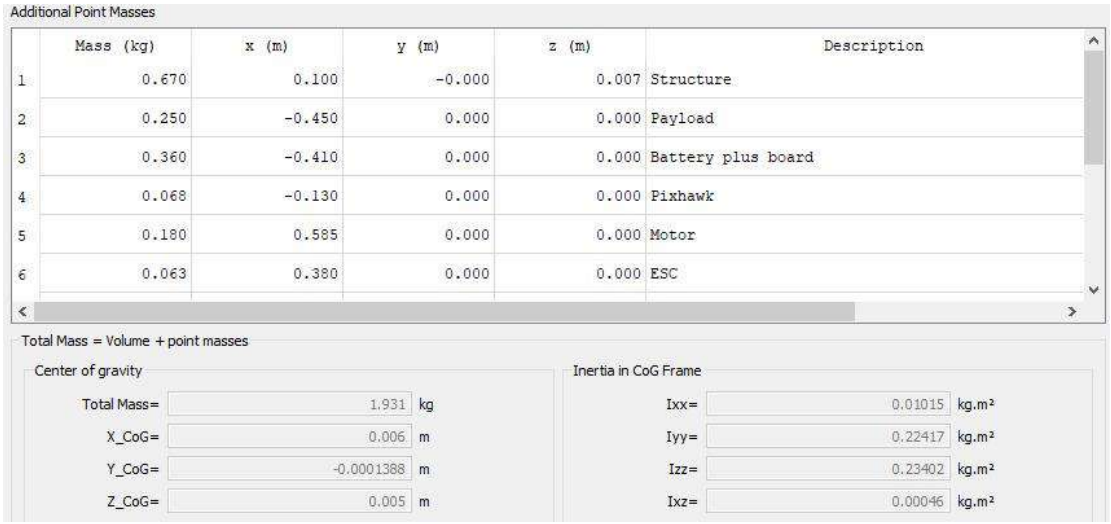

Figure 56: XFLR5 interface with CG

The first thing to check is the stability margin of the plane which indicates how stable is the plane in cruise. Stability Margin is calculated by:

$$S.M = -\frac{C_{m_\alpha}}{Cl_\alpha}$$

Where C_{m_a} is pitching moment derivative and C_{l_a} is lift curve slope. By putting the values of these derivative shown in figure the stability margin comes out to be 7.9 % which is a good value indicating that UAV is longitudinally stable in cruise flight.

```
Longitudinal derivatives
Xu=     -0.14147          Cxu=    -0.023653
Xw=      0.33185          Cxa=     0.055485
Zu=     -0.76123          Czu=    -0.015289
Zw=       -28.74          CLa=       4.8051
Zq=      -3.1921          CLq=       6.0817
Mu=   -0.0025158          Cmu=   -0.0023966
Mw=     -0.39746          Cma=     -0.37863
Mq=     -0.56639          Cmq=      -6.1483
Neutral Point position=   0.07005 m

Lateral derivatives
Yv=       -2.953          CYb=     -0.49373
Yp=     -0.15175          CYp=    -0.042287
Yr=        1.329          CYr=      0.37035
Lv=    -0.089536          Clb=    -0.012475
Lp=      -2.0967          Clp=     -0.48688
Lr=      0.15112          Clr=     0.035093
Nv=       1.2282          Cnb=      0.17112
Np=    0.0089281          Cnp=    0.0020732
Nr=     -0.54122          Cnr=     -0.12568
```

Figure 57: Longitudinal and Lateral derivatives at cruise

Chapter 11: Avionics & Software

11.1 Avionics

In this section we will discuss the avionics components present in our UAV as avionics play an important role in controlling and monetarizing the flight.

11.1.1 Flight Controller

The flight controller is a critical component of a UAV, as it is tasked with stabilizing the aircraft, executing precise flight maneuvers, and providing flight data to the pilot. We have used Pixhawk 6c flight controller for our UAV.

Figure 58: Pixhawk 6c [42]

The Pixhawk® 6C is the latest version Pixhawk® flight controller family. Based on the Pixhawk® FMUv6C Open and Connector Standard it comes with STM32H743 processor and RAM. Additionally, the Pixhawk® 6C comes pre-installed with PX4 Autopilot®. [43]

11.1.2 Telemetry

Telemetry involves the transmission of real-time flight data from the drone to a ground station, allowing the pilot or operator to monitor the drone's status and make adjustments as needed. To ensure the seamless integration with mission planner we use CUAV 3DR Radio Telemetry.

Figure : CUAV 3DR Radio Telemetry 59 [44]

The CUAV 3DR Radio Telemetry is a compact, lightweight, and cost-effective open-source radio platform compatible with Pixhawk 6c making it easy to set up a telemetry connection between your autopilot and a ground station. The radio uses open-source firmware designed to work seamlessly with MAVLink packets and integrate with popular software such as Ardupilot, QGroundControl, Mission Planner, and PX4 Autopilot.

11.1.3 Battery

Batteries are a crucial component of UAV to run the aircraft's electric motors, onboard electronics, and other systems. To ensure all the requirements are met 4S 14.8v Tattu 45C lipo battery is used.

Figure 60: 4S 14.8v Tattu 45C lipo battery

4S 14.8v Tattu 45C lipo battery pack features a battery management system (BMS), compact form factor, self-balancing function gives great battery timing for flight as well power.

11.1.4 Motor

Motors are a critical component of UAV as they provide the necessary thrust to lift the aircraft off the ground and maintain flight. For easier installation with the fuselage, a long shaft motor was desired. Based on the design requirements EMAX GT2826/04 1090KV Thrust 3100 gram 3kg is selected for our UAV.

Figure 62: EMAX GT2826/04 1090KV Thrust 3100 gram 3kg

11.1.5 Propeller

Propellers are a crucial component of unmanned aerial vehicles (UAVs), as they provide the necessary thrust to lift the aircraft off the ground and maintain flight by converting rotary motion into linear thrust. APC 10x5E propeller is used in combination with motor to provide the required thrust according to UAV design and also recommended by the motor manufacturer.

Figure 63: APC 10 × 8E

11.1.6 ESC

An electronic speed controller (ESC) is a critical component of UAV responsible for controlling the speed of the motor that drives the propellers. Hobbywing skywalker 3-4s 40AMP V2 ESC is used in our UAV.

Figure 61: Hobbywing skywalker 3-4s 40AMP V2 ESC

The Hobbywing skywalker 3-4s 40AMP V2 ESC features Safety arming, Throttle calibration function, user programmability and protection against overheat.

11.1.7 Servos

Servos are another essential component of a UAV, used to control the movement surfaces on fixed-wing drones. SG90s full metal gear servo motor is used in our UAV.

Figure 62: SG90s full metal gear servo

SG90s full metal gear servo Motor is a high speed, reliable and optimized servo which provides good torque, holding power, and faster updates in response to external forces.

11.2 Software

11.2.1 Ground Control Station

ArduPilot Mission Planner is used as a Ground Control Station software for calibration of sensors and flight testing of UAV. Mission Planner is a software application that can be used as both a configuration utility and a dynamic control supplement for autonomous vehicles.

As a configuration utility, Mission Planner allows users to configure and customize various aspects of their autonomous vehicle, such as setting up the flight plan,

configuring sensors and cameras, adjusting flight parameters, and calibrating the vehicle's systems.

As a dynamic control supplement, Mission Planner allows users to monitor and control their autonomous vehicle in real-time during flight. This can include tasks such as adjusting the flight path, changing flight modes, and monitoring telemetry data.

Figure 63: Mission Planner Home Screen [45]

Overall, Mission Planner is a powerful tool that can be used to streamline and enhance the capabilities of autonomous vehicles, making them more efficient, effective, and safe.

11.2.2 Sensor Calibration

Mission Planner is used to calibrate different sensors on the Flight Controller (Pixhawk® 6C). The Flight Controller is connected to the Mission Planner and the sensors are calibrated on the Setup screen under the section Mandatory Hardware in Mission Planner. Following sensors are calibrated in in the given order.

11.2.3 Accelerometer

Under the Mandatory Hardware section, Calibrate Accel button is used to calibrate accelerometer. The calibration of accelerometer is done by calibrating the three axes to zero in all the six positions (level, left side, right side, nose down, nose up and back) in the order given by Mission Planner in the accelerometer calibration mode. The six different positions for a tri-copter are illustrated in Figure 38.

Figure 64: Accelerometer Calibration positions

During accelerometer calibration, except for the Level position, the exact angle for the positions is not mandatory. The angle can deviate up to 20 degrees. The important thing is to keep the vehicle still. It is better to calibrate the Flight Controller while mounted on the vehicle.

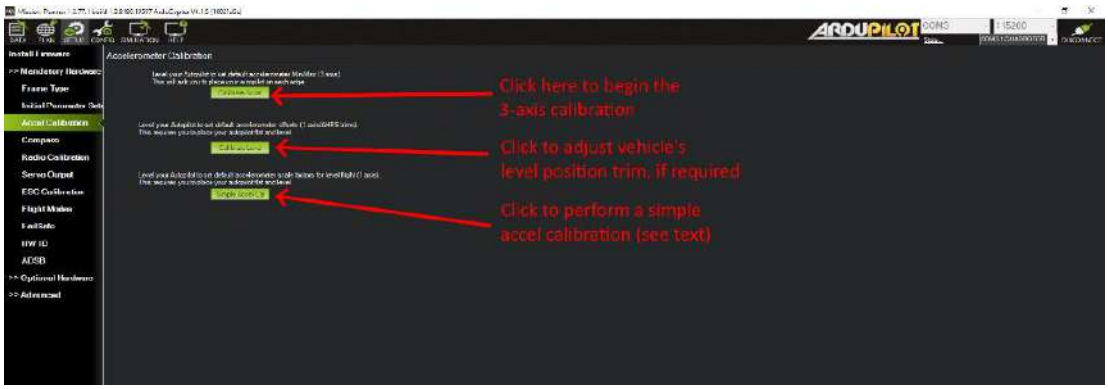

Figure 65: Accelerometer Calibration screen

11.2.4 Compass

The built-in compass of the Flight Controller is also calibrated in the Mission Planner Setup. The calibration is done by rotating the Flight Controller about all the 3 axes after the sound of beep from buzzer when the Start button in Onboard Mag Calibration section is clicked. After complete calibration of compass, the autopilot requires reboot

and reconnect. The compass calibration screen of the Mission Planner is illustrated below.

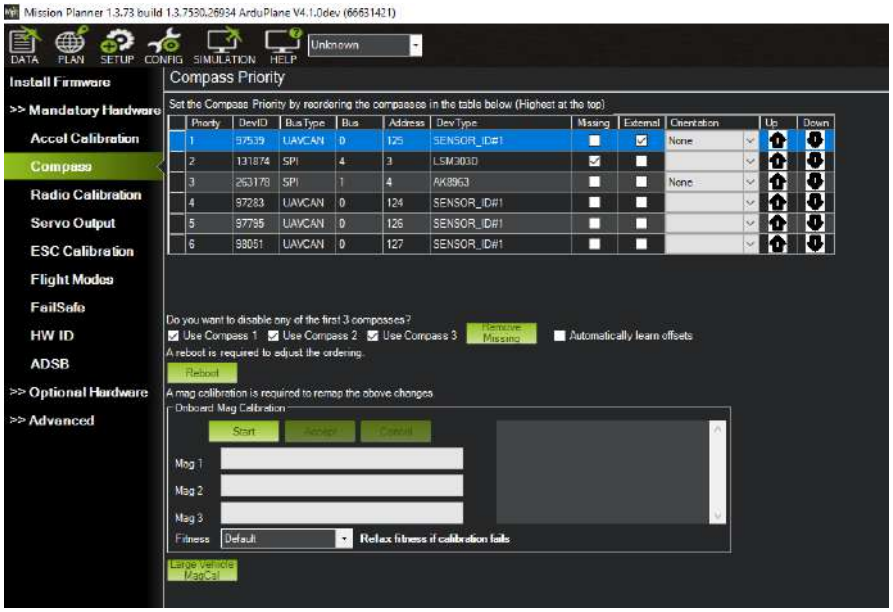

Figure 66: Compass Calibration screen

11.2.5 Servo Output

All the servos are connected to the Flight Controller for calibration and each component is configured in Mission Planner for which the servo is responsible. Also, the minimum, maximum and trimming deflection ranges for the servos are adjusted in this section. The servo functions in Mission Planner are used to assign specific functions to servos as per their use.

11.2.6 Electronic Speed Controller (ESC)

The ESC is calibrated to teach it to which throttle range inputs should it respond to. The calibration is performed using the min-throttle/max-throttle method. For the calibration purpose, ESC is powered separately from Flight Controller. Initially, the ESC is powered down and the safety switch is disabled. Throttle is set to maximum and then ESC is powered up. After that, the throttle is moved to the zero value and once it stops. The ESC makes a beep sound confirming that it has accepted the given maximum to minimum throttle range.

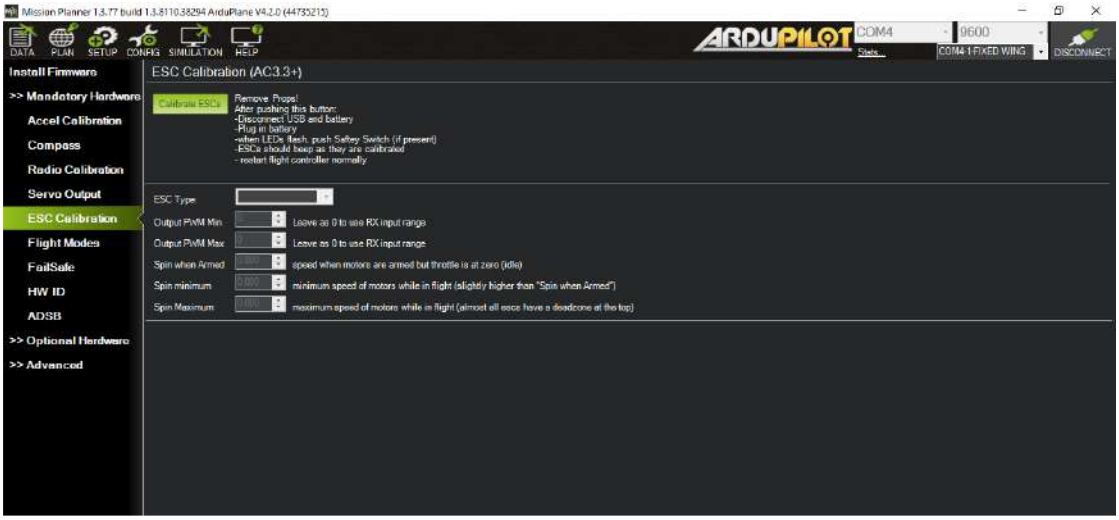

Figure 67: ESC calibration screen (Mission Planner)

11.2.7 Flight Modes

Mission Planner supports several flight modes configurations. Flight modes are initialized from the ground control station. Important flight modes that Mission Planner provides, are elaborated briefly. The Flight Modes selection screen in Mission Planner Setup is illustrated in Figure 42.

Figure 68: Flight Modes Setting Screen (Mission Planner)

11.2.8 Manual Mode

It is the regular RC control mode. This mode does not offer any type of flight stabilization. All the inputs from the controller are directly passed to motors and servos. User has the complete control of flight. Only the arming of vehicle is done by Ground Control Station.

11.2.9 Auto Mode

Auto mode is a fully autonomous flight mode in which the plane follows GPS waypoints established in the Ground Control Station. When a vehicle enters Auto mode, it resumes the mission it was working on previously when it left the auto mode. When the mission ends, if the mission does not end on an undefined or unlimited action that continues indefinitely, the vehicle enters the RTL (return to launch) mode.

11.2.10 RTL (Return to Launch)

Whenever plane enters the RTL mode, it returns to its home location and starts loitering over until given some other instructions. The loiter radius and altitude in the RTL mode are defined using **RTL_RADIUS** and **ALT_HOLD_RTL**, respectively.

RTL_AUTOLAND can be used to setup an auto land sub mode in RTL mode. It automatically lands the vehicle after RTL. The vehicle must have the capability to do automatic landing.

11.2.11 Stabilize Mode

Stabilize mode provides simple stabilization. It stabilizes the plane if the user leaves the sticks. The stabilization in Stabilize Mode, makes it difficult for the user to do maneuvers like rolls and loops. Also, if the user wants the plane to fly mostly by itself just the user telling it where to go, FBWA mode is the preferred mode for this purpose.

11.2.12 FBWA Mode (Fly By Wire_A)

FBWA mode is an assisted flying mode. This mode is best for inexperienced flyers. In this mode, the Plane controls the pitch and roll within the limits provided in parameter configuration under **LIM_ROLL_CD** and **LIM_PITCH_MAX/LIM_PITCH_MIN**. This mode does not control the altitude of the plane which depends on the airspeed. If the user wants the altitude to stay in control, there is an alternate mode for that called FBWB mode. Throttle is manually controlled in FBWA mode within the THR_MIN and THR_MAX limits.

11.2.13 AUTOTUNE Mode

The AUTOTUNE mode works similarly to the FBWA mode. But it automatically tunes roll and pitch control gains during the flight.

11.2.14 Land Mode

In auto Land mode, throttle and altitude are controlled by the Flight Controller. This mode is set by the script only. When the plane enters the LAND_FLARE_ALT meters from the target altitude or LAND_FLARE_SEC seconds from the landing point, it enters the landing mode and will flare to the LAND_PITCH_CD pitch and will stay in the same heading for the final approach.

Chapter 12: Manufacturing and Assembly

12.1 Components Procurement

Procurement of structural and avionics components is underway. Pixhawk and telemetry has been already received and orders for most of the electronics components:

- Servos
- Battery
- Brushless motor
- Power Distribution board

And structural components:

- Hinges
- Servo Connecting Rod
- Carbon fiber rods
- Balsa wood

Have been placed and all these components will be received before 5th of May.

On the other hand, to 3D print formers and ribs, we will visit market and depending upon the quality of print of vendor, order will be placed. So far, we have already made one visit in search of vendors. In order to reduce components printing time, our strategy is to place small orders with multiple vendors.

12.2 Assembly

After procurement of all the components, the next step is to assemble to give it final shape. In this case, the assembly process does not involve any complex operation.

To mold balsa wood into the required shape, first wood will be placed in humid environment due to which wood will become more flexible. After this, wood will be folded to the required and kept in place by tapping. Once the 1-day curing process completes, tape will be removed, glue and epoxy will be used to make permanent connections between 3D-printed components, carbon fiber rods and Balsa wood. Assembly of fuselage, wing and tails will be done separately and after the assembly of individual components, they will be attached together to give UAV a final shape.

12.2.1 Wing Structure

12.2.1.1 Ribs

Starting off with the wings, the ribs of the wings were 3D printed. The purpose of ribs is to support the wing against any stresses that may otherwise break the skin of the wing. The material used for the 3D-printed parts was PLA because of its higher strength and stiffness compared to its other counterparts. With a low melting temperature and minimal warping, PLA is one of the easiest materials to 3D print successfully.

For 3D printing, first, a Standard Tessellation Language (STL) needs to be made of the part that needs to be printed. Then once the STL file has been generated it needs to be opened using suitable 3D printing software that generates a code that can be read by the 3D printer to print the desired part. The 3D printing software used for all the parts that needed to be printed was Cura by Ultimaker. The 3D printer utilized for the 3D printing of all the parts was by Artillery. Once all the ribs were ready, they were fixed accordingly with the distance in the CAD model.

Figure 69 3D Printed Wing Ribs

12.2.1.2 Spars

To provide the wings with support, the spars needed to run through the length of the wings to give much-needed structural integrity to the wings and support the ribs placed along the length of the wing. For the spars, carbon fiber rods were selected as they provide a great strength-to-weight ratio, are lightweight, and can tolerate bending forces much better than other materials.

Figure 70 Carbon Fibre Spars

12.2.1.3 Skin and Ailerons

For the skin of the wing, Balsa wood sheets were first cut into appropriate sizes and then those pieces were cured to give the shape of the airfoil. Once the sheets were in the required shape, the pieces were connected using adhesives and then to the ribs and the rest of the structure. Balsa wood was chosen due to its lightweight qualities and ability to withstand considerable loads with little deformation. In addition to that balsa

wood is very easy to work with, once wettened it can be cured to give it a desired shape. The Ailerons were also made of balsawood by curing it in a similar fashion.

Figure 71 Wing Structure

12.2.2 Fuselage Structure

12.2.2.1 Formers

Much like with the ribs of the wings, the formers were also 3D printed using PLA material. The CAD file was converted to an STL file and then a code was generated to print the formers which were then placed along the length of the fuselage to provide the structure with the required support. The distance between the formers was noted from the CAD design of the fuselage and then the 3D-printed formers were fixed (with carbon fiber stringers going through them) using adhesive with the Balsa wood skin.

Figure 72 3D Printed Formers

12.2.2.2 Skin and Ailerons.

Similar to wings, the skin for the fuselage was made using Balsawood sheets by first cutting them into appropriate sizes and then curing them to get the required shape. Curing was done by first wetting the balsa sheets and then giving them appropriate shapes and keeping a heavy load on them to ensure that the sheets take the desired shape after drying. [46]

Figure 73 Balsa Wood Curing

12.2.2.3 Stringers

For the stringers, carbon fiber rods were utilized due to their lightweight and enormous strength. The stringers were glued to the formers to form a skeleton of the fuselage on which the balsa wood sheets were fused as skin.

Figure 74 Carbon Fiber Stringers attached to Formers

12.2.2.4 Nose

The nose of the aircraft was made detachable to account for the payload that the drone would need to carry. The nose was 3D printed alongside its hooks for attachment to the first former.

12.2.3 Tail Structure

12.2.3.1 Ribs

Unlike wings which had the majority of it made from balsa wood, the whole tail was 3D printed although some parts were printed separately and then attached afterward with adhesives. The tail ribs were one of them, the ribs were printed separately and later joined with the structure with adhesives.

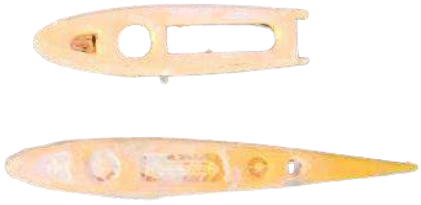

Figure 75 3D Printed Tail Ribs

12.2.3.2 Spars

As with the wings, for the tail carbon fibers were used to contain its rotation about its axis. These spars went throughout the tail, through the ribs, to give structural support to the tail.

12.2.3.3 Elevators

Unlike wings, the elevators for the tails were 3D printed and then attached to the 3D printed tail using a thin metal rod.

Figure 76 3D Printed Tail with Elevators (Orange and White)

Chapter 13: Testing

13.1 Analysis and Simulation

All structural simulations of individual UAV components (wing, tail, fuselage) and simulation on AVL have been completed. To cross check structural simulations and involve aerodynamic forces effect, 1-way FSI of complete drone is to be performed on Ansys. For this process development of simplified model is underway to avoid meshing complications and reduce required computational power requirements.

13.2 Control System

In control system, designing of control system is underway. Pixhawk is being calibrated to control X-tail configuration. For this process, in lab Pixhawk is connected to servos and Pixhawk is rotated by hand to see whether Pixhawk rotate servos as required. So, working on control system will be done in parallel of structure design. But after the assembly of full drone, this designed control system will integrate into drone and three to four test flights will be required to tune Pixhawk parameters to the real-world conditions.

13.3 Testing

Once the assembly of the UAV is complete and all the systems and components have been integrated successfully, the next part is to test the functionality of the UAV to ensure that all the components are behaving in the desired way. Unmanned aerial vehicles (UAVs) are complex systems made up of a variety of parts, such as airframes, propulsion systems, avionics, communication systems, sensors, and payloads. Testing makes sure that these parts are correctly integrated and work as a unit. It aids in the detection of any operational compatibility problems, communication breakdowns, or

system errors that might occur. There are some well-established testing methods that are employed for this testing which are outlined below:

13.3.1 Ground Testing

A UAV (Unmanned Aerial Vehicle) or any other aircraft may be subjected to a number of tests and evaluations while it is on the ground. Before conducting actual flight tests, these tests are normally carried out to evaluate various aspects of the aircraft's operation, systems, and parts. Before the UAV takes to the air operators can test the UAV on the ground to ensure its functionality, reliability, and safety. During the ground testing phase, a number of different tests are employed that encompass different functionality parameters of the UAV. A few prominent tests are outlined below:

13.3.2 Static Wing Loading Test

Static load testing involves subjecting the UAV's structure, airframe, and other critical components to static loads to assess their strength, durability, and structural integrity. This test helps determine the maximum load the UAV can withstand without experiencing deformation or failure. The static wing loading test is a more precise approach that involves placing distributed loads on the wings of the UAV while it is stationary. This helps in the approximation of expected load distribution during flight. For this test, any objects of known mass can be placed on the wings of the UAV and distributed evenly along the wingspan. [47]

Figure 77 Static Wing Loading Test

13.3.3 Power System Testing

The performance, effectiveness, and dependability of the power system that provides the aircraft with electrical power are evaluated during power system testing, which is a crucial component of ground testing for UAVs. As the main source of electrical energy, batteries are frequently used in the UAV's power system. The power systems testing involves Evaluation of the batteries' capacity and performance is part of the battery testing process. To do this, analyze variables including voltage output, charge retention, discharge rates, and general battery health. It ensures that the batteries can deliver the necessary power for the entire trip and that they can be charged and discharged safely.

Testing the system in charge of transferring power from the batteries to the different parts and subsystems of the UAV entails ensuring its effectiveness and operation. To ensure optimum power supply and reduce power losses, this includes evaluating the performance of power distribution circuits, connections, switches, and wiring.

13.3.3.1 Sensor Calibration Testing

Ground testing for UAVs also includes sensor calibration testing because it concentrates on guaranteeing the performance, precision, and dependability of the sensors utilized in the aircraft. Sensors are essential for gathering information for control and navigation. Sensors may develop drift, offsets, or other inaccuracies over time, which may compromise the accuracy and reliability of the data they produce. The sensors' measurements are accurate and reliable thanks to calibration, which helps to correct these mistakes.

13.3.3.2 Motor and Propeller Testing

Electric motor performance parameters including thrust output, torque, RPM (Revolutions Per Minute), and power consumption are assessed during motor testing. To measure the motor's thrust under various operating conditions, a thrust stand or dynamometer is commonly used.

Testing of the motor and propellers enables the propulsion system's effectiveness to be determined. This involves calculating the efficiency of transferring electrical power into thrust, measuring power consumption, and evaluating the power-to-thrust ratio. In order to increase flying endurance and performance, efficiency must be optimized.

Evaluation of the motor's speed response and control is another aspect of the motor and propeller testing process. This involves determining how quickly the motor can adjust its RPM in response to inputs from the controls. The motor and propeller are put through various load circumstances during load testing to assess their performance and reliability. [48]

Figure 78 Motor Thrust Testing

13.3.3.3 Control System Testing

The control system is made up of elements such as autopilot systems, flight controllers, and accompanying software. The functional testing of control system components, including flight controllers and autopilot systems, ensures that they are operating as intended. This entails confirming that the control system can process sensor data, carry out control operations, and receive commands from the ground control station.

13.3.3.4 Centre of Gravity Testing.

In this test a cord was tied around the UAV's fuselage where the Cg was expected to lie and is hung with something to test if the plane leans towards one side or remains balanced. If the plane isn't leaning towards one side, it means it is stable about both x and y axis. [49]

Figure 79 Center of Gravity Testing

13.4 Fully Assembled UAV

After the assembly of the structure and testing has been completed, the control system is integrated into the assembled structure. The final look of the UAV is presented in the figure below:

Figure 80 UAV Fully Assembled

13.5 Final Flight Testing

Once all the tests had been completed, the UAV was finally taken for a flight test but before the flight test, some pre-flight tests were conducted to ensure that the drone behaves in the way that is expected from it. The pre-flight tests included checking all the control surfaces for proper working. The deflection of elevators and ailerons was assessed using a radio controller which overrides the automated control. After that the propulsion motor's throttle was checked using the radio controller. After verifying the proper working of the aforementioned components, the drone was hand launched for the test flight. After the test flight, various parameters of drone's flight were compared to the design parameters. The table below shows the parameters observed during the flight in comparison with the design parameters.

Table 23 Flight Test Parameter Values

Parameter	**Test Flight Values**
MTOW	1.93 kg (can be increased to 2.3 kg)
Cruise Speed	20.8 m/s
Stall Speed	11.66 m/s
Maximum Speed	27 m/s
Rate of Climb	2 m/s
Endurance	22.5 minutes
Range	20.7 km

Figure 81 Hand Launching the UAV

Figure 82 UAV in Climbing

Figure 83 UAV in Cruise

Figure 84 UAV taking a Turn

Figure 85 UAV approaching the Ground

Chapter 14: Conclusion and Future Recommendations

14.1 Conclusion

After a thorough series of processes, the design of a kinetic drone is complete. In this chapter, all the processes will be summarized and then the parameters obtained from the flight test would be compared against the design objectives and finally, some valuable design suggestions and tips will be discussed pertaining to drone design.

After the literature study the first job was to identify the design requirements and then plan accordingly with the requirements. The next step was to work on the conceptual design where the following design configurations were identified: Wing configuration, wing location, tail configuration, propulsion system type, structure configuration etc.

After the conceptual design was preliminary design which constituted evaluating several parameters like motor thrust, battery capacity, MTOW, wingspan etc. The next major design phase was detailed design which focused on design of each major component e.g., wing, tail, fuselage etc., individually. After the detailed design, the required material and components were procured and assembled accordingly with the CAD design. Lastly, a number of tests were performed to check performance and controllability of the drone before finally testing in a test flight and using the flight parameters obtained by the flight controller during the test flight.

Now the table below compares the parameters obtained in the test flight against the target parameters.

Table 24 Comparison of Design and Flight Parameter Values

Parameters	Design objective	Test Flight
MTOW	2 kg	1.93 kg (can be increased to 2.3 kg)
Stall Speed	12 m/s	11.66 m/s
Cruise Speed	20 m/s	20.8 m/s
Max Speed	25 m/s	27 m/s
Rate of Climb	2 m/s	2 m/s
Endurance	16 minutes	17 minutes
Attack Speed	190 km/h	260 km/h
Range	18 km	20.7 km

A close inspection of the comparison table tells that the actual drone boasts a lower stall speed and achieves a higher cruise and top speed than the design objective but at the compensation of battery. It could be also due to the lower MTOW which significantly reduces the stall speed and the thrust required from the motor.

14.2 Future Recommendations

Designing the drone required many tradeoffs and cost cutting to ensure the cost effectiveness and economically viability of the drone but there were some areas that demanded improvements to ensure better functionality and better capability of the drone. These suggested improvements are listed below which can certainly add to improved functionality and better design:

Use of a camera with gimble support and integration of the computer vision modules to isolate the target from the captured camera data to ensure better target locking and tracking in real time in addition to the GPS based locking system that is being utilized currently in the drone.

Since the MATLAB code for the design phases of the drone require extensive calculations and getting the results from them is a time-consuming process and requires many iterations so creation of an application that performs all the calculations using the formulas provided would significantly reduce the effort and would result in quicker iterations and better convergence of results.

References

[1] "Wikipedia," [Online]. Available: https://en.wikipedia.org/wiki/Loitering_munition.

[2] "AeroVironment Switchblade," [Online]. Available: https://www.militaryfactory.com/aircraft/detail.php?aircraft_id=2319.

[3] [Online]. Available: https://www.edrmagazine.eu/switchblade-300-the-combat-proven-munition.

[4] "UVision Hero-30," [Online]. Available: https://www.militaryfactory.com/aircraft/detail.php?aircraft_id=1652.

[5] "Loitering Munition System ALPAGU," [Online]. Available: https://www.stm.com.tr/en/media/press-releases/loitering-munition-system-alpagut#:~:text=ROKETSAN%20and%20STM%2C%20two%20leading%20companies%20in%20the,cruise%20missiles%20with%20its%20cost-effectiveness%20and%20operational%20flexibility..

[6] [Online]. Available: https://www.roketsan.com.tr/en/products/alpagut-smart-loitering-munition-system.

[7] "Raytheon Coyote," [Online]. Available: https://www.militaryfactory.com/aircraft/detail.php?aircraft_id=2001.

[8] M. H. Sadraey, AIRCRAFT DESIGN A Systems Engineering Approach, John Wiley & Sons Ltd, 2012.

[9] M. H. Sadraey, Design of Unmanned Aerial Systems, John Wiley & Sons Ltd, 2020.

[10] "11 Fixed-Wing Drone/UAV Advantages+Disadvantages Explained," [Online]. Available: https://www.thecoronawire.com/fixed-wing-drone-uav-advantages-disadvantages/.

[11] "X-UAV Talon Pro (KIT) 1350mm Wingspan," [Online]. Available: https://runrc.in/product/x-uav-talon-pro-1350mm-wingspan-kit/.

[12] "11 Rotary-Wing Drone/UAV Advantages+Disadvantages Explained," [Online]. Available: https://www.thecoronawire.com/rotary-wing-uav-advantages-disadvantages-explained/.

[13] "PHANTOM 4," [Online]. Available: https://www.dji.com/phantom-4.

[14] A. S. Saeed, A. B. Younes, C. Cai and G. Cai, "A survey of hybrid Unmanned Aerial Vehicles," *Progress in Aerospace Sciences,* 2018.

[15] "XV – Long-Range VTOL Hybrid Dron," [Online]. Available: https://www.unmannedsystemstechnology.com/company/plymouth-rock-technologies/xv-long-range-vtol-hybrid-drone/.

[16] M. Voskuijl, "Performance analysis and design of loitering munitions: A comprehensive technical survey of recent developments," *Defence Technology,* 2020.

[17] "High Wing vs. Low Wing Aircraft (Pros, Cons, and Key Differences)," [Online]. Available: https://airplaneacademy.com/high-wing-vs-low-wing-aircraft-pros-cons-and-key-differences/.

[18] "Wing Configuration," [Online]. Available: https://en.wikipedia.org/wiki/Wing_configuration.

[19] [Online]. Available: https://history.nasa.gov/SP-367/f13c.htm.

[20] M. S. Islam, "Experimental study on aerodynamic characteristics Of NACA 4412 aerofoil with different planforms," 2017.

[21] "Empennage," [Online]. Available: https://en.wikipedia.org/wiki/Empennage.

[22] B. Zhang, Z. Song, F. Zhao and L. Chunhua, "Overview of Propulsion Systems for Unmanned Aerial Vehicles," *Energies*, 2022.

[23] "Electronic speed control," [Online]. Available: https://en.wikipedia.org/wiki/Electronic_speed_control.

[24] "Propeller," [Online]. Available: https://en.wikipedia.org/wiki/Propeller.

[25] M. Yildiz and T. H. Karakoç, "Advantages and Future of Electric Propulsion in UAVs," in *Advances in Sustainable Aviation*, Springer International Publishing AG, p. 237–241.

[26] "Engines & Propulsion Systems," [Online]. Available: https://www.unmannedsystemstechnology.com/expo/engines-propulsion-systems/.

[27] "Fuel Tank," [Online]. Available: https://en.wikipedia.org/wiki/Fuel_tank#Aircraft.

[28] "FLIGHT CONTROLS," [Online]. Available: https://www.lavionnaire.fr/AngFlightControl.php.

[29] A. Basri, A. R. Husain and K. . A. Danapalasingam, "Backstepping Controller with Intelligent Parameters Selection for Stabilization of Quadrotor Helicopter," *Journal of Engineering Science and Technology Review,* 2014.

[30] B. Cuffari, "Using Sensors in Drones," [Online]. Available: https://www.azosensors.com/article.aspx?ArticleID=1149.

[31] D. G. Hull, Fundamentals of Airplane Flight Mechanics, Springer Science & Business Media, 2007.

[32] "Aerodynamic force," [Online]. Available: https://en.wikipedia.org/wiki/Aerodynamic_force.

[33] [Online]. Available: https://www.grc.nasa.gov/www/k-12/VirtualAero/BottleRocket/airplane/ldrat.html.

[34] [Online]. Available: https://www.grc.nasa.gov/WWW/Wright/airplane/geom.html.

[35] [Online]. Available: https://www.daviddarling.info/encyclopedia/A/angle_of_incidence.html.

[36] "Difference Between Static Stability and Dynamic Stability," [Online]. Available: https://www.differencebetween.com/difference-between-static-stability-and-vs-dynamic-stability/.

[37] "Balsa Wood Properties, Uses and Advantages," [Online]. Available: https://www.timberblogger.com/balsa-wood/.

[38] "What Is Wing Spar On An Airplane?," [Online]. Available: https://www.skytough.com/post/airplane-wing-spar.

[39] "Carbon Fibres," [Online]. Available: https://en.wikipedia.org/wiki/Carbon_fibers.

[40] "AM600 3D," [Online]. Available: https://store.tmotor.com/goods.php?id=1207.

[41] D. P. Raymer, Aircraft Design. A Conceptual Approach, American Institute of Aeronautics and Astronautics Inc, 2018.

[42] "Holybro Pixhawk 6c Px4 Autopilot Flight Controller & M8n GPS Module Combo," [Online]. Available: https://nuanqintech.en.made-in-china.com/product/sFVGRpUTHakC/China-Holybro-Pixhawk-6c-Px4-Autopilot-Flight-Controller-M8n-GPS-Module-Combo.html.

[43] "Overview," [Online]. Available: https://docs.holybro.com/autopilot/pixhawk-6c/overview.

[44] "3DR Radio Telemetry 433mhz 433 1000MW Data Telemetry pixhawk apm," [Online]. Available: https://www.smarthobby.pk/product-page/3dr-radio-telemetry-433mhz-433-1000mw-data-telemetry-pixhawk-apm.

[45] "Mission Planner Home," [Online]. Available: https://ardupilot.org/planner/.

[46] "How To Balsa Bending RCTWINS," [Online]. Available: https://www.youtube.com/watch?v=X1ubhW7qaAs.

[47] "Wing Load Test," [Online]. Available: https://www.youtube.com/watch?v=CBczL7qpTFU.

[48] "Brushless Motor Thrust, Current, Watts measurement - DIY RC Flying Hobby Tutoria," [Online]. Available: https://www.youtube.com/watch?v=iZllVgkSs1Q.

[49] "5 Ways to Find CG (CENTER OF GRAVITY) of RC Plane," [Online]. Available: https://www.youtube.com/watch?v=xWwposKZzog.

[50] "AeroVironment Switchblade," [Online]. Available: https://www.militaryfactory.com/aircraft/detail.php?aircraft_id=2319.

[51] "6s 22.2V 10000mah tattu gensace 25C LiPo Battery," [Online]. Available: https://www.smarthobby.pk/product-page/tattu-6s-22-2v-10000mah-25c-lipo-battery.

[52] "APC 15x8E," [Online]. Available: https://arttechhobbies.com/index.php?route=product/product&path=57_83_104&product_id=719.

[53] "Hobbywing skywalker 80Amp esc," [Online]. Available: https://www.smarthobby.pk/product-page/hobbywing-skywalker-80amo-esc.

[54] "MG946R MG946 R 180 Degree Servo Motor in Pakistan," [Online]. Available: https://electronicshub.pk/product/mg946r-mg946-r-180-degree-servo-motor/.

[55] "Accelerometer Calibration," [Online]. Available: https://ardupilot.org/planner/docs/common-accelerometer-calibration.html.

[56] "Compass Calibration," [Online]. Available: https://ardupilot.org/planner/docs/common-compass-calibration-in-mission-planner.html.

Appendix 1: Engineering Drawing

14.3 Assembly Drawing

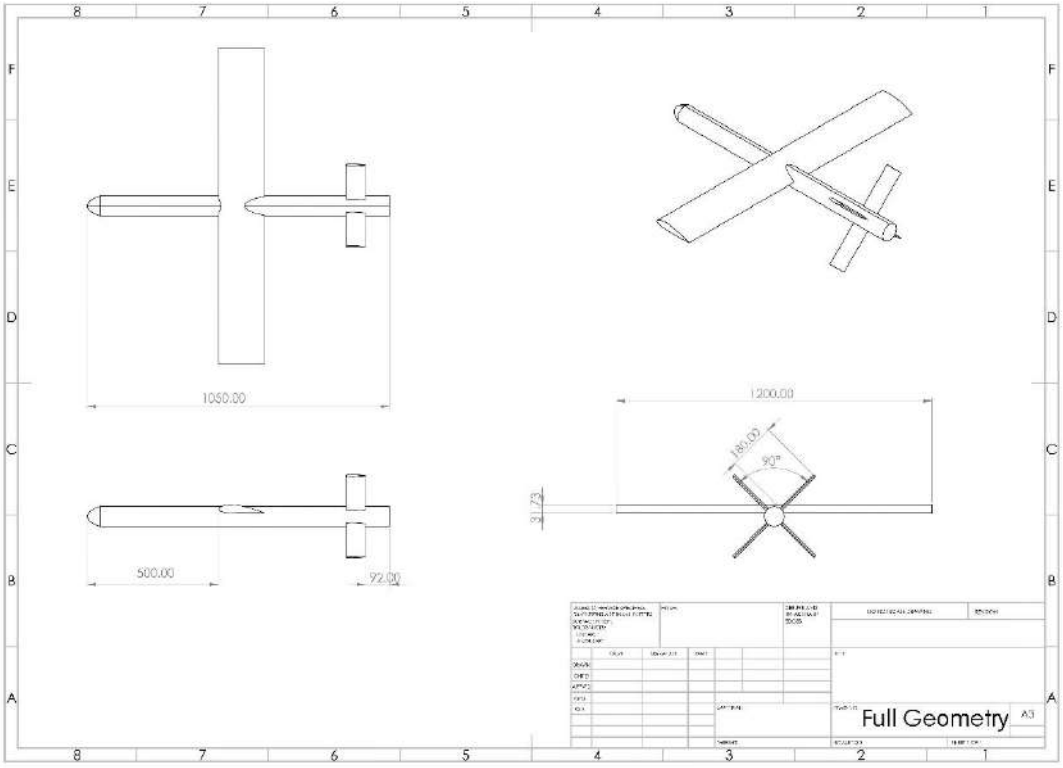

14.4 Wing

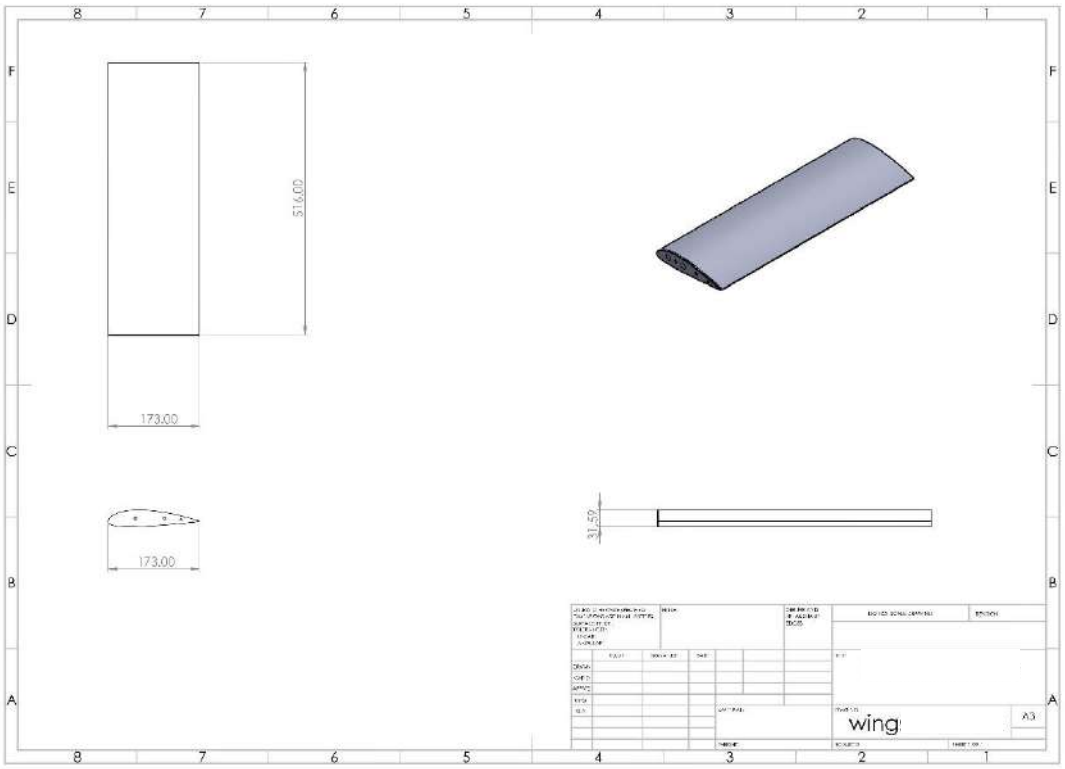

14.5 Tail

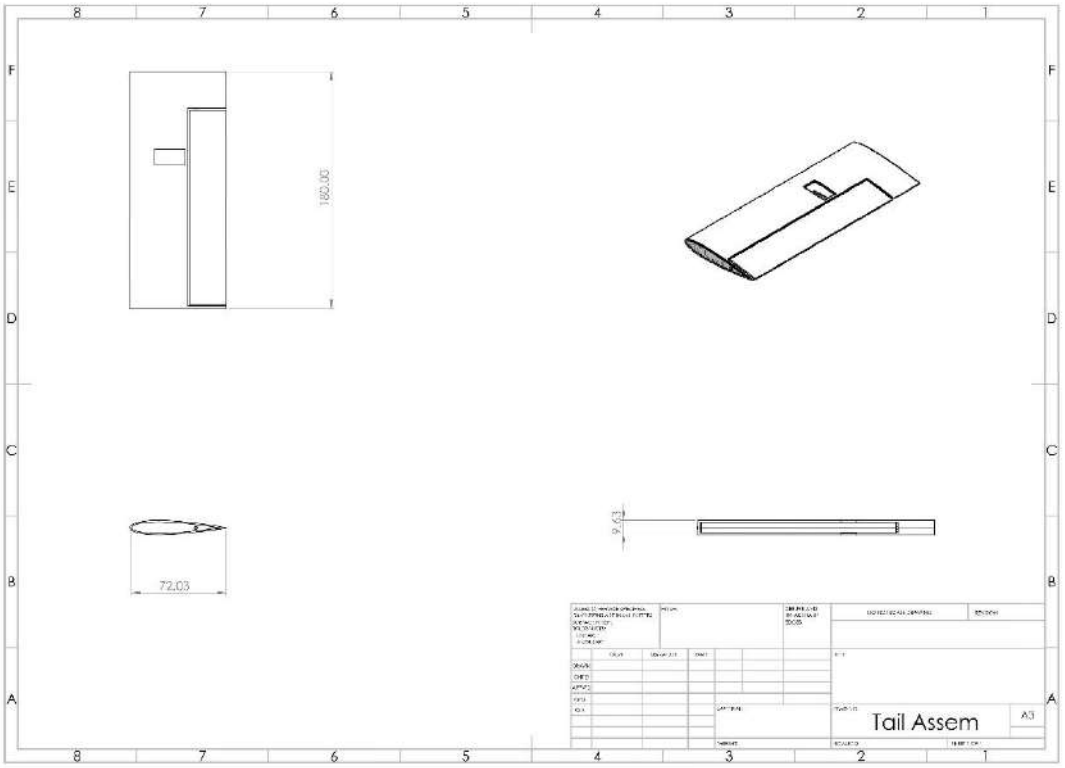

14.6 Fuselage

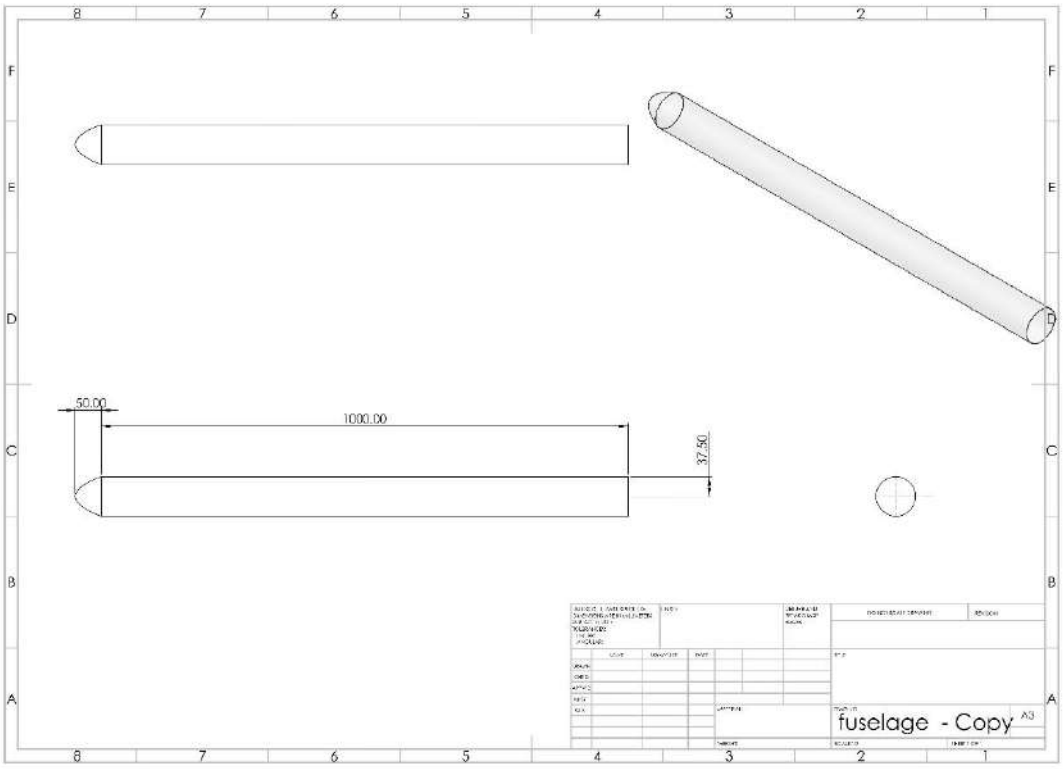

14.7 Former

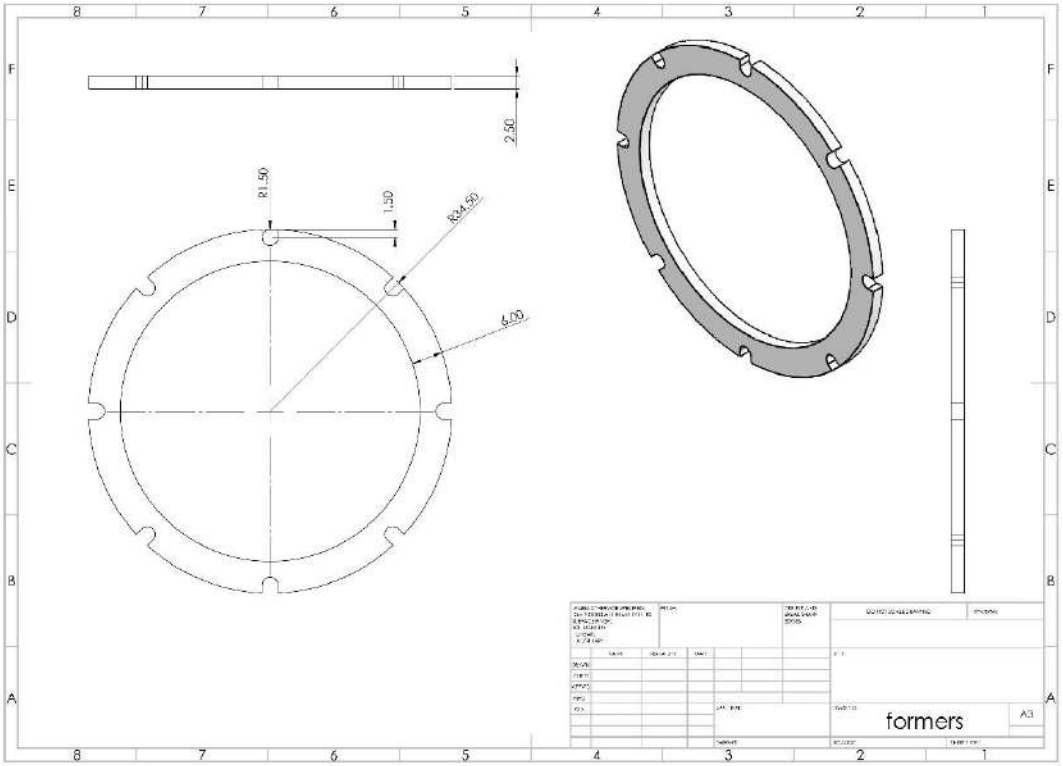

Appendix 2: MATLAB CODES

Prompt to Get Data From User

```
 prompt={'Number of Batteries:','No of Servos','No of Motors:','Payload
Mass:','Battery Mass:','Motor Mass:','ESC Mass:','Propeller
Mass:','Flight Controller Mass:','Mass of GPS:','Mass of Servo:','Mass
of Camera','Weight Fraction of Wires:','Weight Fraction of
Airframe:','Aspect Ratio of the Wing:','Zero Lift Drag
Coefficient','Ostawalds Efficiency','Maximum Lift Coefficient'};
 dim=[1 60];
 title_prompt='Enter the Parameters: ';
 default_Values={'1','6','1','0.3','0.224','0.175','0.109','0.0279','0.
120','0.068','0.013','0.05','0.05','0.38','7','0.04','0.8691','1.4'};
```

Power Loading and Wing Loading Calculation

```
 %(https://wingsofaero.in/calculator/oswald-efficiency-factor-for-
straight-wing/)
 Inputs=inputdlg(prompt,title_prompt,dim,default_Values);
 N_b= str2double(Inputs(1)); %No of batteries
 N_s_1= str2double(Inputs(2)); %no of servos
 N_m_1=str2double(Inputs(3)); %No of Motors
 W_PL=str2double(Inputs(4)); %payload weight
 %From Specsheet of Tattu 45C 14.8V 4S 2300mAh Lipo
 W_b=N_b*str2double(Inputs(5)); %battery weight
 W_m_1= N_m_1*str2double(Inputs(6)); %motor weight
 %From Spechsheet of Hobbywing Skywalker 50A ESC
 W_ESC_1= N_m_1*str2double(Inputs(7)); %ESC Weight
 %From Specsheet of Gemfan 10x6 Nylon Propeller
 W_p_1= N_m_1*str2double(Inputs(8)); %Propellers Weight
 %From Specsheet of Pixhawk 6C Holybro
 W_FC=str2double(Inputs(9)); %Flight Controller weight
 W_Misc= str2double(Inputs(10));
 W_SM_1= N_s_1*str2double(Inputs(11)); %Servo Motors for Control
Surfaces weight
 W_C= str2double(Inputs(12)); % camera
 W_CB=str2double(Inputs(13));
 W_AF=str2double(Inputs(14)); % Estimated Percentage Weight of the
Airframe
 W_MTOW_NAF= W_PL+W_b+W_m_1+W_ESC_1+W_p_1+W_FC+W_Misc+W_SM_1+W_C;
%Maximum Takeoff Weight without airframe
 W_MTOW_S = W_MTOW_NAF*0.2;
 W_MTOW = (W_MTOW_NAF)/(1-W_CB-W_AF);
 W_MTOW = W_MTOW_S+W_MTOW;

 mTOW=inputdlg("Mtow","MTOW calculated",[1 60],{num2str(W_MTOW)});
```

```
 prompt1={'Density at Sea Level in kg/m^3','Density at Maximum Height
in kg/m^3','Power to thrust efficiency at Vmax','Cruise speed','Stall
speed','Zero Lift Drag Coefficient','Power to thrust during
climb','rate of climb:','lift to drag ratio','altitude in
feet','Maximum lift coefficient'};
 dim=[1 60];
 default_Values1={'1.224','1.15','0.6','19.3','12','0.04','0.5','2','10
','400','1.2'};
 Inputs1=inputdlg(prompt1,title_prompt,dim,default_Values1);

 rho_sea= str2double(Inputs1(1)); %Density at Sea Level in kg/m^3
 rho_ceiling= str2double(Inputs1(2)) ;%Density at Maximum Height in
kg/m^3
 eta_p_stall = str2double(Inputs1(3));
 Vc=str2double(Inputs1(4)); %Cruise Speed (Estimation from Statistics)
 Vs=str2double(Inputs1(5)); %Stall Speed (Estimated from Statistics and
Book)
 zero_drag = str2double(Inputs1(6)); %Parasitic Drag
 eta_climb=str2double(Inputs1(7)); %Prop Efficiency for CLimb
 ROC = str2double(Inputs1(8)); %Rate of Climb
 Lift_to_Drag_Ratio = str2double(Inputs1(9)); % Using data available of
2D airfoils
 h_alt=3.28*str2double(Inputs1(10)); %Altitude in meter
 Cl_max_w_2d = str2double(Inputs1(11));
 g = 9.81;

 sigma_ceiling= rho_ceiling/rho_sea; %ratio of desnity of working
altitude to
 Cdo=str2double(Inputs(16)); %zero_lift_drag_coefficient
 AR_w=str2double(Inputs(15)); %Wing Aspect Ratio
 Ostawald_Efficiency= str2double(Inputs(17));
 K=1/(pi()*AR_w*Ostawald_Efficiency); %drag_due_to_lift_coefficient

 % Wing Loading as a Function of Stall Speed
 Power_Loadng_Stall_Speed=1:0.5:300;
 Wing_Loading_Stall_Speed=0.5*rho_sea*Vs.^2*Cl_max_w_2d;

 % Estimation of Maximum Speed
 V_max=1.3*Vc; % 30% greater than cruise speed Vmax = 1.2VC to 1.3VC
(4.58)
 Wing_Loading_Vmax=1:0.5:300;
 Power_Loading_Vmax=(sigma_ceiling*eta_p_stall)./((0.5*rho_sea.*V_max.^
3*Cdo.*(Wing_Loading_Vmax).^-
1)+(2*K.*Wing_Loading_Vmax)./(rho_sea*sigma_ceiling.*V_max));
 % Aircraft Zero Lift Drag Coefficient Estimation
 % Average of 0.04 (Sadraey Book)
 % Estimation of Rate of Climb:
 Wing_Loading_Rate_Of_Climb=1:0.5:300;
 c_ROC=(ROC/eta_climb);
 d_ROC=sqrt((2.*Wing_Loading_Rate_Of_Climb)/(rho_sea*sqrt(3*Cdo/K)))*(1
.155/(Lift_to_Drag_Ratio*eta_climb));
```

```
 Power_Loading_Rate_Of_Climb=(1./(c_ROC+d_ROC));
 % Absolute Ceiling Estimation

 sigma_relative_density=(1-6.873*10^-6*h_alt)^4.26;
 Wing_Loading_Absolute_Ceiling=1:0.5:300;
 ROC_Ceiling=0.1;
 e_ceiling=(ROC_Ceiling/eta_climb);
 f_ceiling=sqrt((2.*Wing_Loading_Rate_Of_Climb)/(rho_ceiling*sqrt(3*Cdo
/K)))*(1.155/(Lift_to_Drag_Ratio*eta_climb));
 Power_Loading_Absolute_Ceiling=sigma_relative_density./(e_ceiling+f_ce
iling);
```

Matching Plot

```
 figure('Position',[0 0 1920 1080])
 hold on
 xline(Wing_Loading_Stall_Speed,'linewidth',3);
 S_w=(W_MTOW*g)/Wing_Loading_Stall_Speed;
 index=round(Wing_Loading_Stall_Speed/0.5);
 Power_Loading_DP=Power_Loading_Vmax(index);
 P_DP=(W_MTOW*g)/Power_Loading_DP;
 b_w=sqrt(AR_w*S_w);
 C_tip_w=b_w/AR_w;

 plot(Wing_Loading_Absolute_Ceiling,Power_Loading_Absolute_Ceiling,Wing
_Loading_Rate_Of_Climb,Power_Loading_Rate_Of_Climb,Wing_Loading_Vmax,Po
wer_Loading_Vmax,'linewidth',3)
 grid on
 axis([0,300,0,1])
 set(gca,'YTick',0:0.20:1)
 title('Matching Plot')
 xlabel('Wing loading (Nm^-2)')
 ylabel('Power loading (NW^-1)')
 disp("The Maximum Take Off Weight is: " +W_MTOW+ " kg")
 disp("The Power Required is: " + P_DP + " Watt")
 disp("The Wing Area Required is: " + S_w +" m^2")
 disp("The Wing Span is: " +b_w+" m" )
 disp("The Wing Chord is:"+C_tip_w+" m")
 plot(Wing_Loading_Stall_Speed,Power_Loading_DP,"Marker","o","MarkerSiz
e",15,"MarkerEdgeColor",'red','Color',[1 0 0])
 legend('Stall Speed','Absolute Ceiling','Rate of
Climb','MaximumSpeed','Design Point')
 set(gca, 'visible', 'on')
 hold off
```

Catapult Speed:

```
V_ctp = sqrt(2*Wing_Loading_Stall_Speed*1.21/(Cl_max_w_2d*rho_sea))
```

Lifting line theory

```
N = 20; % (number of segments - 1)
S_w;
AR_w; % Aspect ratio
lambda_w = 1; % Taper ratio
alpha_twist = 0.0000000000001; % Twist angle (deg)
i_w = 2.5; % wing setting angle (deg)
tbyc_max_w=0.18;
CL_alpha_w_2d = 1.8*pi*(1+0.8*tbyc_max_w); % lift curve slope 2-D
CL_alpha_w_3d=4.04 % obtained using XFLR5
alpha_0 = -3.7; % zero-lift angle of attack (deg)
b_w; % wing span (m)
MAC = S_w/b_w; % Mean Aerodynamic Chord (m)
Croot = (1.5*(1+lambda_w)*MAC)/(1+lambda_w+lambda_w^2); % Chord at
root of wing (m)
theta = pi/(2*N):pi/(2*N):pi/2; % Angle in radians
alpha = (i_w+alpha_twist):-alpha_twist/(N-1):i_w;
% segment angle of attack
z = (b_w/2)*cos(theta);
c = Croot * (1 - (1-lambda_w)*cos(theta)); % Mean Aerodynamics
%Chord at each segment (m)
mu = c * CL_alpha_w_2d / (4 * b_w);
LHS = mu.*(alpha-alpha_0)/57.3; % Left Hand Side
% Solving N equations to find coefficients A(i):
for i=1:N
for j=1:N
D(i,j) = sin((2*j-1) * theta(i)) * (1 + (mu(i) * (2*j-1))
/sin(theta(i)));
end
end
C=D\transpose(LHS);
for i = 1:N
sum1(i) = 0;
sum2(i) = 0;
for j = 1 : N
sum1(i) = sum1(i) + (2*j-1) * C(j)*sin((2*j-1)*theta(i));
sum2(i) = sum2(i) + C(j)*sin((2*j-1)*theta(i));
end
end
CL = 4*b_w*sum2 ./ c;
CL1=[0 CL(1) CL(2) CL(3) CL(4) CL(5) CL(6) CL(7) CL(8) CL(9) CL(10)
CL(11) CL(12) CL(13) CL(14) CL(15) CL(16) CL(17) CL(18) CL(19) CL(20)];
y_s=[b_w/2 z(1) z(2) z(3) z(4) z(5) z(6) z(7) z(8) z(9) z(10) z(11)
z(12) z(13) z(14) z(15) z(16) z(17) z(18) z(19) z(20)];
plot(y_s,CL1,'-o')
```

```
grid
title('Lift distribution')
xlabel('Semi-span location (m)')
ylabel ('Lift coefficient')
CL_w_3d = pi * AR_w * C(1)
```

Tail Desgin (Horizontal Tail Design)

```
% Step 1: Horizontal Tail Volume Coefficient
V_h = 0.45; %0.45 from Table 6.2 (Sadraey Book)
% Step 2: Calculation of Horizontal Tail Moment Arm
D_F = 0.065; % Maximum diameter of fuselage required to place all
objects inside fuselage (obtained from cad)
Kc = 1.05; % Fudge Factor its value varies between 1(for cylinderical
tail) and 1.4(for conical tail)
l_h_opt = Kc*sqrt((4*MAC*S_w*V_h)/(pi*D_F))
% Step 3: Horizontal tail Planform Area
SF = 1.3 % Safety Factor in tail design
S_h = SF*(V_h*MAC*S_w)/l_h_opt % Tail Planform Area
% Step 4: Wing/Fuselage Aerodynamic Pitching Moment Coefficient
Cm_w_2d = -0.08 % Maximum Airfoil Pitching Moment
sweep_angle_w = 0;
alpha_w_t = 0;
Cm_w_3d = -0.15 %Using XFLR5
% Step 5: Cruise Lift Coefficient
CLc_w_3d = 0.42458
% Step 6: Horizontal tail desired lift coefficient at cruise
dCm = 0-(-0.1); % from http://airfoiltools.com/
d_alpha = (16-1)*(pi())/180; % from http://airfoiltools.com/
h = 0.43; % Initiate by selecting value 0.5 and then iterate untli
Cl_h_req approach zero
ho = -dCm/(d_alpha*2*pi())+0.25 % From CAD
Cl_h_req = -(Cm_w_3d + (CLc_w_3d*(h-ho)))/V_h % Required Tail Lift
Coefficient
% Step 7: Horizontal Tail Airfoil Selection
% NACA 0015
% • Optimum -ve Cl at -3 degree
% • Does not stall before wing.
% Step 8: Horizontal Sweep & Dihedral Angle
sweep_angle_h = 0
dihedral_angle_h = 45*pi()/180;
% Step 9: Horizontal Tail Aspect Ratio & Taper Ratio
AR_h = (2/3)*AR_w
Lambda_h = 1
% Step 10: Horizontal Tail Lift Curve Slope
tbyc_max_h=0.15 %NACA 0015
CL_alpha_h_2d=1.8*pi*(1+0.8*tbyc_max_h);
CL_w_3d_0 = 0.288; %Using XFLR5
CL_alpha_h_3d=3.43 %Using XFLR5
% Step 11: Horizontal Tail Angle of Attack at Cruise
```

```
alpha_h_i = Cl_h_req/CL_alpha_h_3d % Required tail incidence angle
alpha_h_i_deg= (alpha_h_i*180)/pi
alpha_f= 0 %Fuselage angle of attack
i_w_rad = (i_w*pi)/180
e_not = 2*CL_w_3d_0/(pi*AR_w)
de_alpha = 2*CL_alpha_w_3d/(pi*AR_w)
e = e_not + de_alpha*(i_w_rad);
i_h = -alpha_f + alpha_h_i + e; % Effective tail incidence angle
i_h_deg = i_h * 180/pi % If your tail and wings are inline
% Step 12: Horizontal Tail Span, Root Chord, Tip Chord, MAC
b_h = sqrt(AR_h * S_h)
C_root_h = b_h/AR_h
C_tip_h = Lambda_h*C_root_h
MAC_h=2/3*C_tip_h*((1+Lambda_h^2+Lambda_h)/(1+Lambda_h))
Mean_Tail_Area=b_h*MAC_h
```

Pitching Moment Calculation

```
CL_alpha_h_3d=3.43 %Using XFLR5
alpha_0 = 0.000001; % zero-lift angle of attack (deg)
b_h; % tail span
MAC_h = S_h/b_h; % Mean Aerodynamic Chord
Croot = (1.5*(1+Lambda_h)*MAC)/(1+Lambda_h+Lambda_h^2); % root chord
% Step 13: Final Check for Longitudinal Stability Check
eta_h=0.75; %Efficiencyiy of horizontal tails
C_m_alpha=CL_alpha_w_3d*(h-ho)-
CL_alpha_h_3d*eta_h*(Mean_Tail_Area/S_w)*(l_h_opt/C_root_h-h)*(1-
de_alpha) %If negative than tail is stable , (Lognitudinal_Stability)
C_m_alpha = -0.35 % from xflr5 (%If negative than tail is stable ,
(Lognitudinal_Stability))
```

Vertical Tail Design

```
V_v = 0.07; % Sadray UAV book pg 121
l_v_opt = l_h_opt;
S_v = (b_w*S_w*V_v)/l_v_opt
tbyc_max_v=0.09
CL_alpha_v_2d=1.8*pi*(1+0.8*tbyc_max_v)
CL_alpha_v_3d=CL_alpha_v_2d/(1+CL_alpha_v_2d/(pi*AR_h))
Lambda_v = 1
i_v = 0
Alpha_Sweep_v= 0
dihedral_v = 45
b_Vtail=sqrt(S_v*AR_h)
C_tip_v = b_Vtail/AR_h;
C_root_v = Lambda_v*C_tip_v
MAC_v = (2/3)*C_root_v*((1+Lambda_v+(Lambda_v^2))/(1+Lambda_v))
Mean_S_v=b_Vtail*MAC_v
```

```
% Vertical Tail Stability Check
K_f = 0.65 %From Sadray pg 322 (typical value is 0.65 and 0.85)
dsigma_beta = 0
eta_v = 0.75
Cn_beta_v = K_f*CL_alpha_v_3d(1-
dsigma_beta)*eta_v*l_v_opt*S_v/(b_Vtail*S_w)%Positive value means plane
is stable, typical value is 0.2-0.4/rad
```

Projections

```
%Since Horizontal tail is larger than vertical tail, horizontal tail
(limiting tail) is
%used to calculate X-tail
% Horizontal Tail Projection
P_h_Area = (Mean_Tail_Area/cos(dihedral_angle_h))/2
P_b_h = sqrt(AR_h * P_h_Area)
P_C_root_h = P_b_h/AR_h
P_C_tip_h = Lambda_h*P_C_root_h
P_MAC_h=2/3*P_C_tip_h*((1+Lambda_h^2+Lambda_h)/(1+Lambda_h))
P_Mean_Tail_Area=P_b_h*P_MAC_h

% Vertical Tail Projection
% Vertical Tail Stability Check
K_f = 0.65 %From Sadray pg 322 (typical value is 0.65 and 0.85)
dsigma_beta = 0
eta_v = 0.8
S_v = P_h_Area*cos(dihedral_angle_h)*2
b_Vtail = sqrt(AR_h * S_v)
V_v = S_v*l_v_opt/(b_w*S_w)
Cn_beta_v = K_f*CL_alpha_v_3d*(1-
dsigma_beta)*eta_v*l_v_opt*S_v/(b_Vtail*S_w) % if Cn_beta_v is greater
than 0.4, your design is good
```

Fuselage length parameter calculation

```
%Distances from Main Wing tip
x_cg = h*C_tip_w
x_ach = l_h_opt+(ho*C_tip_w)-(0.25*P_MAC_h)
x_ac=ho*C_tip_w
```

Design Tests

```
C_mq = -2*CL_alpha_h_3d*V_h*(x_ach-x_cg)
if(C_mq<C_m_alpha)
    disp("Test Passed. C_mq is good");
else
    disp("Stability Test Failed due to C_mq");
end
X_np=x_cg-(C_m_alpha/CL_alpha_w_3d);
```

```
 if(X_np-x_cg>0)
     disp("Test passed")
 else
     disp("Test failed move x_cg forward of X_np")
 end
 SM= (X_np-x_cg)/C_tip_w
 if(0.05<SM>0.4)
     disp("Test passed")
 else
     disp("Test failed")
 end
```

Propeller Size Estimation

```
 V_max_ts=150;
 C_dc=Cdo+K*CLc_w_3d^2;
 D_c=0.5*rho_ceiling*V_max^2*S_w*C_dc
 n_p=(D_c*V_max)/P_DP
 P_reqc=(D_c*Vc)/n_p
 K_np = 1;
 FOS_p = 1.2;
 AR_p = 7:0.1:15;
 for Cl_p=0.2:0.05:0.4

D_p=sqrt((2*P_reqc*n_p)/(rho_ceiling*0.7*V_max_ts*Cl_p*Vc)).*sqrt(AR_p)
;
     plot(AR_p,D_p,"linewidth",2);
     hold on;
 end
 grid on
 title('Propeller Diameter vs Aspect Ratio');
 xlabel('Aspect Ratio of Propeller');
 ylabel('Diameter of Properller');
 legend("CL_p = 0.2","CL_p = 0.25","CL_p = 0.3","CL_p = 0.35","CL_p =
0.4");
 hold off;
 prompt3={'Enter the diameter of propeller: ', 'Enter Aspect Ratio: ',
'Enter Cl_p: '};
 dim=[1 60];
 title_prompt='Enter the Parameters: ';
 default_Values3={'0.4','10','0.2'};
 answer = inputdlg(prompt3,"Propeller data",dim,default_Values3)
 dia_p = str2double(answer(1));
 AR_p= str2double(answer(2));
 Cl_pr= str2double(answer(3));
 limiting_D_p=K_np*sqrt((2*P_reqc*AR_p*FOS_p)/((rho_ceiling*(0.7*V_max_
ts)^2)*Cl_pr*V_max)); % Diameter of propeller in meters

 V_ts=sqrt(V_max_ts^2-V_max^2); % Maximum Tip Speed
 rot_speed = 2*V_ts/dia_p;
```

```
limiting_omega_p=(rot_speed*(60/(2*pi))); % RPM of Motor
disp("Propeller RPM should be less than limiting_omega_p")

if (dia_p>limiting_D_p)
    disp("Diamter of Propeller is good")
else
    disp("Propeller diameter is below lower limit")
end
```

Aileron Design

Design Requirement

- Should be able to control plane
- Low cost and easy to manufacture
- Dimension must be feasible when compared to main wing dimensions

Aileron Purpose

- Roll control
- Should be able to rotate by 60 degree in 2.6 s

Aircraft class

- Class 1

Flight critical phase:

- Phase B

Acceptibility level

- 3

Handling Quality design of Requirement

```
t_req = 3.4;
phi_req = 45;
I_xx = 0.71551;
```

Position of Aileron

```
bai_by_b = 0.6; % lies between 0.6-0.8
ba_by_b = 0.4; % lies between 0.2-0.4
bao_by_b = 1; % cannot be less than bai_by_b and greater than 1
```

Chord to Wing Ratio of Aileron

```
Ca_by_C = 0.25; % lies between 0.15-0.25
```

Aileron Effectivenesss Parameter

```
 tau_a = -6.108*(Ca_by_C)^4+11.59*(Ca_by_C)^3-
8.2457*(Ca_by_C)^2+3.3255*(Ca_by_C); % from page 681 of Sadraey
```

Derivative of Rolling Moment Coefficients

```
 yi = bai_by_b*b_w/2
 yo = bao_by_b*b_w/2
 C_r = 1.5*MAC*((1+lambda_w)/(1+lambda_w+lambda_w^2));
 Cl_delta_A =
((2*CL_alpha_w_3d*tau_a*C_r)/(S_w*b_w))*((yo^2/2+(2/3*((lambda_w-
1)/b_w)*yo^3))-(yi^2/2+(2/3*((lambda_w-1)/b_w)*yi^3)))
```

Maximum Deflection of Aileron

```
 delta_Amax = 20 %typical value in degree is ±25
```

Aircraft rolling moment coefficient (Cl)

```
 Cl = Cl_delta_A*delta_Amax*pi/180
```

Aircraft rolling moment (LA)

```
 V_T = Vs*1.3; %true speed of plane
 L_A = 0.5*rho_sea*(V_T^2)*S_w*Cl*b_w
```

Steady-State Roll Rate

```
 % Drag moment arm
 y_D = 0.4*b_w/2 % assumption of 40 percent
 % Wing horizontal/tail vertical tail rolling
 % drag coefficient
 C_D_R = 1 % from sadraey book page 681
 P_ss = ((2*L_A)/(rho_sea*(S_w + P_h_Area*2)*C_D_R*(y_D^3)))^0.5
```

Bank Angle

```
 phi_l = (I_xx*log(P_ss^2))/(rho_sea*(S_w + P_h_Area*2)*C_D_R*(y_D^3))
```

Aircraft roll rate

```
 P_dot = (P_ss^2)/(2*phi_l)
```

Area Calculation

```
 if(phi_l>phi_req)
     t_2 = ((2*phi_req*(pi/180)/P_dot)^1/2)
 else
     t_2 = ((2*phi_l*(pi/180)/P_dot)^1/2)
```

```
end
if(t_2 < t_req)
    disp("Requirements of Aileron has been met")
else
    disp("Requirements for designing Aileron has not been met. Either
increase geometry of aileron or increase deflection angle. If
increasing Aileron geometry does not work, entire wing is need to be
redesigned.")
end
b_a = yo-yi
MAC_a = 0.2*MAC
S_a = 2*b_a*MAC_a
if((0.05*S_w)<S_a & S_a<(0.1*S_w))
    disp("Area of Aileron lies in range");
else
    disp("Area of Aileron lies out of recommended range")
end
```

Reduction in Stall Angle of wing

```
stallAngle_w = 14.5;
r = MAC_a/C_tip_w;
reduction_table = [0,0,0,0,0,0,0,0,0,0,0;
    0,0.3,0.5,1.1,1.6,2.2,2.7,3.3,3.9,4.4,5;
    0,0.6,1,2.1,3.2,4.4,5.5,6.6,7.7,8.9,10;
    0,0.9,1.5,3.2,4.9,6.5,8.2,9.9,11.6,13.3,15;
    0,1.2,2,4.2,6.5,8.7,11,13.2,15.5,17.7,20;
    0,1.6,2.5,5.3,8.1,11,13.7,16.5,19.4,22.2,25;
    0,1.9,3,6.4,9.7,13.1,16.5,19.9,23.2,26.6,30];
row = ceil(delta_Amax/5)+1;
column = int16(r*10+1);
stallAngle_w = stallAngle_w - reduction_table(row,column)
```

Elevator Design

Low Cost & Manufacturability

Selection the Elevator Span

```
b_E = 0.83*b_h % Elevator Span ( from table 12.3 Sadraey)
```

Select max elevator deflection from table 12.3 of Sadraey

```
maxdefl_E = 15; % Max Deflection of Elevator
```

Choose desired Tail lift coefficient

Calculate angle of attack effectiveness of elevator using eq 12.75 (Sadraey)

```
effectiveness_E = 1 % Attack Effectiveness of Elevator
```

Calculate Chord ratio of Elevator from Figure 12.12 of Sadraey

```
 Chord_ratio_E = 0.38; % Use effectivenes_E in Figure 12.12
 C_E = Chord_ratio_E*C_tip_h % Elevator Chord
```

Find Tail lift coefficient using CFD techniques at max negative elevator deflection and compare.

If equal, move to next step

Calculate the Elevator Effectiveness Derivatives using eqs 12.51-53 of Sadraey

```
 Cm_changedefl_E = (-
CL_alpha_h_3d*eta_h*V_h*(b_E/b_h)*effectiveness_E); %Longitudinal
Control Power Derivative
 CL_changedefl_E =
(CL_alpha_h_3d*eta_h*(S_h/S_w)*(b_E/b_h)*(effectiveness_E));%
Contribution of Elevator to Aircraft Lift
 Cl_h_changedefl_E = (CL_alpha_h_3d*effectiveness_E); % Contribution of
the Elevator to Tail Lift
```

Calculate Elevator Deflection required for Longitudinal Trim

```
 Cmo=0.01546; % Aircraft cruise pitching moment
 CL_slope=0.07626521; % Aircraft cruise lift curve slope
 Cm_slope=0.00539271; % Aircraft cruise pitching moment curve slope

 tau_e = -6.108*(Chord_ratio_E)^4+11.59*(Chord_ratio_E)^3-
8.2457*(Chord_ratio_E)^2+3.3255*(Chord_ratio_E) % from page 681 of
Sadraey
 CL_o=0.4165;
 q_bar=0.5*rho_ceiling*Vc^2;
 CL_1=W_MTOW*9.81/(q_bar*(S_w));
 alpha_nose = (((CL_1-CL_o)*Cm_slope
+Cmo*CL_slope)/(CL_alpha_w_3d*Cm_slope-C_m_alpha*CL_slope))*180/pi; %
Angle of Attack at which max deflection of elevator required for
longitudinal trim
 defl_E =(((-CL_alpha_w_3d*Cmo)-C_m_alpha*(CL_1-
CL_o))/((CL_alpha_w_3d*Cm_slope)-(C_m_alpha*CL_slope)))*180/pi() %
required Deflection of Elevator for Longitudinal trim
```

Check if within the maximum permissible Elevator Deflection & check for horizontal tail stall

Optimize Elevator

Find Planform area of elevator and draw top view

```
 S_E=b_E*C_E % Elevator Planform Area
```

Pitch Rate calculation

```
 instant_dE=-5:1:15;
 I_yy=0.7;
 L_w=0.5*rho_ceiling*Vc^2*S_w*(CL_w_3d+CL_slope.*instant_dE);
 M_ac=0.5*rho_ceiling*Vc^2*(Cm_w_3d+Cm_changedefl_E.*instant_dE)*S_w;
 M_tail=0.5*rho_ceiling*Vc^2*(Cm_changedefl_E.*instant_dE)*P_h_Area*2;
 theta_oo= (W_MTOW*9.81*(x_cg-x_ac)+M_ac+M_tail)/I_yy; %ignored tail
pitching moment, assumed drag and thrust acts at longitudnal axis,
acceleration = 0
 plot(instant_dE,theta_oo,"linewidth",2)
 grid on
 title('Pitch rate parametric study')
 xlabel('Elevator deflection')
 ylabel('Pitch Rate')
 plot(instant_dE,theta_oo,"linewidth",2)
```

Rudder Design

List data and identify cg locations, weight combination and altitude for spin recovery

Determine the Aircraft AOA during Spin Maneuver

```
 alpha_spin = 40; %in degrees.
 %This value is approximated as being close to (and beyond) the angle
of attack of stall, and from Internet.
```

Aircraft Mass Moments of Inertia in the body axis Coordinate System

```
 I_xx_B = 0.0509 %rolling inertia
 I_zz_B = 0.213 %yawing inertia
 I_xz_B = -0.0029 %product of inertia
 %Calculated via FEA of the model.
```

Mass Moments of Inertia in the wind axis Coordinate System

```
 [I] = [(cosd(alpha_spin))^2 (sind(alpha_spin))^2 -
(sind(2*alpha_spin)); (sind(alpha_spin))^2 (cosd(alpha_spin))^2
sind(2*alpha_spin); 0.5*sind(2*alpha_spin) -0.5*sind(2*alpha_spin)
cosd(2*alpha_spin)]*[I_xx_B;I_zz_B; I_xz_B]
 I_xx_W = I(1,1) %rolling inertia
 I_zz_W = I(2,1) %yawing inertia
 I_xz_W = I(3,1) %product of inertia
```

Desirable Rate of Spin Recovery

```
 R_dot_SR = 1.4; %desired rate of yaw, taken from 12.122. of Sadraey.
It is 80 in deg/s^2. This is the typical value used in aircraft design.
```

Required Counteracting Yawing Moment

```
 N_SR = R_dot_SR*(((I_xx_W*I_zz_W)-(I_xz_W^2))/I_xx_W) %Eq. 12.120 of
Sadraey
```

Effective Vertical Tail Volume Ratio

```
 V_v_e = 0.18 %Same as actual ratio.
```

Rudder Span-to-Vertical Tail Ratio

```
 span_ratio_R = 0.83; %Assumption from Table 12.3 (Sadraey) bR/bV
```

Effective Rudder Span

```
 %Same as actual.
```

Max Rudder Deflection

```
 delta_R = 15; %This is in +- degrees. Assumed from Table 12.3 of
Sadraey
```

Rudder AOA Effectiveness, Chord Ratio & Control Derivative

```
 chord_ratio_R = 0.38; %Assumption from Table 12.3 CR/CV
 tau_R = -6.108*(chord_ratio_R)^4+11.59*(chord_ratio_R)^3-
8.2457*(chord_ratio_R)^2+3.3255*(chord_ratio_R) % from page 681 of
Sadraey
 eta_v = 1;
 C_n_delta_R = -CL_changedefl_E*V_v_e*eta_v*tau_R*span_ratio_R
```

Rudder Span, Chord & Planform Area

```
 b_R = b_Vtail
 C_R = MAC_v
 S_R = b_R*C_R
```

Rudder Design Validation

```
 chord_ratio_R = 1; %Assumption from Table 12.3 CR/CV
 delta_R_1 = (2*N_SR*57.298)/(rho_ceiling*(Vs^2)*S_w*b_w*C_n_delta_R)
 if abs(delta_R_1) < delta_R && C_n_delta_R<0
  disp("Rudder geometry is acceptable.")
 else
  disp("Rudder geometry is unacceptable.")
 end
```

Stall Angle checking

```
row = ceil(abs(delta_R_1)/5)+1;
column = int16(chord_ratio_R*10+1);
Tail_stall_ang = delta_R - reduction_table(row,column);
if Tail_stall_ang>0
    disp('Design acceptable')
else
    disp('Design unacceptable')
end
```